Felsic crust development in the Kaapvaal Craton, South Africa: A reference sample collection to investigate a billion years of geological history

Jean-François Moyen, A J Mccoy-West, Emilie Bruand, M A Millet, O Nebel, P A Cawood, N Saji, A Ladwig, Martijn Klaver, M Elburg

Earth-Science Reviews 250 (2024) 104680

Contents lists available at ScienceDirect

Earth-Science Reviews

journal homepage: www.elsevier.com/locate/earscirev

Invited Review

Felsic crust development in the Kaapvaal Craton, South Africa: A reference sample collection to investigate a billion years of geological history

J.F. Moyen [a,*], A.J. McCoy-West [b,c], E. Bruand [d,g], M.A. Millet [e], O. Nebel [c], P.A. Cawood [c], N. Saji [e], A. Ladwig [c], Martijn Klaver [e], M. Elburg [f]

[a] Université Jean-Monnet, Laboratoire Magmas et Volcans, UCA-CNRS-IRD, Aubière F-63170, France
[b] IsoTropics Geochemistry Laboratory, Earth and Environmental Science, James Cook University, Townsville, QLD 4811, Australia
[c] Department of Earth, Atmosphere and Environment, Monash University, Clayton, Victoria 3800, Australia
[d] Laboratoire Magmas et Volcans, UCA-CNRS-IRD, Aubière F-63170, France
[e] School of Earth and Ocean Sciences, Cardiff University, Park Place, Cardiff CF10 3AT, UK
[f] Department of Geology, University of Johannesburg, South Africa
[g] Geo-Ocean, CNRS-IFREMER-UBO-UBS, Plouzané F-29280, France

ARTICLE INFO

Keywords:
Tonalite-trondhjemite-granodiorite
TTG
SWASA
Archaean
Continental crust
Kaapvaal craton

ABSTRACT

The crust of the Kaapvaal craton accreted throughout the Archaean over nearly 1 billion years. It provides a unique example of the various geological processes that shape Earth's continental crust, and is illustrated by a reference collection of granitoids and mafic rocks (SWASA collection). This sample collection is fully characterised in term of age, major and trace elements, and documents the following multistage history of the craton. In the Barberton area, the initial stages of accretion (stage B.I, > 3.33 Ga and B.II, 3.28—3.21 Ga) correspond to the formation of a sodic (TTG) crust extracted from a near-chondritic reservoir. Stage B.III (ca. 3.1 Ga) corresponds to reworking of this crust, either through intracrustal melting, or via recycling of some material into the mantle and melting of this enriched mantle. Stage B.IV (2.85—2.7 Ga) corresponds to the emplacement of small, discrete plutons involving limited intracrustal reworking. The Northern Kaapvaal craton corresponds to a mobile belt flanking the Barberton cratonic core to the North. Stage NK.I (> 3.1 Ga) resembles stages B.I and B.II: formation of a TTG crust from a chondritic reservoir. In contrast, stage NK.II. (2.97–2.88 Ga) witnesses probable rifting of a cratonic fragment and formation of greenstone basins as well as a new generation of TTGs with both the mafic and felsic magmatism extracted from an isotopically depleted mantle (super-chondritic) reservoir. Intra-crustal reworking dominates stage NK.III (2.88–2.71 Ga), whereas sanukitoids and related granites, involving a mantle contaminated by recycled crustal material, are common during stage NK.IV (ca. 2.67 Ga).

The SWASA collection are available as a reference collection to investigate the behavior of other systems of interest during a variety of crust evolution modes.

1. Introduction

The formation of continents has influenced most geological processes on Earth, from the thermal structure of the mantle to the regulation of climate and the development of life. In order to fully understand the role of crustal evolution in the development of the Earth's surface towards its present-day habitable state, it is critical to ascertain the mechanisms by which continents have formed through time and how these may be linked to specific geodynamic environments. As such, the determination of the growth rate and composition of the continental crust are key endeavours that have remained at the forefront of research in Earth Sciences since its earliest days.

Decades of studies have shown that the present-day continental crust, which is largely generated in subduction zone settings, has an approximately andesitic bulk composition (Rudnick and Gao, 2014; Taylor and McLennan, 1985). Similarly, estimates of the present-day

* Corresponding author.
E-mail address: Jean_Francois.MOYEN@uca.fr (J.F. Moyen).

https://doi.org/10.1016/j.earscirev.2024.104680
Received 25 August 2023; Received in revised form 6 December 2023; Accepted 15 January 2024
Available online 20 January 2024

rates of growth and destruction of continental crust appear to be currently balanced (Cawood et al., 2013; Scholl and von Huene, 2007, 2009) Stern, 2011; Stern and Scholl, 2010). In the Archaean, the geological record shows that compositions of crust-forming magmas were significantly different, with sodic tonalite-trondhjemite-granodiorite (TTG) suites making up the bulk of Archaean granitoids rather than K-rich granites (Moyen and Laurent, 2018). However, significant uncertainty remains regarding the proportion of mafic rocks (Dhuime et al., 2015; Greber and Dauphas, 2019; Greber et al., 2017; Tang et al., 2016) and the Archaean crustal growth rate, with estimates ranging from c. 20 to 80% of present-day continental crust volume extracted from the mantle by 2.5 Ga (Armstrong, 1981; Korenaga, 2018; McCoy-West et al., 2019).

These uncertainties, in addition to the inescapable preservation bias that affects the early Earth geological record, have led to intense debate around the geodynamic setting of continent formation. Since conventional geochemical and petrological approaches have so far not provided scientific consensus, multiple research groups have attempted to use novel geochemical and petrological tools to study Archaean granitoids and crust-forming processes. This approach, while potentially extremely useful, is typically limited by one or several of the following: i) limited sample characterisation prior to analysis; ii) limited size and/or representativity of sample sets; iii) sample preparation methods may not be appropriate for novel analytical work; and iv) limited sample accessibility of the analysed samples to the community for further work. As such, a new approach in the study of Archaean terranes is required that combines best practice in sampling, analysis and curation.

We attempt to resolve these limitations by presenting and characterising a reference sample suite for the Kaapvaal Craton, which we hereafter refer to as the SWASA suite. The SWASA sample suite consists of 152 samples collected in SWAziland (now eSwatini) and South Africa. The samples were put together by a multi-disciplinary team combining expert field geologists, petrologists and geochemists with the specific aim to build a sample suite that is representative of the crustal formation history of the Kaapvaal Craton, while being prepared to the standard to meet modern petrological and geochemical analytical needs. After interrogating the major and trace element characteristics of the samples, we discuss how the SWASA suite fits within the larger literature database for the Kaapvaal Craton, demonstrating the spatial and temporal distribution of three to four broad tectonomagmatic regimes. Finally, we provide a sample sharing policy that will be applied for dissemination of the samples.

2. Cratonic architecture

The Kaapvaal Craton (Fig. 1) occupies the northeastern third of the Republic of South Africa (and extends into neighboring eSwatini, Lesotho and Botswana). It is best defined from geophysics, as a region underlain by a thick, cold lithosphere (Fouch et al., 2004). Although the total geophysical extent of the craton is about 700,000 km^2, ~ 80% of it is covered by younger sedimentary sequences, starting in the Mesoarchaean (the Pongola and Witwatersrand supergroups) and extending into the Phanerozoic (the Karoo Supergroup). The most regionally extensive cover sequence corresponds to the Transvaal Supergroup, whose basal unit [the Black Reef quartzite, ca. 2.6 Ga; Eriksson et al., 2006] unconformably overlies the Archaean granites and gneisses. The Transvaal Supergroup (and the Archaean basement) are intruded by the ca. 2.05 Ga Bushveld complex (Zeh et al., 2015).

The craton is surrounded by younger mobile belts (Johnson et al., 2006): the Palaeoproterozoic Limpopo and Kheis to the north and west, respectively; the Mesoproterozoic Namaqua-Natal belt to the south; and by the Indian Ocean passive margin to the east.

Based on geophysics, as well as surface age distributions (Anhaeusser, 2006; de Wit et al., 1992b; Eglington and Armstrong, 2004; Poujol et al., 2003), the craton can be subdivided into several domains (Fig. 1). The *Swaziland*[1] and *Witwatersrand blocks* form the old core of the craton, with rocks as old as 3.64 Ga (Compston and Kröner, 1988; Kröner et al., 1996b), although the bulk of the outcropping rocks are much younger, ca. 3.2–3.1 Ga (Poujol and Anhaeusser, 2001; Robb et al., 2006). The Colesberg Lineament separates this ancient core from younger, mostly ca. 2.7 Ga rocks of the (poorly exposed) *Kimberley Block*, to the west. North of the cratonic core, the Thabazimbi-Murchison Lineament (TML) marks the boundary with the *Pietersburg Block*, part of the *Northern Kaapvaal Craton*. Debate surrounds the status of the high-grade portion of the Pietersburg Block. While it is customarily interpreted as a thrusted allochthon forming the *Southern Marginal Zone (SMZ)* of the composite *Limpopo Mobile Belt* (Van Reenen et al., 2019), geochronological and isotopic data rather suggest that the SMZ represents the same crustal segment as the rest of the Pietersburg Block, although it experienced a higher grade, late-Archaean metamorphic event not seen in the rest of the Pietersburg Block (Laurent et al., 2019; Zeh et al., 2009). We treat the SMZ as part of the Pietersburg Block. The Pietersburg Block is much younger than the cratonic core: ages range from 3.4 to 2.65 Ga, but the majority of the rocks formed during the 2.9–2.7 Ga interval (Laurent et al., 2019). During this period, the cratonic core to the south was already stable and covered by intracratonic successions of the Pongola, Dominion (Marsh, 2006) and Witwatersrand (super)groups (McCarthy, 2006).

Only 20% of the basement rocks of Kaapvaal Craton are exposed (Fouch et al., 2004). Archaean outcrops occur in the following regions: (1) The largest, continuous outcrop occurs on the eastern and northern margins of the craton: a large Archaean inlier ranges from eMkhondo (*Piet Retief*) in northern Kwazulu-Natal, to eSwatini (*Swaziland*), the Makhjondo mountains around eMindjini (*Barberton*), the Lowveld region from Mbombela (*Nelspruit*) to Phalaborwa, to the Limpopo province around and north of Polokwane (*Pietersburg*). This paper focuses on this region and offers a section through the Archaean crust from the cratonic core of the Swaziland Block, to the SMZ. (2) In the north-west province, as dispersed outcrops of the Kimberley Block in the poorly exposed region of Amalia and Kraaipan Greenstone Belts. (3) In small windows through the (mostly) Proterozoic cover: the Johannesburg and Vredefort domes, the latter corresponding to basement uplifted by a ca. 2.023 Ga meteorite impact (Reimold and Gibson, 1996).

3. The SWASA collection

3.1. Sample collection and representativity

The SWASA samples were collected over a two-week field campaign in May 2018 by the SWASA team (Fig. 3). The collection includes 152 samples, with strong emphasis on granitoids and gneisses (80 samples;~ 52%). Forty-three samples of mafic lavas and amphibolites were also collected (ca. 26%); the rest of the collection consists of miscellaneous lithologies such as felsic volcanics, and sedimentary rocks, many of which were not further processed. The final collection thus includes only 128 samples. As much as possible, samples were taken from outcrops that have already been studied in other work, and when possible (Table A1) from the same part of the outcrop or at least from the same phase, or rock type. The equivalence between SWASA and other literature samples is given Table A1. Sample sites were selected on the basis of their representativity, relying on published work. The SWASA collection

[1] Since 1994, many Southern African places, in particular cities in the Republic of South Africa, changed names. However, geological features named after these places retained their previous names. This text therefore uses the current gazetted toponyms (mentioning older names when appropriate, for easier reference to published literature) but refers to the former denomination when it corresponds to an established geological name, and uses names approved by the South African Committee for Stratigraphy (SACS) for geological units.

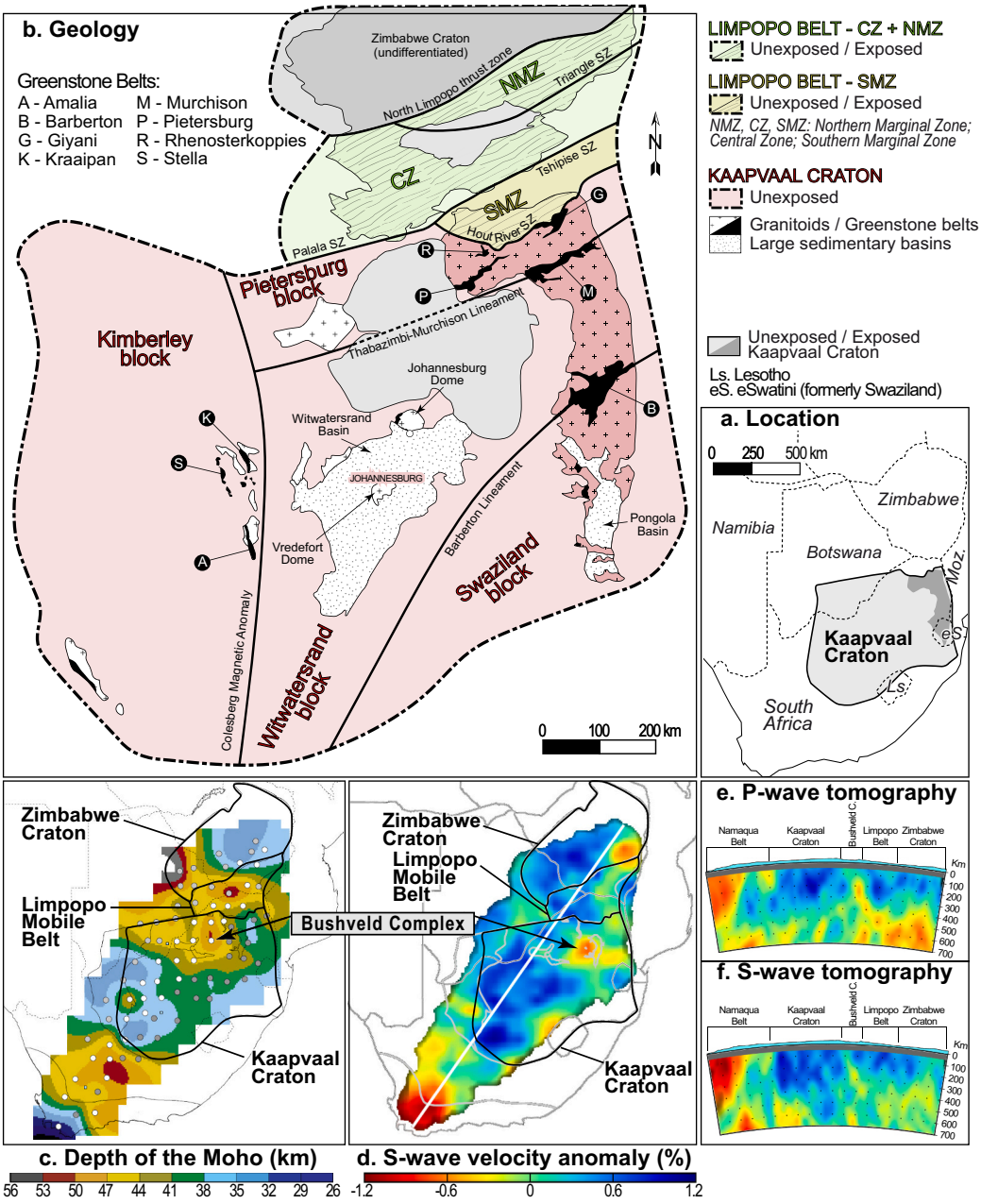

Fig. 1. Anatomy of the Kaapvaal Craton. a) Location map of the craton in southern Africa. b) Simplified geological map of the craton, modified after Laurent (2012) [compiled from (Anhaeusser, 2006; Eglington and Armstrong, 2004; Poujol et al., 2003)]. c-f) Geophysical properties of the Kaapvaal Craton, modified from Laurent (2012). Moho depth (c) from Nguuri et al. (2001); lithospheric mantle (d-f) from Fouch et al. (2004). The section line of panels (e) and (f) corresponds to the white line in panel (d).

thus includes representative samples of all major units previously identified in the literature. In addition, our interpretations below also draw on a large compilation of published data: ca. 1600 samples from the Barberton area, and ca. 550 from Northern Kaapvaal. The various diagrams used in this paper show that the SWASA samples invariably fall within the range defined by literature samples from the same groups, giving us confidence that the SWASA collection is as representative as it size permits and offers as comprehensive a record as possible.

3.2. Sample preparation

In the field, care was taken to select the least altered portions of outcrops. To obtain a representative collection, very large samples, generally ~3–5 kg (minimum of 2 kg), were collected using sledge hammers and chisels, and then cleaned in the field as much as practical to remove any remaining weathering rinds. Following the field campaign, three days were spent at University of Johannesburg sawing the samples to remove any remaining weathered parts and to split them into more manageable pieces for shipping.

The main mass of the samples was then sent to Cardiff University for further processing and preparation of representative sample powders. Thin section blocks and samples for mineral separates were sent to Laboratoire Magmas et Volcans (LMV) and Monash University, respectively. Prior to milling, each sample, ~ 200–300 g was cut in <5 cm blocks using a diamond saw. Each block was then individually polished using a diamond lap to remove any potential contamination from the saw blades. The samples were then milled to a fine powder using agate planetary ball mills. A minimum of 100 g of powder (most often 200 g)

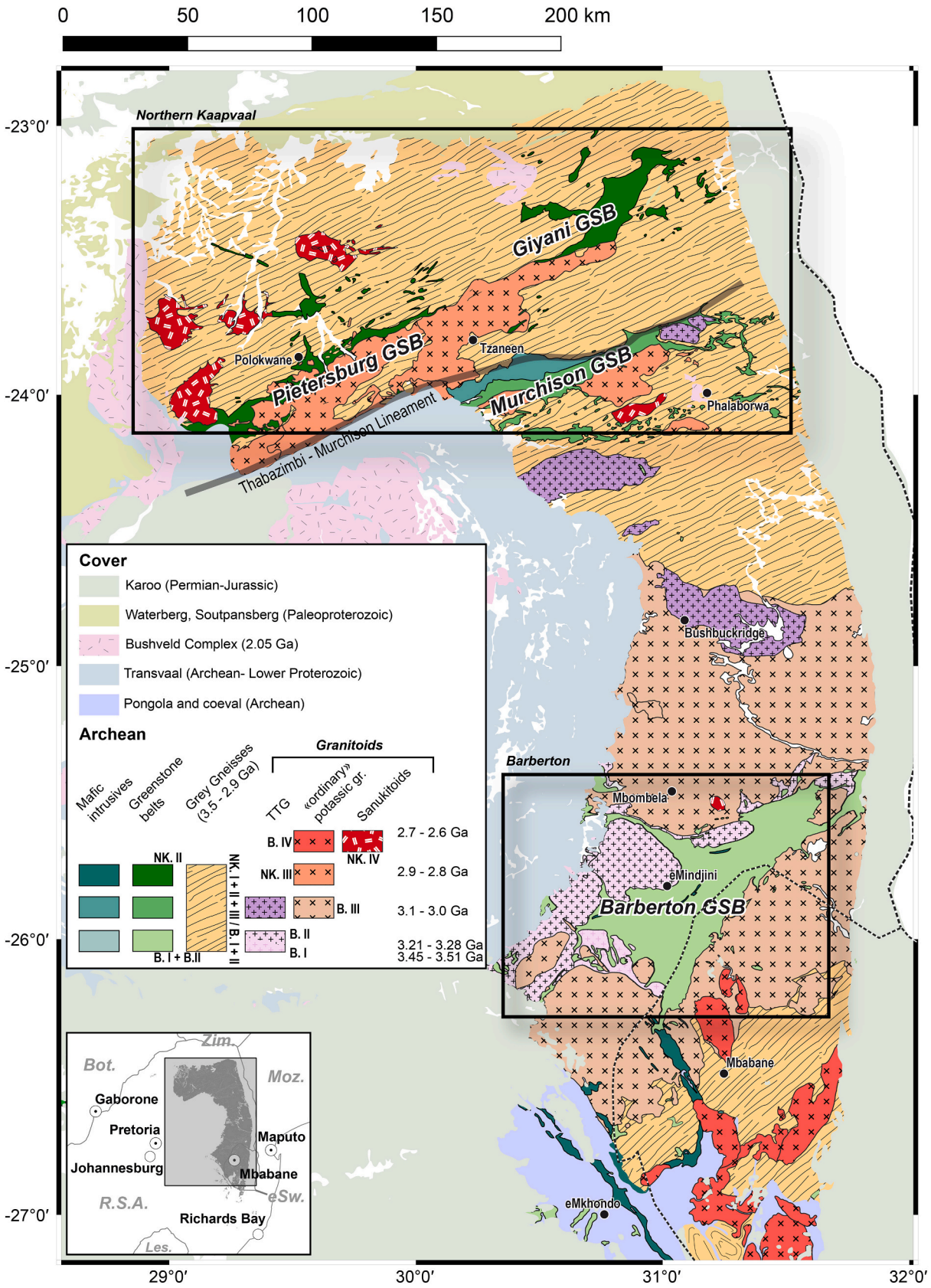

Fig. 2. Geological map of the main Archaean outcrop in the eastern and northeastern Kaapvaal Craton. Redrawn from the 1/1000000 Geological Map of South Africa. The two boxes labelled "Barberton" and "Northern Kaapvaal" identify the two focus areas of this paper (the two regions with the best Archaean outcrops). GSB = Greenstone Belt. The stages discussed in the text for Barberton and Northern Kaapvaal evolution are indicated in the caption ("B·I", "NK.II", etc.). Grey Gneisses from both areas are composite and include rocks from several stages (see text).

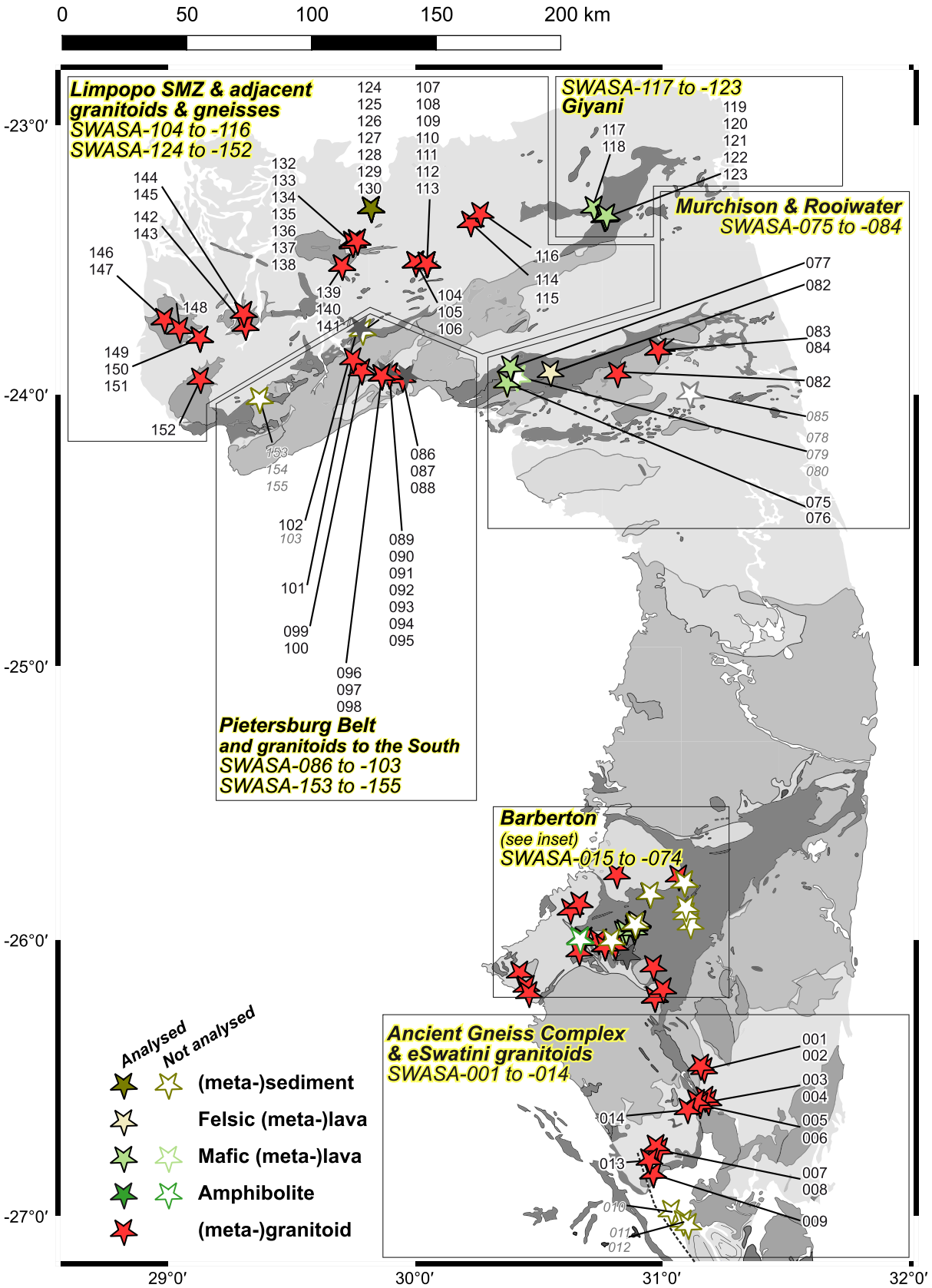

Fig. 3. Location of SWASA samples (same map as Fig. 2). Barberton area is magnified on next page. Samples labelled in grey have not been analysed. In many cases several samples were collected from one locality (or from adjacent localities). All sample numbers are prefixed by "SWASA-".

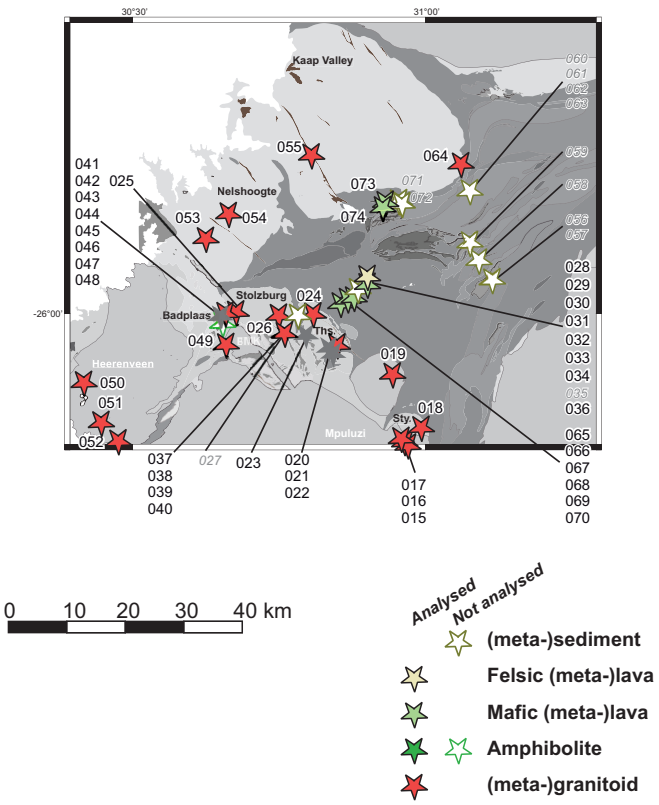

Fig. 3. (*continued*).

was generated for each sample and splits can be requested from the author team (see sample sharing policy, Appendix A).

3.3. Major and trace element analyses

A total of 128 samples (all granitoids and most mafic rocks) has been prepared and analysed for major and trace elements (Supplementary Table 1). The analyses were conducted in two separate analytical programs with data quality monitored with a range of international rock standards available from USGS. The first analytical program, at Monash University, Australia, consisted of 89 samples. Major element and loss on ignition (LOI) data were obtained at the CODES Analytical Laboratories, University of Tasmania, using established techniques (Robinson, 2003; Watson, 1996). Major element compositions were determined on glass discs made by adding 0.6 g of rock powder and 5.4 g 12:22 flux (lithium tetraborate-metaborate mix) using an Axios Advanced Wavelength Dispersive X-ray Fluorescence (XRF) spectrometer with a 4 kW Rh tube. Analyses were performed in two batches (March 2019 and January 2020) with rock standards (G-2, GSR-1) used for quality control, with measured values (Supplementary Table 2) within uncertainty of recommended values (Jochum et al., 2016).

Trace element concentrations were determined for 71 samples at the Isotopia Laboratories, Monash University. All acids used had undergone sub-boiling distillation twice. One hundred mg (± 1) of rock powder was weighted out into 3 mL Savillex PFA vials along with 1 mL 29 M HF and 0.5 mL 16 M HNO_3 and placed inside pressure sealed Parr bombs and heated at 200 °C for at least 72 h. Following cooling, an additional 0.5 mL 16 M HNO_3 was added, and the samples were then evaporated to dryness at 85 °C. The samples were then brought into solution in 2 mL 16 M HNO_3 at 120 °C and transferred to 7 mL Savillex Teflon vials. Multiple refluxes of 16 M HNO_3 and 12 HCl were then undertaken as required to ensure complete dissolution of the sample. Once the sample was completely dissolved it was brought into solution in 5 mL of 3 M HNO_3. A 5% aliquot was then taken and diluted using 2% HNO_3 in preparation for analysis. Samples were then analysed for 40 trace elements using a Thermo Scientific iCAP quadrupole inductively coupled plasma mass spectrometer (Q-ICP-MS). The instrument was calibrated using multi-element solutions ranging from 0.1 to 100 ppb (0.1, 1.0, 10, 50, 100 ppb). Raw counts per second data had a blank subtraction applied (the digestion blank for each element; $n = 3$) and then absolute concentrations were calculated. Most analyses represent the average of two replicate measurements from separate analytical sessions. Absolute concentration data were corrected for mass bias-induced signal fluctuations using rock standard BHVO-1 (Jochum et al., 2016) monitored throughout the analytical session every 8–10 samples. International rock standard G-2 treated in a similar way produces average values (Supplementary Table 3) within ≤5–10% of the recommended values (Jochum et al., 2016) for all elements, except Sn and Tl where relative uncertainties are <13%. Further confirmation of the accuracy of the trace element data is provided through comparison of more abundant trace elements Sr and Ba, which were independently determined by both XRF and ICP-MS (Supplementary Fig. 1) and over a wide concentration range fall close to unity. Furthermore, Nd and Sm concentrations obtained here using ICP-MS are in excellent agreement falling along a 1:1 regression line with isotope dilution data (following McCoy-West et al., 2020) obtained using multi-collector instruments for the same samples (Supplementary Fig. 2).

The second batch of 39 additional samples was analysed at LMV, France (Supplementary Table 1). Loss on ignition was calculated based on the mass difference following 1 g of sample being placed in an oven at 110 °C for 2 h (H_2O+) and then 1000 °C for a further 2 h (H_2O-), with the total LOI being the sum of these values. For element analyses, 100 mg of sample powder was mixed with 300 mg of $LiBO_2$ flux in a graphite crucible and placed in a furnace at 1000 °C allowing complete melting of the sample. The obtained glass was then dissolved immediately with 1% HNO_3 before being diluted for analysis in solution mode. Major elements have been analysed using an Agilent 5800 ICP- optical emission spectrometer (OES) at LMV. Analyses were performed over two sessions

(July and November 2021). For each of these sessions, rock standard BHVO-1 was used for data quality control purposes (Supplementary Table 4). Trace element compositions were determined from a separate dissolution. Fifty mg of sample powder was mixed with solid NH_4HF_2 using the method described in Zhang et al. (2012). Following dilution, the samples were analysed for 49 trace elements using the Agilent 7500 ICP-MS at LMV. Analyses were performed over four sessions between February and July 2021. For each of these sessions, rock standard GSP-2 was used as primary reference material while AGV-2 was used as secondary standard for quality control purposes (Supplementary Table 5). International rock standard AGV-2 analysed as unknown produces average values within ≤5–10% of the recommended values (Jochum et al., 2016) for most elements except for few elements (Sc, Zn, Tl, Tb, Er, Pb) for which the relative uncertainty was ≤10–15%.

4. Assessment of alteration within the SWASA collection

The SWASA collection contains a range of representative rock types that showcase the variability observed throughout the Kaapvaal Craton. During sampling all reasonable precautions were taken to obtain the most pristine samples possible. We have conducted a preliminary investigation of the degree of chemical alteration within the SWASA sample suite based on their major element compositions (Fig. 4). The majority of samples ($n = 112/128$) shows relatively low (≤ 2 wt%) loss on ignition (LOI) values, a potential indicator of secondary hydrous mineral formation. Alternatively, the mass transfer of mobile elements versus immobile elements can be used to assess the extent of chemical weathering. The most prominent of these is the Chemical Index of Alteration (CIA; Fig. 4a) of Nesbitt and Young (1982), for which fresh basalts have values from ~30 to 45, granitoids would be expected to have higher values of ≈ 45 to 55, and average shales values of ≈ 70 to 75, due to their elevated clay contents. An alternative approach to quantifying alteration, hopefully less sensitive to initial bulk rock composition, has been developed by Ohta and Arai (2007). Their Mafic-Felsic-Weathered (MFW) diagram (Fig. 4b) uses principle component analyses of 8 major elements to assess the consequences of alteration.

The majority of SWASA samples show little evidence for chemical weathering. The only samples that display significant degrees of alteration (either high CIA or LOI, sometimes but not always reflected in high MFW) correspond to altered mafic/ultramafic units in particular in the Hooggenoeg Formation of the Barberton Greenstone Belt, where (Archaean) seafloor alteration related to the development of chert units is well described (Hofmann and Harris, 2008). All the granitoids on the other hand, and all but one amphibolite, show no evidence for alteration.

The assessment presented here has only focused on major element mobility, and detailed consideration of specific trace elements has not been attempted as they can vary over an order of magnitude between different sample types. As a rule, major and trace elements mobility are seldom disconnected (e.g. Chavagnac, 2004; Furnes et al., 2012; Lahaye et al., 1995; Parman et al., 2001; Schneider et al., 2019; Trépanier et al., 2016), so there is little ground to assume significant trace element mobility in the absence of major element mobility. Also, the various trace element diagrams we use in this paper, comparing SWASA samples with published samples, do show that they do not differ significantly. Lastly, trace element mobility has long been a topic of discussion e.g. in Barberton mafic rocks, clearly including highly silicified horizons (Hofmann and Harris, 2008). Yet, non-silicified ones preserve pristine trace elements signatures (Chavagnac, 2004; Furnes et al., 2012; Parman et al., 2001; Schneider et al., 2019). Thus, the SWASA collection did at least not suffer more from trace element mobility than any other Kaapvaal sample ever studied. Nonetheless, interested researchers should ensure they carefully scrutinise the data regarding the specific trace elements or isotopic systematics they are interested in for potential more subtle effects of alteration prior to making detailed interpretations.

5. The Barberton Granite—Greenstone Terrain (and adjacent Ancient Gneiss complex)

5.1. Summary of the geological history

The Barberton-Granite-Greenstone Terrain (BGGT), and the adjacent Ancient Gneiss Complex (AGC) in eSwatini, record nearly 1 GYr of geological history (from 3.64 to 2.67 Ga), both as supracrustal (the Barberton Greenstone Belt proper, BGB) and intrusive rocks. For recent syntheses of the complex geology of the BGGT and AGC, the reader is referred to: Moyen et al. (2018) for the TTG magmatism; Lowe et al. (2012) and Byerly et al. (2018) for the supracrustal sequences; Schmitz and Heubeck (2021) for the structures; Hoffmann and Kröner (2018) for the evolution of the AGC, and of course the older but still invaluable geological maps and comments by Anhaeusser et al. (1981, 1983) and Wilson (1982).

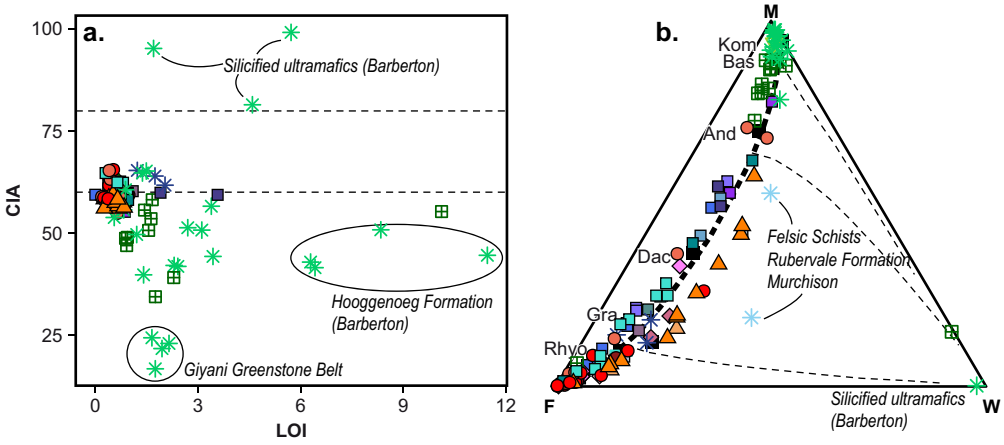

Fig. 4. An assessment of the extent of alteration within the SWASA sample collection. Caption as in Figs. 6–17. (a) Loss on ignition (LOI) versus chemical index of alteration (CIA), where CIA = $[Al_2O_3/(Al_2O_3 + CaO + Na_2O + K_2O] \times 100$ (Nesbitt and Young, 1982). The intensity of chemical weathering can be considered intermediate when CIA is c. 60–80, and extreme when CIA > 80 (Fedo et al., 1995). Some clearly altered samples correspond to fuchsite alteration zones in the Barberton Greenstone Belt, or to samples from the Hooggenoeg Formation close to chert bands. (b) MFW ternary plot after Ohta and Arai (2007). Rhyo, Gra, Dac, And, Bas, Kom: compositions of average rhyolite, granite, dacite, andesite, basalt and komatiite. The majority of samples within the SWASA collection plot close to the igneous rock trend. Sanukitoids and other hornblende-bearing granitoids of the Northern Kaapvaal plot slightly away from the main "igneous" trend of Ohta and Arai (2007), outlining that the "igneous" trend of this work has been fitted on calc-alkaline rocks and is not very appropriate for more potassic samples.

The AGC consists of composite, meso-crustal (amphibolite to granulite facies) grey gneisses. It is tectonically juxtaposed to the Barberton Greenstone Belt, which is a thick, folded sequence of low-grade (subgreenschist to greenschist facies) supracrustal rocks. Traditionally, the BGB is described in terms of a simple stratigraphy (Onverwacht, Fig Tree and Moodies groups from bottom to top, respectively), although, as we will see, this simplified view does not describe the complex geology of this unit adequately. Granitoids (as opposed to composite gneisses) occur as plutons mainly intruding into the BGB, and belong to several successive generations and petrological types.

For the purpose of this paper, crustal development in the region can be summarised as four main stages, labelled B.I to B.IV (Table 1):

Stage B.I 3.6–3.3 Ga: the original crustal nucleus. The dominantly mafic/ultramafic extrusive sequence of the lower Onverwacht Group is intruded by TTG plutons [TTG1 and TTG2 of Moyen et al. (2018)] around the BGB. The oldest components of the AGC, which are predominantly TTG in composition, formed at the same time.

Stage B.II 3.3–3.2 Ga: the main tectono-magmatic event. During this rather complex event, the supracrustal rocks record (of the Fig Tree and Moodies groups) evolve from mafic extrusive rocks towards terrigenous sediments, initially being represented by banded iron formations (BIF) and felsic volcanoclastics of the Fig Tree Group, followed by quartz-rich sands and conglomerates of the shallow marine (deltaic) Moodies Group. Younger TTGs [TTG3a and 3b of Moyen et al. (2018)] intruded, and younger components of the AGC emplaced. Broadly during the same period, complex deformation in the BGB is responsible for the formation of the main structures and the juxtaposition of these diverse rock units. These events are collectively responsible for most of the present day map pattern.

Stage B.III ca. 3.1 Ga: craton stabilisation. Throughout the craton, a large volume of granitoids (granodiorites, monzogranites and syenogranites, the GMS suite) intrude the older rocks during a short time interval [about 10 MYr; Moyen et al., 2021c]. As a result, rocks from the GMS suite cover large swathes of the BGGT, perhaps about one third of the surface.

Stage B.IV ca. 2.7 Ga: late granites. In the late Archaean, a series of small (<10–20 km), well-delimited plutons intruded the now rigid crust.

From a geographic perspective, the BGGT comprises several juxtaposed domains, each preserving only part of the history. This has been well documented in the BGB. Lithological and stratigraphic mapping, as summarised in Lowe et al. (2012), shows that the belt consists of different domains with distinctive stratigraphies (i.e. rock packages of distinct nature and ages). These domains were then complexly deformed and imbricated, mostly during ca. 3.29–3.21 Ga (Stage B.II) deformation events (Drabon and Lowe, 2021; Schmitz and Heubeck, 2021). The surrounding intrusive rocks also show different ages in each domain. Lately, The domain boundary has been proposed to correlate with the geophysical boundary between the Swaziland and Witwatersrand blocks of the Kaapvaal Craton (de Wit et al., 2018).

Table 1 summarises the occurrences of rocks from each stage in the various domains.

The center and southeast of the BGB, corresponding to the

Table 1
Summary of the main rock units in the (BGGT) and (AGC). For age references, see text, as well as mentioned review papers (Byerly et al., 2018; Hoffmann and Kröner, 2018; Moyen et al., 2018 offer comprehensive summaries).

	Age (Ga)	Barberton Northwest		Barberton South-Central		Ancient Gneiss Complex	
Stage B.IV	2.7 2.85?	"Late" intrusive plutons: Mpageni, Mbabane, Ngwempisi, Sinceni, Sicunusa, etc.					
Stage B.III	ca. 3.1	GMS suite: Nelspruit, Pigg's Peak, Mpuluzi and Heerenveen Batholiths					
Stage B.II	3.21	Kaap Valley, Nelshoogte plutons Lomati River Gabbro	Moodies		Moodies	Usutu suite Youngest components of Ngwane Gneiss	
	3.25–3.23	Late components of Badplaas (and Inyoni) Gneisses	"Northern" Fig Tree (< 3.24 Ga) (Ulundi, Sheba, Belvue Road & Schoongezicht formations)		"Southern" Fig Tree (< 3.28 Ga) (Mapepe & Auber Villiers formations)		
	3.25–3.28	Early components of Badplaas Gneisses	Weltvreden Formation of Onverwacht Group* Jamestown "arm" of the BGB Schapenburg fragment				
Stage B.I	3.42–3.33				Kromberg & Mendon formations	Mhlatuzane Gneisses (3.33 Ga)	
	3.445			Stolzburg and Theespruit plutons	H6 felsic lavas	Tsawela gneisses Components of Ngwane Gneiss	
	3.47–3.45				Theespruit, Komati and Hoogenoeg formations of Onverwacht Group		Protoliths of supracrustal suites (*Mankayane, Dwalile, Kibuta-Shishelveni*)
	3.51–3.55 Ga			Protoliths of Steynsdorp gneiss	Protoliths of amphibolites?		
	> 3.55 Ga					Oldest remnants of Ngwane Gneiss	

* The Welvreden Formation is traditionally placed in the Onverwacht Group, although it is now known to be an age equivalent of the Fig Tree Group of South-Central Barberton (Byerly et al., 2018).

"Songimvelo Block" (Byerly et al., 2018; Lowe et al., 2012), comprise mainly stage B.I rocks (both plutonic and supracrustal). They include the supracrustals from the Onverwacht anticline and the "Stolzburg block" (Mühlberg et al., 2021) plutons to the South that intrude it. Supracrustal rocks from the Songimvelo Block are uncomformably overlain by stage B.II rocks of the Fig Tree and Moodies groups [of the "Umuduha Block"; (Byerly et al., 2018)], although the preserved contacts are mostly tectonic.

In contrast, the **northwest of the BGB** [the "Kaap Valley" Block; (Byerly et al., 2018; Lowe et al., 2012)] is dominated by stage B.II rocks and lacks older components. Relatively young mafic rocks, traditionally placed within the Onverwacht Group although they are age equivalent of the Fig Tree Group further South,include (i) the ca. 3.28 Ga Weltevreden Formation (Lahaye et al., 1995; Puchtel et al., 2014), (ii) deformed fragments in the Jamestown Schist Belt (the "arm" of the BGB protruding to the NW; Anhaeusser, 2019) and (iii) the Schapenburg Schist Belt (a small, schistose fragment, West of the main BGB; Anhaeusser, 1983). These rocks are capped by Fig Tree rocks, younger and stratigraphically distinct from the "southern" Fig Tree (Drabon and Lowe, 2021), followed by Moodies Group sedimentary rocks, and intruded by late stage B. II (3.23–3.21 Ga) plutons.

The **Ancient Gneiss Complex** of eSwatini records a similar evolution history, but at mid-crustal levels. The dominant lithology (the Ngwane Gneiss) is a complex orthogneiss consisting of different phases, some of which are TTG-like and some of which represent periods of crustal reworking (Hoffmann and Kröner, 2018; Kröner et al., 2019). The Ngwane Gneiss also include enclaves of amphibolites and metasediments (the Dwalile, Mankayane and Kubuta-Shishelveni suites), and numerous leucosomes, pegmatites and aplites. Collectively, this unit is akin to the (much younger) Grey Gneisses of the Northern Kaapvaal Craton, discussed below. It corresponds to a protracted period of formation and reworking of an early felsic crust, including TTG as well as more potassic (intra-crustal melting?) components (Hoffmann and Kröner, 2018), all of which were imbricated and transposed into a common foliation during their history. Ages for the Ngwane Gneiss range from 3.66 to 3.20 Ga (Hoffmann and Kröner, 2018), with a gap between 3.43 and 3.30 Ga (i.e. between stage B.I and B.II). Some well-delineated phases are also mappable, including the tonalitic Tsawela Gneiss, intruded at ca. 3.45 Ga, in the Mankayane area of southwestern eSwatini; as well as the ca. 3.33 Ga Mhlatuzane tonalitic to dioritic gneiss of the Kubuta region in the South-East of the country (Hoffmann and Kröner, 2018). Collectively, this age range covers Barberton stage B.I and stage B.II. Further stage B.II rocks are represented by the diorite-granodiorite Usutu Suite (ca. 3.23 Ga), which intruded the Ngwane Gneiss.

Stage B.III and Stage B.IV intrusives occur in all three domains (Central-South Eastern BGB, Northwest BGB and AGC) described above, irrespective of their unique older histories.

5.2. Mafic rocks of the BGGT and associated supracrustals

In the BGGT, mafic rocks include both amphibolite fragments in older (stage B.I) plutons (mostly in the TTG2 suite) as well as the thick basalt-komatiite sequence of the Onverwacht Group (stage B.I). Rare mafic rocks are reported during stage B.II [e.g. Moodies lavas (Heubeck et al., 2013) or Lomati River gabbroic sill (van Rensburg et al., 2021)] but few analyses are available for them; they tend to be deeply weathered and therefore were not sampled as part of the SWASA collection.

Amphibolite fragments are older than the surrounding ca. 3.45 Ga plutons, and are generally regarded as high-grade equivalents of the lowermost Onverwacht Group [the Sandspruit and Theespruit formations; Anhaeusser and Robb, 1980]. To our knowledge they have not been dated, although felsic schists (Mühlberg et al., 2021) and metasedimentary rocks (Moyen et al., 2021c) associated with the amphibolite xenoliths give emplacement or depositional ages of 3.56–3.51 Ga. The Ngwane Gneiss of the AGC also includes amphibolite fragments that are probable equivalents.

The stage B.I mafic sequences of the Onverwacht Group form a ca. 9 km thick sequence in the south-central portion of the belt (the Onverwacht anticline). In very general terms, komatiites are more common at the base and basalts near the top. Eruption ages range from ca. 3.47 to ca. 3.3 Ga (Lowe et al., 2012). At ca. 3.45 Ga [the age of the plutons to the south of the belt; (Laurent et al., 2020)], a series of hypovolcanic units connect the plutons to a felsic extrusive complex near the top of the Hooggenoeg Formation [H6 member in (Lowe et al., 2012)].

The mafic volcanic rocks range in composition from komatiites to basalts, in subequal proportions, locally extending to more differentiated compositions (andesites). Irrespective of their type, Barberton mafic lavas plot between a N-MORB and *E*-MORB composition in terms of trace elements (Fig. 5b). In comparison with Archaean mafic rocks worldwide (Moyen and Laurent, 2018), they occupy the "MORB-like" extremity of the compositional range: many Archaean mafic rocks plot between this MORB-like composition, and a "crust like" composition with higher Th (and Th/Yb, Th/Nb) levels. There is no clear change with stratigraphy, and the main control on trace elements patterns appears to be the rock type (from komatiite to basalt, with rare andesites), probably reflecting varying degrees (and possibly depth) of melting of a similar mantle source (de Wit et al., 2018; Furnes et al., 2012).

The amphibolites also plot in the field of Archaean mafic rocks. Amphibolites that did not undergo any melting event (such as brittle xenoliths from the Theespruit Pluton, SWASA-21 to −23) plot close to the depleted side of the Archaean field, and are indeed probable equivalents of lower Onverwacht lavas. On the other hand, amphibolites that experienced melting and/or injection by latter granitoids (such as the samples from Inyoni Zone, SWASA-41 to −45) occur towards the "crustal" side of the field and overlap with the composition of granitoids. These are of course samples composite at the scale of the hand specimen, due to the presence either of in-situ leucosomes or injected veins (and caution should be exercised when interpreting their whole rock geochemistry). The amphibolites from the AGC, described by Kröner et al. (2019), also present the same enrichments in incompatible elements compared to metabasalts and probably reflect the same sort of mixed signature.

5.3. Granitoids of the BGGT

Granitoid formation occurred during the four stages of evolution of the Kaapvaal Craton, with each stage having distinctive characteristics reflecting progressive craton accretion and evolution. In general one of the key chemical discriminators for granites is their aluminosity (Bonin et al., 2020), however, this becomes largely irrelevant for Archaean granitoids as they are dominantly metaluminous (Moyen, 2020). In terms of major elements, the main descriptor is the Na-Ca-K balance, that we here depict using the O'Connor (1965) feldspar normative diagram (Fig. 6).[2] We also show the two ternary diagrams used by Laurent et al. (2014a), that allow several geochemical features to be summarised (Fig. 7). For trace elements, rather than more common variants of Sr—Y and La—Yb systematics, we use a combined projection (Sr/Y vs. La/Yb, in log scale; Fig. 8). In addition, Supplementary Fig. 3 shows some diagrams more useful for TTG rocks (Moyen et al., 2018): SiO_2 – Na_2O/CaO (separates the trondhjemitic from tonalitic series), and SiO_2 – Sr. The latter separates the low- from high-Sr series, an important feature in distinguishing low- from high-pressure series (Moyen and Martin, 2012). In the BGGT, the existence of distinct low- and high-Sr series has long been demonstrated (Anhaeusser and Robb, 1983a; Robb and Anhaeusser, 1983), and is a key observation. Note that both diagrams are not particularly useful for the potassic granites. Lastly, Supplementary Fig. 4 summarises the shape of the REE patterns, using the lambda-

[2] The plotting script (and ancillary files), in R language, is supplied as supplementary files MMC3 and MMC4

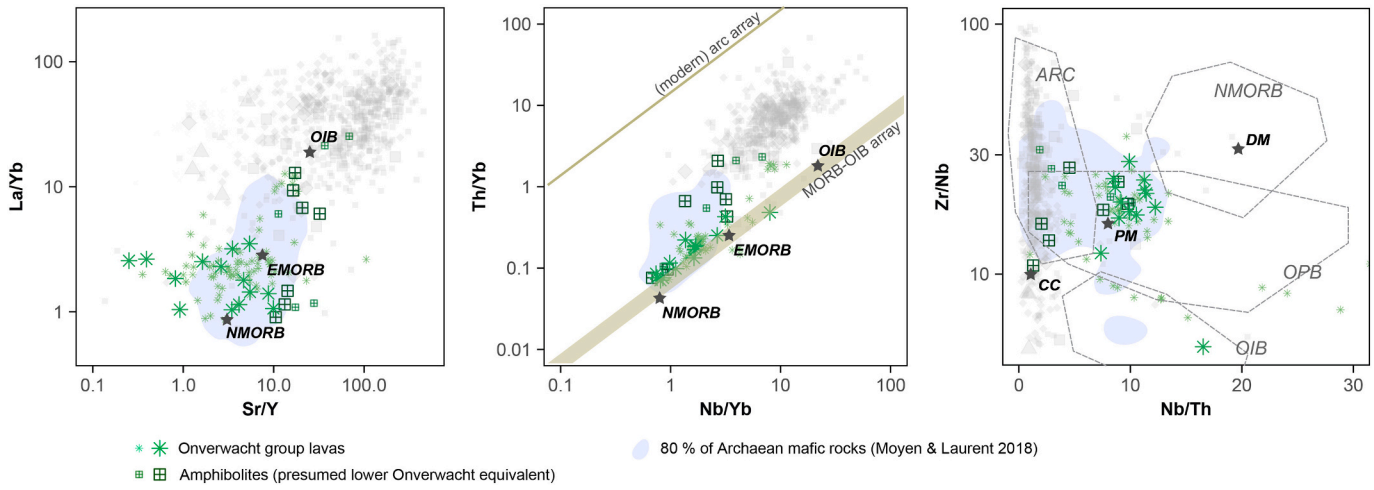

Fig. 5. Trace element characteristics of mafic rocks of the BGGT. (a) La/Yb versus Sr/Y diagram (log-log). (b) Th/Yb vs. Nb/Yb diagram of Pearce (2008), showing the inferred "MORB-OIB" and "modern arc" arrays. (c) Zr/Nb vs Nb/Th diagram of Condie (2005a). The Nb/Th axis mostly separates "arc" from "non-arc" rocks, as in Pearce's projection. Zr/Nb permits the distinction between depleted and enriched components (an OIB-MORB range). SWASA samples are represented by larger symbols. Grey symbols in the background show the composition of BGGT granitoids (Fig. 6 to Fig. 8) for comparison. Light blue fields show where 80% of the Archaean mafic rocks from the global compilation of Moyen and Laurent (2018) plot. (For interpretation of the references to colour in this figure legend, the reader is referred to the web version of this article.)

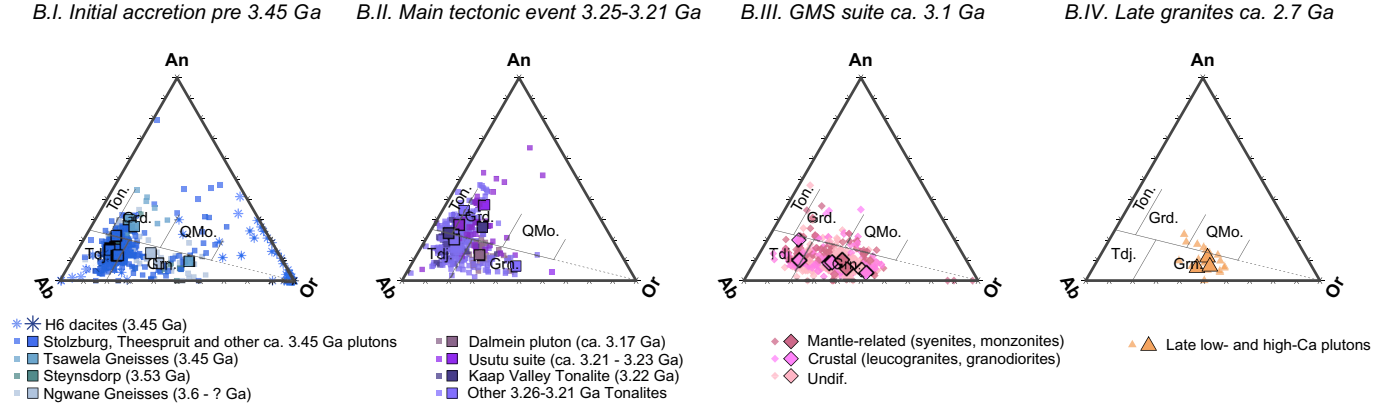

Fig. 6. Feldspar-normative diagrams for the granitoids of the BGGT after O'Connor (1965). Abbreviations: Ton.: tonalite; Tdj.: trondhjemite; Grn.: granite; Grd.: granodiorite; QMo.: quartz-monzonite. SWASA samples are represented by larger symbols with black outlines, smaller dots correspond to literature data.

parameters of O'Neill (2016). Figs. 6–8, and 12–14, are all constructed in a similar manner: (i) SWASA samples are depicted by larger symbols with black outline, whereas literature samples are shown by smaller paler symbols; (ii) the whole dataset (SWASA + literature) is shown in the background as grey symbols, whereas compositions belonging to a given age band are shown in colour and in the foreground; (iii) the shape of the symbols corresponds to rock types, as explained in the caption. Symbols and colors remain consistent throughout the paper.

Granitoids of **stage B.I** are in vast majority tonalites and trondhjemites (Fig. 6). About 2% of the dataset forms a "tail" towards the right-hand side of the feldspar normative diagram; half of these samples correspond to the diorites that Laurent et al. (2020) interpreted as primitive liquids, the other half are minor granitic phases in the AGC or the Steynsdorp Gneiss, the latter already identified by Moyen et al. (2018). Unsurprisingly, the granitoids are similar to compositions related to melting of low-K mafic rocks (Fig. 7). They define medium- to high-Sr series (Supplementary Fig. 3; also Robb and Anhaeusser (1983)). They have on average higher Sr/Y and La/Yb ratios (ca. 85 and 50, respectively) than subsequent generations of TTGs (Fig. 8; also Supplementary Fig. 4) and are more sodic compared the more calcic younger TTGs [i.e. stage B.I are trondhjemites compared to stage B.II leucotonalites; also see Moyen et al., 2018]. All these features are the basis of the "high pressure" signature as defined by Moyen and Martin (2012), but it is worth noting that these are also the signatures interpreted by Laurent et al. (2020) as evidence for plagioclase accumulation within the magma chamber.

Stage B.II granitoids are concomitant with the main deformation event(s) observed in the BGGT and although they are also mostly tonalites and trondhjemites, they show systematic differences from the stage B.I rocks. Compared to stage B.I, stage B.II plutonic rocks tend to be calcic rather than sodic, i.e. they are tonalites more often than trondhjemites (Fig. 6). They have also lower Sr content (Supplementary Fig. 3) and tend to have higher Sr/Y (ca. 100) but lower La/Yb (ca. 30) ratios (Fig. 8), i.e. they define a low- to medium-pressure signature (Moyen and Martin, 2012) but seldom a high-pressure one (Moyen et al., 2018). A particular noteworthy aspect is the presence of a large, relatively mafic intrusion, the 3.22 Ga Kaap Valley pluton (Robb et al., 1986). This large intrusion (at ca. 750 km^2 it is the largest in the BGGT) is atypical in that it is made of leuco-diorites to hornblende tonalites (60 < SiO_2 < 65 wt%), much more mafic than typical TTGs seen in the BGGT and elsewhere in the craton. Kaap Valley has low Sr contents for these SiO_2 values (ca. 500 ppm at 65% SiO_2; other Barberton TTGs reach 800 ppm at this silica content) and has low La/Yb (ca. 20) and, in fact, does not (or barely) fulfill the defining criteria for TTGs (Moyen and Martin,

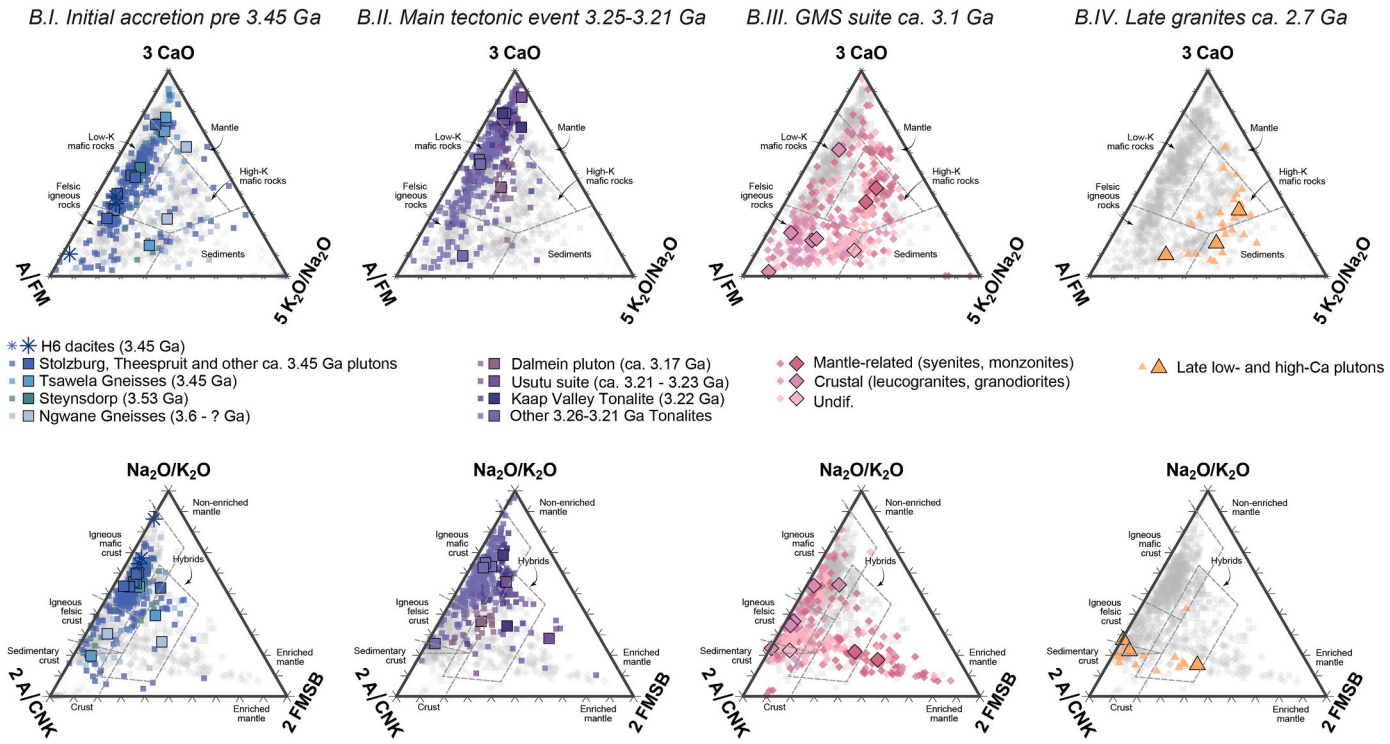

Fig. 7. Summary ternary diagrams of Laurent et al. (2014) for BGGT granitoids. A/FM = Al2O3/(FeOt+MgO); A/CNK = molecular Al/(2Ca + Na + K); FMSB = (FeOt+MgO) × (Sr + Ba). SWASA samples are represented by larger symbols with black outlines, smaller dots correspond to literature data. Grey symbols show the whole dataset, coloured symbols in each panel correspond to the age band considered.

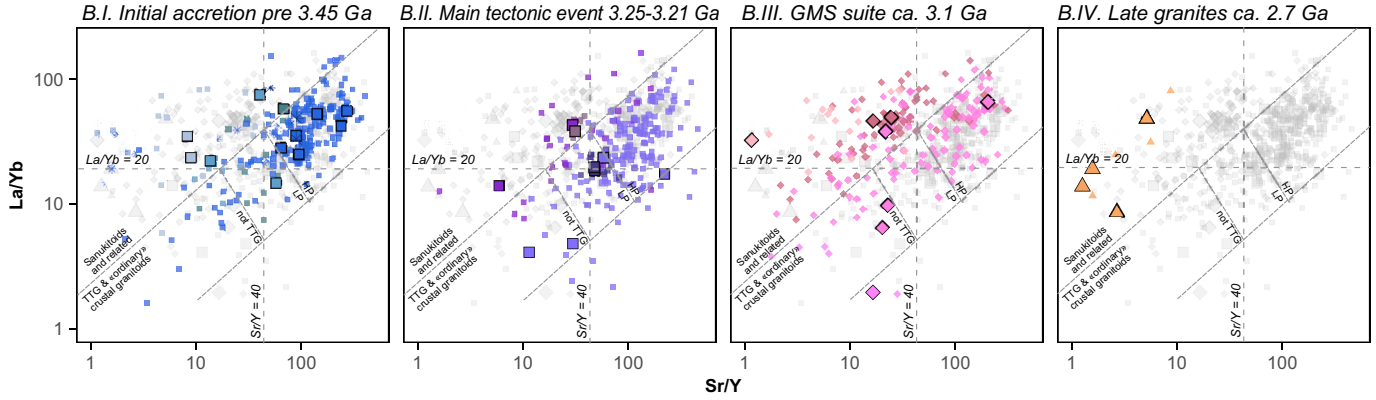

Fig. 8. Sr/Y versus La/Yb diagram for BGGT granitoids. The fields separating the rock types (grey lines) are drawn visually from the dataset in this paper.

2012). Some components of the coeval Usutu suite in eSwatini have been previously reported (Hoffmann and Kröner, 2018) and show similar features.

The Dalmein Pluton (poorly studied, and not represented in the SWASA database) emplaced at ca. 3.17 Ga (Lana et al., 2010), post-dating the main deformation of the BGB. It is a K-feldspar porphyritic granite, strongly distinct from both stage B.II and stage B.III granitoids.

Stage B.III corresponds to the volumetrically dominant GMS suite at ca. 3.11 Ga. Four large batholiths, probably emplaced between syn-magmatic shear zones (Anhaeusser and Robb, 1983b; Belcher and Kisters, 2006a, 2006b; Robb et al., 1983), were emplaced in a short period of time at ca. 3.11 Ga (Moyen et al., 2021c). The batholiths are dominated by granites, but also include minor granodiorite and syenite components (Fig. 6). The granites and granodiorites likely formed by melting of an older felsic basement such as TTG, grey gneisses or sedimentary derived from them (Clemens et al., 2010; Moyen et al., 2021c). These rocks resemble the "low-Ca" granitoids of the Yilgarn craton (Champion and Sheraton, 1997); similar rocks probably occur in other cratons, where they tend to be lumped with tonalites and trondhjemites (they form the "G" of the "TTG" suite). Yet the BGGT example highlights the distinction between trondhjemites (stage B.I), tonalites (stage B.II) and granodiorites (stage B.III). The GMS granites and granodiorites are coeval with syenites, monzonites and some mafic components, the petrogenesis of which is best explained by a contribution of an enriched mantle source (Moyen et al., 2021c) (Fig. 7). An interesting feature of BGGT's GMS suite is the fact that the mantle-derived components are contemporaneous to the crustal melting-derived granitoids, whereas in other areas such as the Northern Kaapvaal, the syenites or "mafic granites" tend to form a younger, very distinctive event (e.g. Laurent et al., 2014a).

Stage B.IV granites have attracted only limited attention (Meyer et al., 1994) and are poorly documented. These post-tectonic rocks are emplaced at 2.8–2.7 Ga as discrete intrusions with sharp contacts. They are made of granites s.s. (Fig. 6), belonging to two groups: a slightly

peraluminous one (associated with Sn mineralisation), and a metaluminous series. The latter group is rather similar to the ubiquitous post-tectonic potassic granites found in most cratons (Laurent et al., 2014a). The SWASA collection includes only samples from the metaluminous plutons ("high Ca" of Meyer et al., 1994).

5.4. Isotopic evolution of the BGGT

The granitoids of the BGGT have been widely studied in terms of Hf isotopes compositions (mostly by in-situ laser ablation on zircon) (Fig. 9), from which some conclusions based on the literature can be drawn (Hoffmann et al., 2016; Hoffmann and Kröner, 2018; Jele, 2015; Kröner et al., 2013, 2014, 2016; Moyen et al., 2021c; Reinhardt et al., 2015; van Schijndel et al., 2017; Zeh et al., 2009, 2011, 2013).

Most granitoids from stages B.I and B.II define a narrow range of average $\varepsilon Hf_{(t)}$ values, near-chondritic to slightly supra-chondritic. Strikingly, rocks with a clear depleted mantle signature are almost totally lacking, the exceptions being some primitive outliers from rock units (e.g. Theespruit Formation) that are more typically near-chondritic. A group of old rocks from the AGC, all older than ca. 3.5 Ga, as well as some of the lavas from the 3.51–3.53 Ga Theespruit Formation, have negative $\varepsilon Hf_{(t)}$ values around −2. Using an average crustal $^{176}Lu/^{177}Hf$ value of 0.0113, this could reflect reworking of a ca. 3.7–3.8 Ga near-chondritic protolith; or of a much older (4.0–4.1 Ga) depleted-mantle like protolith. Rare Eoarchaean or Hadean zircons were found in the BGGT (Drabon et al., 2021; Kröner et al., 1996b), attesting to the presence of a crustal component of that age.

There is some debate on the meaning of the predominantly near-chondritic compositions. One interpretation, based on the presence of rare Hadean zircons, postulates the existence of an ancient crustal reservoir. Near-chondritic signatures, in this view, could reflect either reworking of such an old, DM-like mafic component (Kröner et al., 2014; Naeraa et al., 2012; Zeh et al., 2011); or mixing between a younger (3.4–3.2 Ga) DM component assimilating, evolved felsic crust (Hoffmann and Kröner, 2018; Kröner et al., 2019). On the other hand, such an old component would be very cryptic indeed and is not directly preserved in the rock record, neither globally (Moyen and Laurent, 2018; Nägler and Kramers, 1998) nor in the BGGT, and this contrasts with the Northern Kaapvaal which, as we describe in this paper, does feature rock units with DM signatures. Thus, the alternative model is that most stage B.I and B.II rocks formed by tapping into the same reservoir, a chondritic to slightly supra-chondritic component. A similar conclusion has been inferred based on the worldwide compilation by Guitreau et al. (2012), who similarly concluded that the bulk of continental crust through time was generated from a reservoir with similar near- to slightly supra-chondritic Hf.

The difference between stage B.I and stage B.II rocks is small – it is magnified by the use of averages in Fig. 8, as the spread of individual $\varepsilon Hf_{(t)}$ values from rocks of both age groups is essentially similar, as outlined by dotted boxes in Fig. 8. (Moyen et al., 2021c; Zeh et al., 2009). Within the stage B.II rocks, the Kaap Valley Tonalite occupies the most radiogenic end of the range (average $\varepsilon Hf_{(t)}$ of ca. +2), whereas the other rocks (all other TTG3 plutons as well as the Usutu suite) have lower, slightly sub-chondritic values. These sub-chondritic values could be obtained by recycling an older crust, but barely: it would require selectively recycling the most radiogenic of the ca. 3.45 Ga rocks but none of the others.

Stage B.III rocks, in contrast, cluster around average $\varepsilon Hf_{(t)}$ values of −2, a composition best explained by reworking of the older stage B.I and B.II rocks (Moyen et al., 2021c; Zeh et al., 2009). Importantly, there is no difference between the more granitic, and the more syenitic components, with both being isotopically similar. Moyen et al. (2021c) explained that this could be the result of multiple recycling modes of the crustal component, either directly by melting of the crust, or indirectly

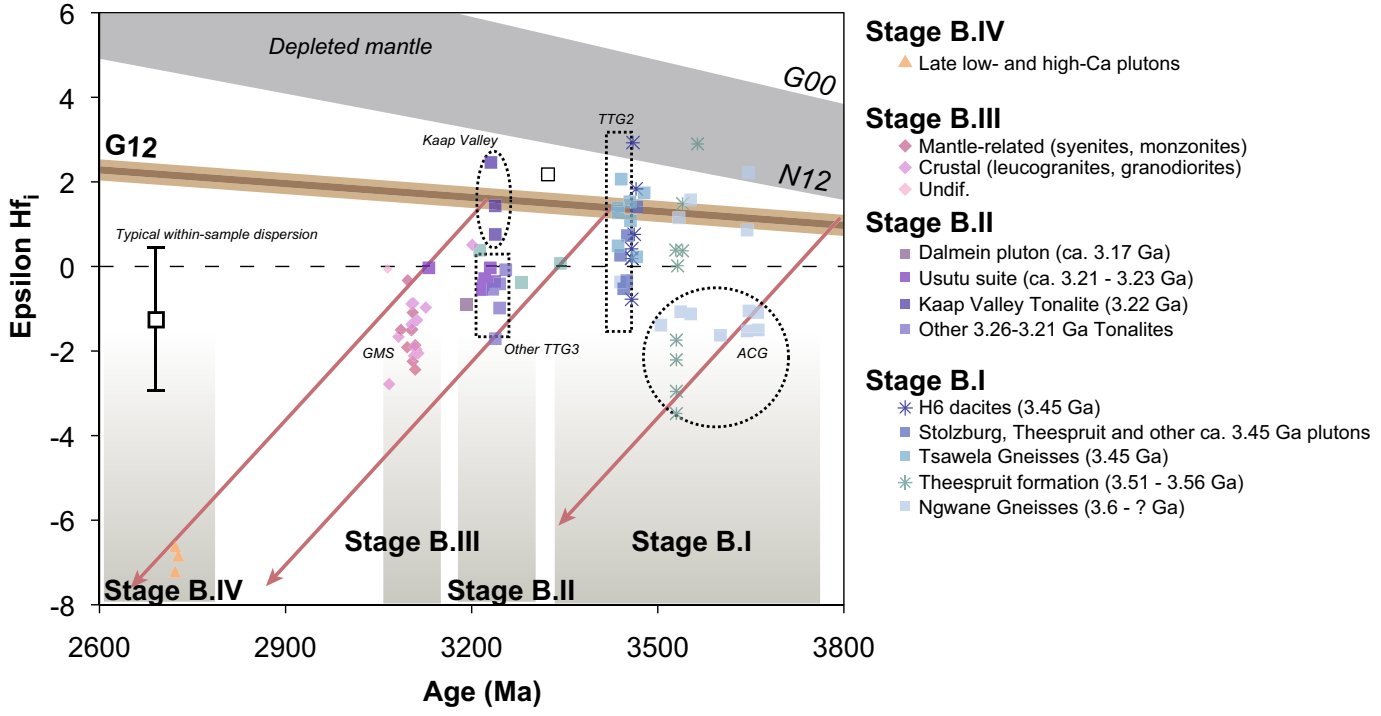

Fig. 9. Literature review of the Hf isotopic evolution of the BGGT. Each sample is only reported in terms of the average of individual analyses, recalculated at the time of emplacement; using the median instead gives indistinguishable results. Note that the relatively high within-sample dispersion may be influenced by analyses that accidentally included younger zircon domains. The depleted mantle range is bounded by curves calculated using Griffin et al. (2000) (top, G00) and Naeraa et al. (2012) (bottom, N12) values, and encompasses the range of likely DM compositions. The brown curve (G12) is the near-chondritic mantle source advocated by Guitreau et al. (2012) as the most likely source for continental crust through time. The red arrows show the evolution of a typical continental reservoir ($^{176}Lu/^{177}Hf$ = 0.113), starting on the Guitreau et al. (2012) curve at various times. Symbols as in Fig. 6. Data are from numerous sources (see text). (For interpretation of the references to colour in this figure legend, the reader is referred to the web version of this article.)

by recycling of this component into the mantle, imparting a similar, crust-like signature to enriched portions of the mantle that subsequently melted (Couzinié et al., 2017; Laurent and Zeh, 2015). The stage B.III rocks (except one sample) plot between crustal evolution lines derived from a ca. 3.2 and ca. 3.4 Ga old crustal protolith, with near-chondritic εHf at the time of formation.

Currently little is known of the origin of stage B.IV granitoids. They also plot on a crustal evolution array, extending from stage B.I/B.II, through stage B.III to stage B.IV rocks. However, this observation carries little implications on the mode of recycling – as for stage B.III, both

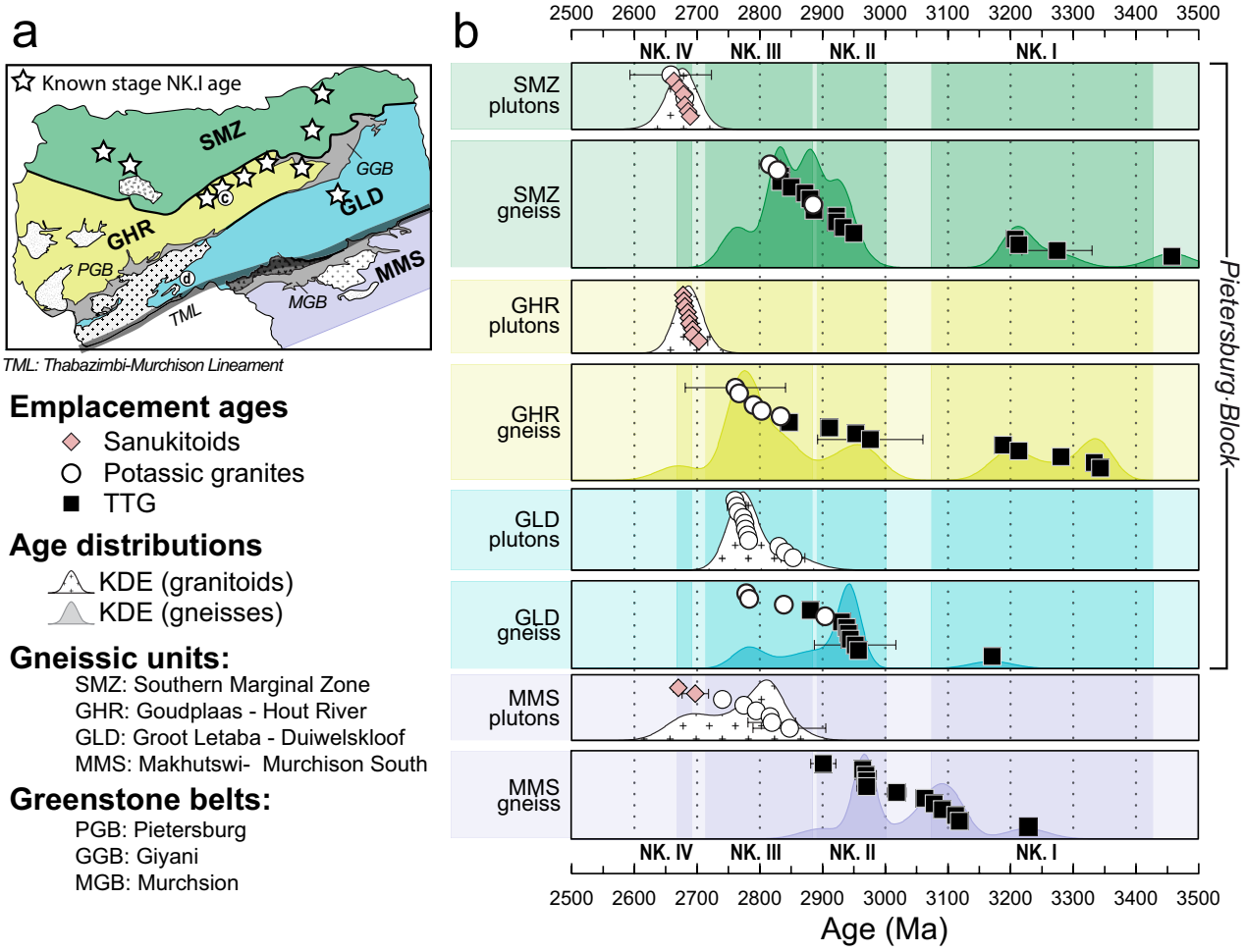

Fig. 10. Characteristics of Grey Gneisses from the Northern Kaapvaal, adapted from Laurent et al. (2019). (a) Sketch geological map indicating the delineation in 4 domains (comments in text). The Pietersburg Block corresponds to the portion North of the Thabazimbi-Murchison Lineament (TML). Stars indicate the location of (known) stage NK I rocks, mostly in the northeastern portion of the GHR domain. Locations of (c) and (d) are shown. (b). Summary of the published emplacement ages in the Northern Kaapvaal, from Laurent et al. (2019). Points indicate individual samples; density curves are constructed to better represent the age distributions. (c) and (d), two examples of Grey Gneiss outcrops from the Northern Kaapvaal, indicated in panel (a). At both localities different phases are found, and in these examples emplacement ages of different phases are known (Laurent et al., 2013; Laurent and Zeh, 2015; Laurent et al., 2019); approximate ages are shown, typical uncertainty is ±5 Ma. The stage to which they belong is indicated in roman numerals, and equivalent SWASA samples are indicated. (c) "Goudplaas" locality in the GHR domain; (d) roadcut along road R71 ca. 20 km East of Mankweng in the GLD domain.

crustal melting, or cycling through the mantle are equally plausible alternatives (Laurent and Zeh, 2015).

6. Gneisses between Barberton and Murchison

The area between the BGGT and the Northern Kaapvaal / Limpopo is poorly exposed and therefore poorly known. Very few geochemical data are available in this region, which was only briefly visited as part of the SWASA project. Accordingly, we provide only a brief summary of its geology.

The Barberton belt is flanked to the north by the Nelspruit batholith, part of the GMS suite (Robb, 1978). The Nelspruit batholith extends to the north for ca. 150 km to Bushbuckridge, in progressively more adverse outcrop conditions. Its large size as well as the better accessibility of other members of the GMS suite has so far seriously limited investigations (Robb, 1978).

North of this batholith, in the region from Bushbuckridge to the Murchison Greenstone Belt, exposure is poor and covered by deep weathering profiles, and the land is mostly used by nature reserves and game farms. Therefore, the outcrop situation as well as accessibility are problematic, and little is known of this area. The published geological maps report distinct phases within the Grey Gneisses, emplaced between 3.0 and 3.1 Ga (Poujol and Robb, 1999)(Fig. 10), as well as a couple of separately-mapped "TTG" plutons (Cunning Moor and Harmony), presumed to be ca. 3.0 Ga old, without much more information (Robb et al., 2006). A late potassic pluton, the Mashishimale Pluton, similar to the stage NK.IV ca. 2.67 Ga plutons (see below) of the North Kaapvaal offers reasonable outcrops but has not been investigated further. Small greenstone remnants are also mapped south of the Murchison Belt (for example near the locality of Mica, which derives its name from the muscovite-bearing pegmatites mined there). The situation improves around the Murchison Belt, owing to its economic interest (Sb and Au mines). Excellent 1/50000 scale maps are available (Vearncombe et al., 1992) and several studies described aspects of the local geology (Block et al., 2013; Jaguin et al., 2012a; Jaguin et al., 2012b; Kröner et al., 1996a; Poujol, 2001; Poujol and Robb, 1999; Schwarz-Schampera et al., 2010; Vearncombe et al., 1992).

7. The Northern Kaapvaal

7.1. Summary of the geological history

The "Northern Kaapvaal Craton" is a geographic term encompassing the Pietersburg Block (North of Thabazimbi-Murchison Lineament; Fig. 2) as well as the adjoining Murchison Greenstone Belt and the plutons that flank it. The bulk of the region is made of composite Grey Gneisses, in which various components (belonging to stages NK·I to NK.III as defined below) are interstratified (Fig. 10c) and span >600 MYr, sometimes over a few square meters (Fig. 10c)(Laurent et al., 2019). Based on age distribution and field features, Laurent et al. (2019) subdivided the gneisses into four domains (Fig. 10a), separated by geophysical and/or structural features.

In contrast with the Barberton Greenstone Belt, the greenstone belts of the Northern Kaapvaal are narrow, strongly deformed schist belts, often metamorphosed to upper greenschist or amphibolite grades (Block et al., 2013; de Wit et al., 1992a; de Wit et al., 1992c; Kramers et al., 2014; Vearncombe et al., 1992). The Murchison Greenstone Belt, the southernmost one, corresponds to the major Thabazimbi-Murchison Lineament, a first order craton-wide geophysical feature (Fig. 1). It is flanked to the north by a layered mafic/ultramafic complex, the coeval Rooiwater Complex (Vearncombe et al., 1992; Zeh et al., 2013). The Pietersburg and Giyani belts are aligned some 45 km to the north-northeast and define a second-order boundary between two gneiss domains. Their age is poorly known. The Rhenosterkoppies greenstone belt (Passeraub et al., 1999) is a small fragment, another 20 km north-northeast of the Pietersburg Belt. Lastly, high-grade, dismembered slivers of greenstone lithologies form the Bandelierkop Formation, mostly made of amphibolites associated with uncommon but spectacular metapelites (Kramers et al., 2006; Van Reenen et al., 2019) in the high-grade portion of the Pietersburg Block.

Late plutons, clearly intrusive and with sharp contacts with the composite gneisses occur mostly in the western part of the region (Matok, Mashashane, Moletsi, Matlala), as well as the Mashishimalle pluton south of the Murchison Belt, and they define the final stage, NK.IV, ca. 2.67 Ga ago (Laurent et al., 2013).

The northernmost portion of the Pietersburg Block experienced high-grade conditions (upper amphibolite to granulite facies), spectacularly expressed in metapelites (Stevens and van Reenen, 1992; Taylor et al., 2014; Van Reenen et al., 2019). The rest of the region experienced amphibolite facies peak conditions (Block et al., 2013; Kramers et al., 2014). This observation forms the basis of the "conventional" model, whereby the high-grade portion is regarded as a component of a larger, neoArchean (ca. 2.72 Ga) orogen (i.e. the "southern Marginal Zone" of the "Limpopo Belt") corresponding to an allochthon thrusted over the Kaapvaal continent (Van Reenen et al., 2019). However, recent geochronological findings challenge this idea, as: (i) the age and isotopic evolution of the gneisses are similar in the SMZ and south of it (Kreissig et al., 2000; Laurent et al., 2019; Vézinet et al., 2018; Zeh et al., 2009); (ii) both domains experienced a similar complex, polyphase metamorphic evolution during the same time (Kramers et al., 2014; Laurent et al., 2019; Madlakana et al., 2020). In this light, the "Southern Marginal Zone" appears as simply a deeper portion of the Pietersburg block, that underwent higher metamorphic grades in particular towards the end of its evolution (at ca. 2.72 Ga) and was subsequently exhumed against shallower portions of the same crust.

Here we adopt the geochronological framework of Laurent et al. (2019) (Table 2):

Stage NK·I: older crustal remnants (> 3.1 Ga). In the eastern portion of the Pietersburg Block, around the Giyani Greenstone Belt (Laurent et al., 2019), the protoliths of some Grey Gneisses crystallised between 3.4 and 3.2 Ga. The Giyani Greenstone Belt is very poorly known, but one of the two dated rocks (Kröner et al., 2000) is a 3.2 Ga andesite. The old (NK·I) components of the Grey Gneisses are petrologically similar to the younger trondhjemitic gneisses of stage NK.II, and typically cannot be distinguished in the field (i.e. based on outcrop mapping). In rare localities (e.g. Fig. 10c), it is possible to observe old gneisses forming large (ca. 10 m^2) enclaves in the younger components of stage NK.II. On the other hand, the distribution of the old ages is regionally consistent, as they mostly were reported from a relatively restricted, ca. 60 × 20 km region (Fig. 10a).

These ages are broadly similar to the ages of the cratonic core of the BGGT. It is therefore possible that these rocks represent fragments of the older Kaapvaal crust, heavily modified by subsequent (stages NK.II to IV) events.

Stage NK.II: the main crust-forming event (2.97–2.88 Ga). The most common ages of TTG gneisses in the Pietersburg Block are between 2.95 and 2.88 Ga (Fig. 10): this period corresponds to the formation of the bulk of the felsic crust in the area. It starts with the formation of the Murchison Greenstone Belt (Poujol, 2001; Schwarz-Schampera et al., 2010; Zeh et al., 2013), the adjacent Rooiwater Complex (Laurent and Zeh, 2015; Zeh et al., 2013), and presumably the Pietersburg Belt (Kröner et al., 2000), at 2.97–2.95 Ga. Amphibolite remnants within the Grey Gneisses also have the same age (Laurent et al., 2013).

Stage NK.III: crustal reworking (2.88–2.71 Ga). A protracted period of crustal reworking is marked by abundant anatectic features, granitic dykes and plutons. In places it overlaps with the previous stage – the earliest granitic dykes were emplaced at ca. 2.92 Ga (Vézinet et al., 2018), i.e. before the youngest tonalitic gneisses (2.88 Ga). In the high-grade portion, stage NK.III rocks are represented by in-situ melts (often associated with peritectic minerals such as garnet or cordierite), either in Grey Gneisses or in metapelites. The anatectic metapelites have been the focus of many metamorphic studies, as reviewed by Van Reenen

Table 2
Summary of the main rock units in the Northern Kaapvaal. For age references, see text as well as mentioned papers (in particular Laurent et al., 2019 for a summary).

		Pietersburg Block					
	Age (Ga)	SMZ	GHR	Pietersburg (and Giyani?) Greenstone Belts	GLD	Murchison Greenstone Belt	MMS
Stage NK IV	Ca. 2.67 Ga	Matok Pluton	Matlala, Moletsi, Mashashane plutons. Some dykes				Mashishimale Pluton
Stage NK III (2.88–2.71 Ga)	2.72–2.71 Ga	Melting features in metapelites					
	2.78–2.77 Ga	Numerous veins, dykes and small plutons	Melting features in metapelites Numerous veins, dykes and small plutons		Turfloop batholith (2.77 Ga) Plutons and dykes collectively defining the "Duiwelskloof Batholith" (ca. 2.78 Ga)		Lekkersmaak and Willie plutons
	2.85–2.77 Ga				Numerous veins, dykes and small plutons		
	2.88–2.85 Ga	Latest phases of tonalitic gneisses	Latest phases of tonalitic gneisses				
Stage NK. II	2.97–2.88 Ga	Emplacement of the precursors of most gneisses	Emplacement of the precursors of most gneisses	Eruption/ deposition of greenstone belt supracrustals	Emplacement of the precursors of most gneisses	Eruption/ deposition of greenstone belt supracrustals Rooiwater Complex	Emplacement of the precursors of most gneisses
Stage NK I	3.45–3.10 Ga	Older gneiss relicts	Older gneiss relicts	Possible old components in Giyani Belt?			

et al. (2019): melting in the pelites occurred around ca. 2.71–2.72 Ga, at ca. 850° and 9–10 kbar. Melting in the gneisses covers a larger time range, starting at ca. 2.92 Ga [(Laurent et al., 2019) and Fig. 10] and extending to ca. 2.75 Ga. No P-T constraints are available for melting of the gneisses, although the occurrence of peritectic garnet suggests similar upper amphibolite/granulite facies conditions. Further south, stage NK.III corresponds to the injection of dykes and small bodies of granites and pegmatites in the gneisses (Fig. 10). Adjacent to the Giyani Belt, these bodies become larger (kilometre-sized) and more numerous, collectively corresponding to the "Duiwelskloof batholith" (Robb et al., 2006). Finally, still further south, large (10's of km) intrusions of granite *s.s.* form the Turfloop batholith (ca. 2.77 Ga; Henderson et al., 2000) or the 2.82–2.73 Ga Lekkersmaak and Willie (composite) plutons (Poujol et al., 2021).

The depositional age of the Bandelierkop metapelites remains unclear. On one hand, Kreissig et al. (2000) have shown that they derive from a ca. 2.95–3.0 Ga protolith, i.e. stage NK.II, meaning that they could have been deposited in the basins floored by mafic rocks of a similar age. On the other hand, Nicoli et al. (2015) interpret the zircon age pattern in metapelites as reflecting a maximum deposition age of 2.73 Ga (late stage NK.III), shortly before the ca. 2.71 Ga metamorphism.

Stage NK.IV: late plutons (2.67 Ga). The final stage of evolution of the Pietersburg Block is marked by the emplacement of half a dozen of plutons over a short time interval at ca. 2.67 Ga (Laurent et al., 2013). Four of them are clustered to the west of the domain in the GHR (Matlala, Moletsi, Mashashane Plutons) and adjoining SMZ (Matok Pluton), another one occurs south of the Murchison Belt (Mashishimalle Pluton), and some related dykes are known throughout the area. These intrusions have sharp contacts with the surrounding country rocks and are well-delimited bodies. They are chemically distinctive from the proceeding magmatism, all having "hybrid" compositions, akin to the sanukitoid group (Laurent et al., 2014a; Laurent et al., 2014c).

7.2. *Mafic rocks of the Pietersburg Block*

In the Pietersburg Block, mafic rocks correspond to: (i) fragments of greenstone belts, (ii) amphibolite remnants of similar age, within the Grey Gneisses; (iii) the layered mafic to ultramafic Rooiwater complex and (iv) diorites with a sanukitoid affinity emplaced during the stage NK.IV.

Greenstone (meta)lavas and amphibolites are very similar to their Barberton counterparts (Fig. 11), perhaps slightly richer in incompatible elements, in particular fluid-mobile elements such as Th. Compared to the global Archaean array, they are slightly closer to the crust-like end-member. Strangely, these schists resemble average igneous rocks and more supracrustal rocks from the Barberton Greenstone belt (Fig. 4), probably because Northern Kaapvaal rocks did not experience the intense seafloor alteration so prominent in the Onverwacht Group.

Only a few samples from the Rooiwater Complex have been analysed, and they correspond to a layered mafic sequence: they are quite likely to be cumulates and not primary liquids, such that comparisons are difficult. Nonetheless, existing samples are strongly depleted, and do not plot within the array defined by Archaean rocks. As will be shown, they also have very radiogenic isotopic signatures, such that the depleted character may well represent a feature inherited from the primary liquids.

Finally, the sanukitoid diorites, similar to their counterparts worldwide, are very distinctive from the other mafic rocks sampled in the SWASA collection, much more enriched with arc-like compositions. This has already been noted in many places in the world, and is a distinguishing feature of these rocks (Fowler and Rollinson, 2012; Heilimo et al., 2013; Laurent et al., 2014a; Laurent et al., 2014b; Martin et al., 2005; Moyen, 2020; Shirey and Hanson, 1984).

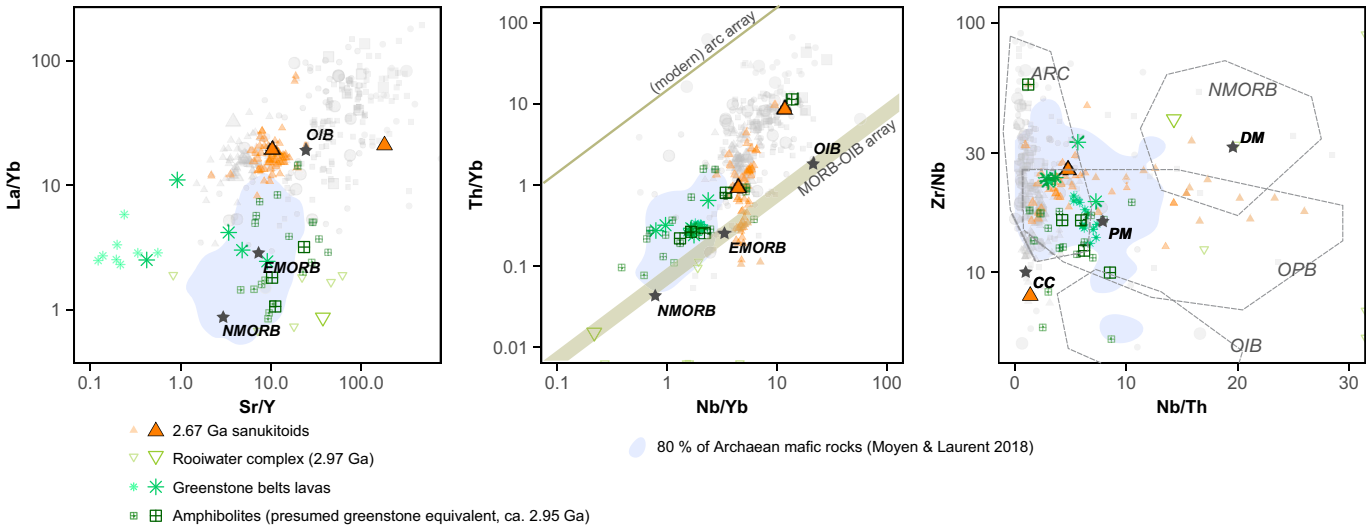

Fig. 11. Mafic rocks of the Pietersburg Block (North Kaapvaal) area. (a) La/Yb versus Sr/Y diagram (log-log). (b) Th/Yb vs. Nb/Yb diagram after Pearce (2008), showing the inferred "MORB-OIB" and "modern arc" arrays. (c) Zr/Nb vs Nb/Th diagram after Condie (2005a). SWASA samples are represented by larger symbols. Grey symbols in the background show the composition of North Kaapvaal granitoids for comparison. Light blue fields shows where 80% of the Archaean mafic rocks lie, from the global compilation of Moyen and Laurent (2018). (For interpretation of the references to colour in this figure legend, the reader is referred to the web version of this article.)

7.3. Granitoids of the Pietersburg Block

Granitoids were formed during all stages of the Pietersburg Block evolution, and we depict them using the same diagrams as we did for Barberton granitoids: the O'Connor (1965) normative feldspar triangle; the composite ternary diagrams of Laurent et al. (2014a), and Sr/Y vs. La/Yb, in log scale. Supplementary Fig. 5 shows SiO_2 – Na_2O/CaO and SiO_2 – Sr diagrams and Supplementary Fig. 6 summarises the shape of the REE patterns, using the lambda-parameters of O'Neill (2016). We use similar colour coding as for Barberton samples.

In the field, stage NK.I and NK.II gneisses are intimately associated and often it is not possible to associate a given rock to a period (unless they have specifically been dated, which by necessity applies to only a small fraction of the dataset). Since few systematic differences in composition appear between the two stages, we describe them together here. We therefore report stage NK·I and NK.II together as "Initial accretion 3.4-3-2.88 Ga" in Figs. 12 to 14.

Gneisses from **stages NK·I and NK.II** are mostly TTG, trondhjemites more commonly than tonalites (Fig. 12), and they show mostly high Sr and Sr/Y as well as high La/Yb values, similar to the high pressure type of Moyen (2011) (Fig. 14; Supplementary Fig. 5 and Supplementary Fig. 6).

Stage NK.III (2.87–2.71 Ga) is the dominant event and is represented by features ranging in size from small leucosomes, veins or dykelets, to small plutons, to large (10s of km) batholiths. They are plotted with different symbols on Figs. 12–14, although their compositions largely overlap in these diagrams.

The large plutons are more granitic and the leucosomes are generally trondhjemitic, in chemical terms. This reflects the facts that the leucosomes are dominated by plagioclase+quartz (± garnet, cordierite, orthopyroxene) assemblages and generally lack K-feldspar and biotite. Such rocks are unlikely to correspond to chilled melts, and are best interpreted as early accumulations of plagioclase (possibly peritectic) in former melt sites (Madlakana and Stevens, 2018; Nicoli et al., 2017; Taylor et al., 2014). It is therefore slightly misleading to compare their composition with that of genuine igneous compositions. Collectively,

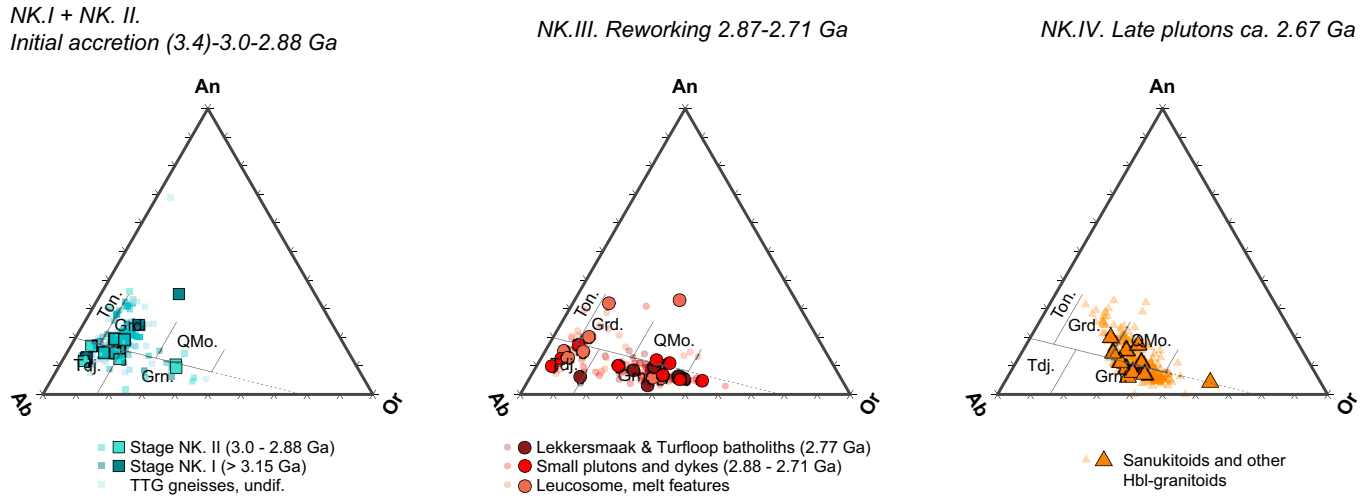

Fig. 12. O'Connor (1965) feldspar-normative diagrams for granitoids of the Northern Kaapvaal region. Ton.: tonalite; Tdj.: trondhjemite; Grn.: granite; Grd.: granodiorite; QMo.: quartz-monzonite. This figure (and the following) are constructed as the Barberton ones, Figs. 6 to 8, with SWASA samples as larger dots with black outlines, literature samples as smaller and paler dots.

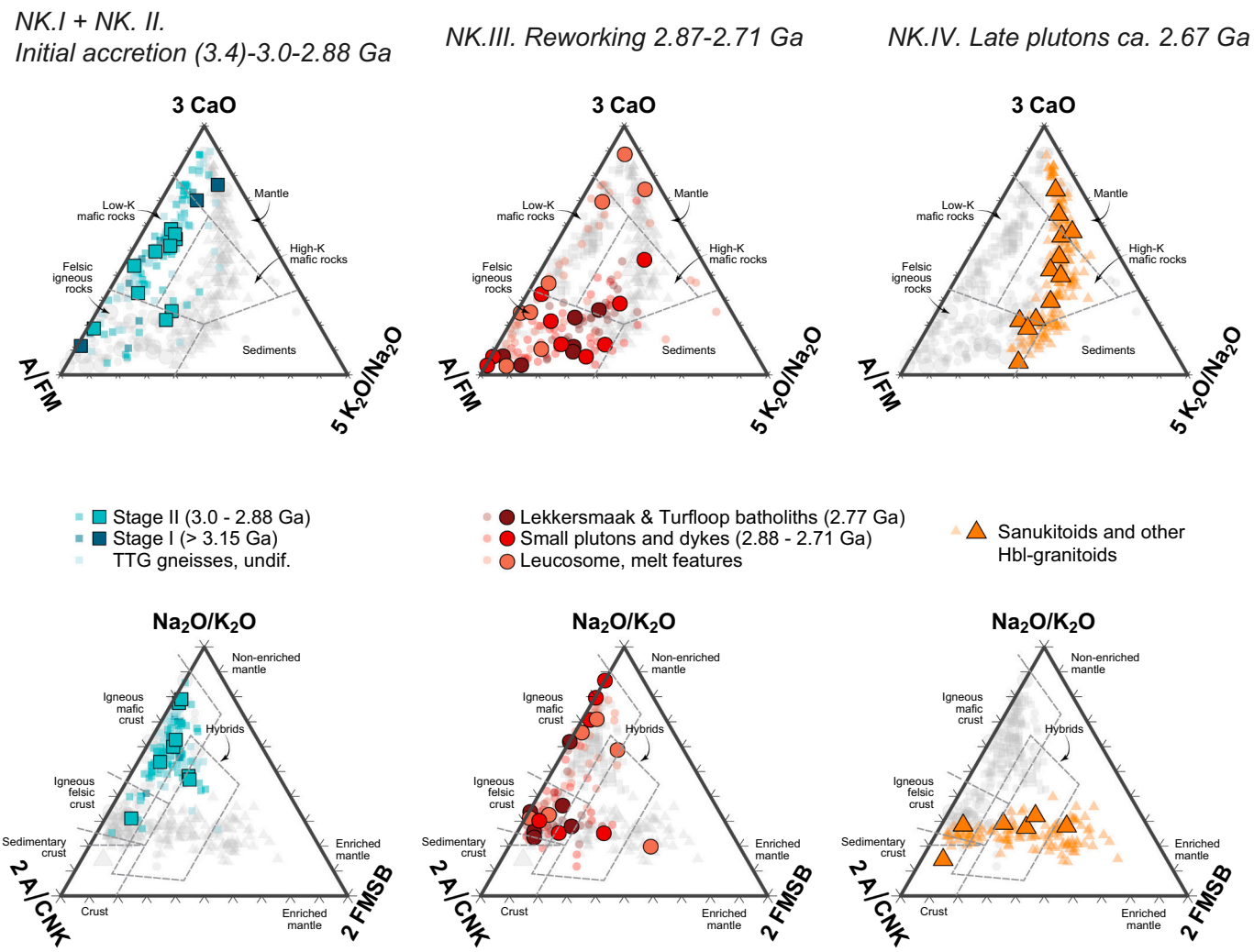

Fig. 13. Summary ternary diagrams of Laurent et al. (2014) for Northern Kaapvaal granitoids. A/FM = Al2O3/(FeOt+MgO); A/CNK = molecular Al/(2Ca + Na + K); FMSB = (FeOt+MgO) × (Sr + Ba). Grey dots in the background show the full dataset, coloured dots correspond to individual age bands.

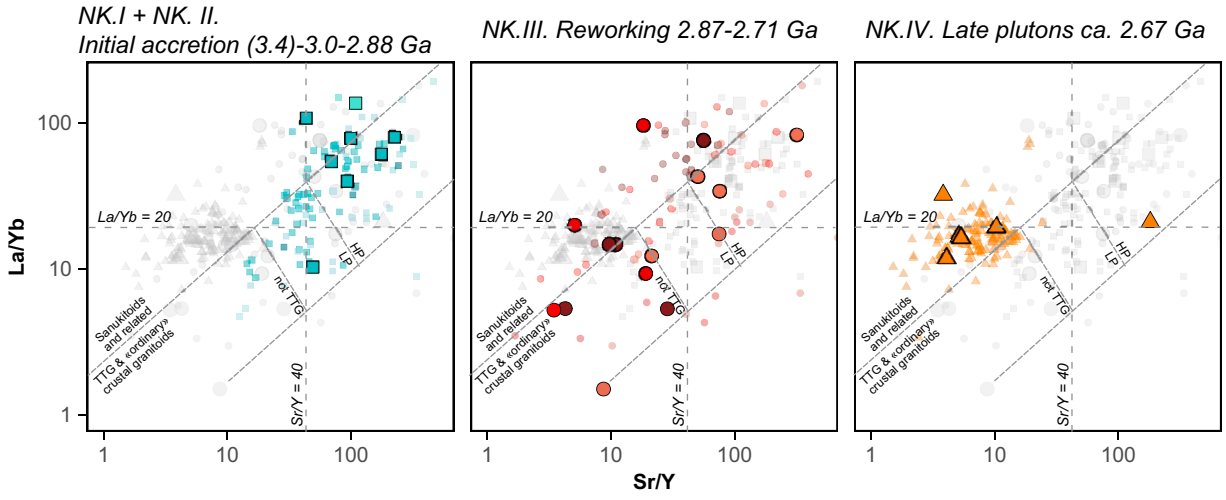

Fig. 14. Sr/Y vs. La/Yb diagram for Northern Kaapvaal granitoids. See comment in Fig. 6 for the construction of the diagram. Caption as Figs. 12–13.

the composite Northern Kaapvaal (NK·I + NK.II + NK.III) samples cover the range from (uncommon) tonalites, to trondhjemites, to granodiorites, representing the full range of the popular TTG acronym – but also illustrating that the Grey Gneiss unit of the Northern Kaapvaal is really a composite of several different rock types, in this case several trondhjemitic (± tonalitic) igneous units interstratified with granodioritic (± trondhjemitic and granitic) leucosomes and small melt pockets. It would, therefore, be unwise to try to draw global conclusions from the chemical composition of the evolution of the continental crust based on Grey Gneisses without further qualification or separation of individual components.

In contrast with leucosomes and small veins, larger features (plutons proper) are granitic to granodioritic, weakly deformed and clearly intrusive into the older, composite gneisses. At the time of their emplacement, the deeper crust further north was undergoing partial melting and/or injection of small granitic (s.l.) components (Fig. 10b). Consistent with this observation, the compositions of the plutons are best explained by partial melting of an already felsic crust (Fig. 13), as has indeed long been established (de Wit et al., 1992a; Henderson et al., 2000; Laurent et al., 2014a). In some details, it is possible to identify plutons sourced from specific components of the crust, for instance the peraluminous plutons of the Lekkersmaak suite, south of the Murchison belt, appear to be S-type, related to melting of a metasedimentary component (Poujol et al., 2021).

The **NK.IV plutons** (2. 67 Ga; Figs. 12–14) were previously studied by Laurent et al. (2014c), who described them as "hybrids", with petrogenetic processes akin to the sanukitoid family (Fig. 13). All appear to be related to an enriched, potassic dioritic component, sourced in a mantle metasomatised by crustal material.

7.4. Isotopic evolution of the Northern Kaapvaal

The Hf isotopic evolution of the Northern Kaapvaal largely reflects the geological and petrological history (Fig. 15). **Stage NK·I** rocks are near-chondritic, similar to their Barberton counterparts of stages B.I and B.II; here, too, a proper depleted mantle component is lacking.

In contrast, **stage NK.II** is marked by a sudden influx of a juvenile, depleted-mantle like component – a situation strikingly different to that observed in Barberton, where the bulk of TTG samples plotted below the Guitreau et al. (2012) line. This radiogenic excursion is even more remarkable when taking into account the Rooiwater layered mafic Complex, one of the rare rock units in the Kaapvaal craton (other exceptions would be represented by some komatiites in the S.E. part of the craton) that plots squarely into the field of depleted mantle. In the Makoppa dome, a probable Western extension of the North Kaapvaal, the Vaalpenskraal trondhjemite (3.01–3.03 Ga) also carries the same depleted mantle signature (average ε_{Hf} of +4 to +5) (Elburg and Poujol, 2020).

The compositions of **stage NK.III** rocks are broadly consistent with reworking of this radiogenic, ca. 2.95 Ga crust. However, as noted by Laurent and Zeh (2015), their ε_{Hf} compositions (ca. 0 to −1) imply an evolution line with $^{176}Lu/^{177}Hf$ values of only ca. 0.0022, significantly lower than the average continental crust (0.0113) or of a mafic crust (0.022). Such a slope, in Laurent and Zeh (2015)'s interpretation, reflect

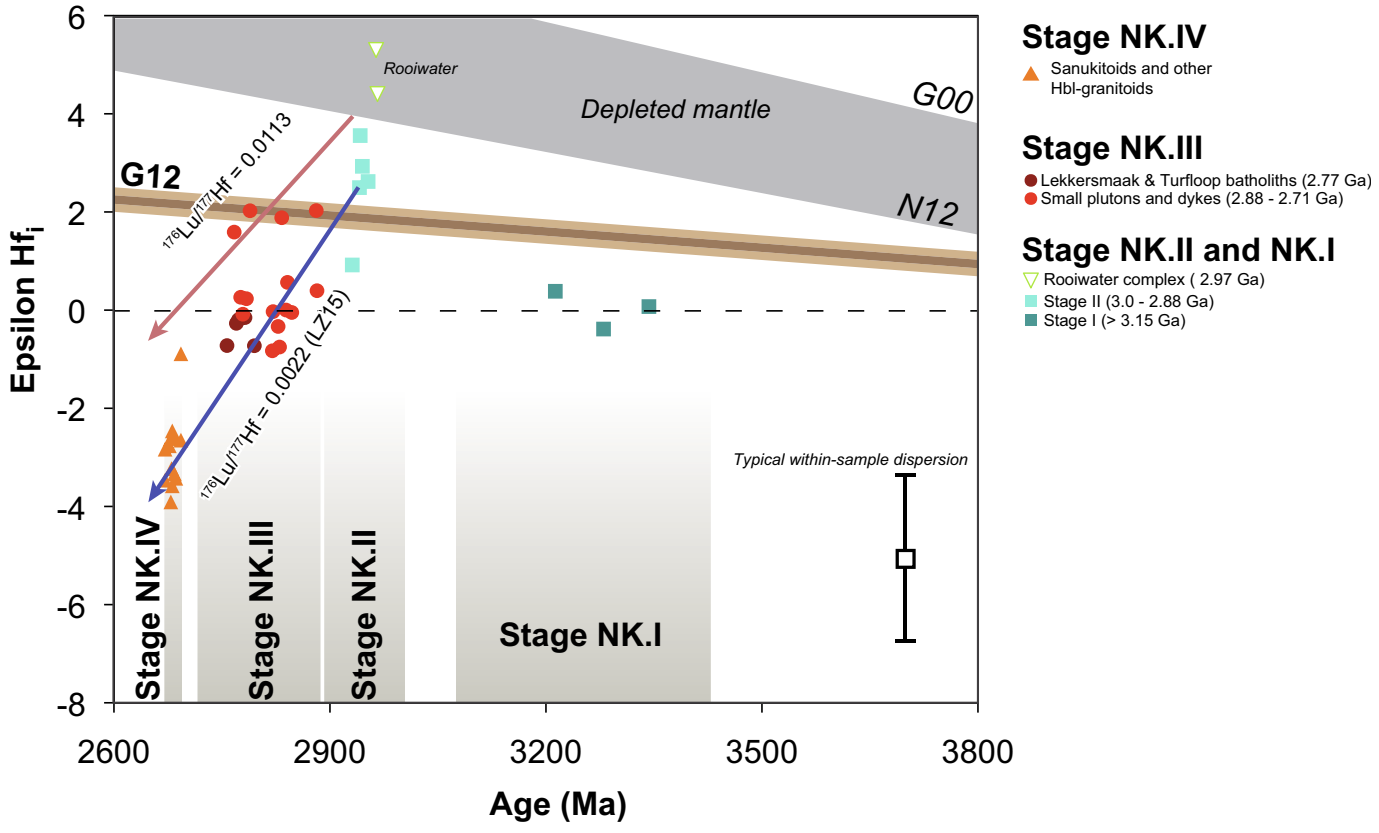

Fig. 15. Literature review of the Hf isotopic evolution in the Northern Kaapvaal. Each sample is only reported in terms of the average of individual analyses, recalculated to the time of emplacement. The depleted mantle range is bounded by curves calculated using Griffin et al. (2000) (top, G00) and Naeraa et al. (2012) (bottom, N12) values, and encompass the range of likely DM compositions. The brown curve (G12) is the near-chondritic mantle source advocated by Guitreau et al. (2012) as the most likely source for continental crust through time. The red arrows show the evolution of a typical continental reservoir ($^{176}Lu/^{177}Hf$ = 0.113), starting on the DM curve at the time of emplacement of Rooiwater complex. The blue arrow, from Laurent and Zeh (2015), shows evolution from stage NK.II compositions with $^{176}Lu/^{177}Hf$ = 0.0022, which they interpret as lack of retention of zircon in the source. Together these curves bracket stage NK.III and NK.IV rocks. Symbols as in Fig. 11. Data from (Vézinet et al., 2018; Zeh et al., 2009). (For interpretation of the references to colour in this figure legend, the reader is referred to the web version of this article.)

almost total zircon dissolution and in this context it is noticeable that the most radiogenic samples of stage NK.III come from the Goudplaas – Hout River domain, i.e. they are neither granulite-facies leucosomes, nor large granites (that may be the mid/upper crustal expression of granulite facies melting deeper), but probably low degrees of melting occurring near the melting front in the upper amphibolite-facies middle crust.

Lastly, **stage NK.IV** samples are interpreted as carrying a crustal signature (Laurent and Zeh, 2015), and similar to the GMS syenites previously discussed, they inherited this composition from crustal reworking of the older batches of magmatism in the region.

8. Discussion

8.1. Crustal development in the (eastern) Kaapvaal craton

Combining the information presented above, we summarise the evolution of the study area. In light of the controversies surrounding "plate tectonics" in the Archaean, cluttered by semantic issues (Chelle-Michou et al., 2022; Hawkesworth et al., 2020; Moyen et al., 2021b), we stay clear as much as possible from geodynamic inferences, and try to simply focus on processes occurring at the crustal scale – the scale we can directly observe. Table 3 lists the number of SWASA samples relevant for each stage.

8.1.1. Before 3.5 Ga: earliest crustal fragments (pre B.I)

The presence of rare zircons (Drabon et al., 2021) and crustal fragments attest the presence of some felsic crust from before 3.5 Ga in the Kaapvaal craton. Apart from its presence, little is known of this early crust, including its nature, or its extent.

8.1.2. 3.5–3.2 Ga: formation of a cratonic nucleus (B.I, B.II, NK.I)

The BGGT presents a good record of the processes that occurred during the formation of an early cratonic nucleus. The process was long-lived (300 MYr) and is still surrounded by many controversies, despite the fact that the BGGT is one of the few places in the world where the events relating to the original crustal accretion have not been over-printed by younger events. Several lines of evidence have been used to unravel this complex history: petrology and geochemistry, on which we commented in this paper; sedimentology, as we have a rich record in the Barberton Belt of the various stages of evolution (e.g. Byerly et al., 2018, for an up-to-date summary); metamorphism (Stevens and Moyen, 2007); structures and tectonics, which are a very contentious, and not fully resolved issue (Schmitz and Heubeck, 2021 for a review of the evidence and models).

At ca. 3.45 Ga – the oldest event we can confidently describe – TTG plutons were emplaced in a thick mafic pile, probably mostly or fully submarine (an oceanic plateau?). How much of the present-day strain that we observe in these rocks relates to their emplacement, as opposed to younger (ca. 3.2 Ga) events is still unclear, and of course it is hard to comment on the possible tectonic conditions.

This situation is in stark contrast with the evolution at ca. 3.2 Ga. At this time, the sedimentary basin was receiving clastic components eroded from a nearby (and felsic) continent (Heubeck and Lowe, 1999; Toulkeridis et al., 1999), suggesting at least some exhumation and topography. Slices of sediments were imbricated as they were deposited (Drabon and Lowe, 2021), and coherent units of rocks were buried to amphibolite-facies conditions and exhumed in short-lived P-T loops (Diener et al., 2005; Dziggel et al., 2002; Mühlberg et al., 2021). Irrespective of the actual model preferred for this period, it is clear that the crustal accretion at ca. 3.2 Ga occurred in a much more dynamic setting, with regional deformation – the relative importance of far field strain and gravitational instabilities still remains to be decided (Schmitz and Heubeck, 2021).

These processes collectively resulted in the formation of a proto-continent, covering most of the present-day Swaziland and Witwatersrand blocks (Poujol et al., 2003). In the Northern Kaapvaal (Pietersburg block), we only have dismembered fragments of rocks of this age. Their composition does not require a different formation process, but it is not clear whether this region was already juxtaposed to the cratonic core, of represents an exotic terrane accreted at a later stage.

8.1.3. Ca. 3.1 Ga: craton stabilisation (B.III)

The period of protocrust formation culminated in a phase of cratonic stabilisation that likely affected the whole lithosphere, and conferred it a stable and stiff nature. This seemed to occur in a rather limited period of time at ca. 3.1 based on the observation that ca. 3.1 Ga ages are found throughout the craton (Poujol et al., 2003). Moreover, this also appears to be the period during which the sub-continental lithospheric mantle also stabilized. Brey and Shu (2018) noted that only 3% of the Re-depletion model ages in Kaapvaal peridotites are older than 3.1 Ga.

Moyen et al. (2021c) speculated that what rendered this period possible was the progressive stabilisation of recycling systems from the crust to the mantle [regardless of their actual nature, subduction or not: Chelle-Michou et al., 2022], and specifically the priming of the upper mantle and the crust by adding fertile components into them it. This in turn allowed pervasive melting of the upper lithospheric mantle and crust, and the formation of large volumes of granitoids. Consequently, the lower reaches of the lithosphere were depleted (or perhaps further depleted), the heat-producing elements carried near the surface, and the resulting structure was stiff, cold and durable – it formed a continent, on top of which intra-cratonic sequences were deposited almost immediately [Pongola Supergroup and Dominion Group; Marsh, 2006; McCarthy, 2006; Paprika et al. (2021)].

The lithosphere of the Swaziland and Witwatersrand blocks was not significantly modified after this period. It was intruded and heated by intrusions and covered by (intra-cratonic) sediments, but did not undergo any further pervasive deformation, melting or dynamic metamorphism. In contrast, in the Pietersburg block (where ca. 3.1 Ga ages are almost entirely lacking), the subsequent period from 3.0 to 2.7 Ga was a period of intense activity. It appears that the northern portion of the Kaapvaal craton escaped cratonisation, and was subsequently continuously deformed against the rigid buttress of the cratonic core.

8.1.4. 3.0–2.7 Ga: long-lived reworking of the northern margin (NK.II and NK.III)

In the Northern Kaapvaal (Pietersburg block), i.e. outside of the main cratonic core, which by then had been stabilized and underlain by a stiff lithosphere, the crust was still undergoing active deformation and modification. Two processes seem to have operated, broadly in

Table 3
Distribution of the samples from the SWASA collection amongst the major magmatic stages observed in the Kaapvaal Craton.

	Stage	Regime	Granitoid samples (n =)	Mafic samples (n =)
Barberton	B.I (3.6–3.3 Ga)	Chondritic TTG crust	13	15
	B.II (3.3–3.2 Ga)	Chondritic TTG crust	7	4
	B.III (ca. 3.1 Ga)	Recycling	9	–
	B.IV (ca. 2.7 Ga)	Recycling	3	–
Northern Kaapvaal	NK.I (> 3.1 Ga)	Chondritic TTG crust	3	–
	NK.II (2.97–2.88 Ga)	Rifting and tapping into DM reservoir	6	13
	NK.III (2.88–2.71 Ga)	Recycling (mostly intra-crustal)	24	–
	NK.IV (ca. 2.67 Ga)	Recycling (mostly via the mantle)	14	–

succession.

At ca. 2.95 (and until perhaps 2.88) Ga, fracturing of the crust resulted in the formation of greenstone belt basins, dominated by mafic rocks; intrusion of layered mafic intrusions; and formation of TTG components, with a more radiogenic Hf isotopic signatures than any of the older components described above. This depleted reservoir had previously rarely been melted (or only in small volumes which are not preserved in the current rock record), or it did not exist. It is tempting to envision this process as rifting at the edges of the craton, similar to what has been suggested in the Abitibi Province (Harris and Bédard, 2015) or Eastern Goldfields of the Yilgarn Craton (Czarnota et al., 2010; Mole et al., 2014). How TTGs are formed under these conditions, however, remains to be elucidated – the vast majority of current models for the formation of TTGs require, in some form, the burial (rather than exhumation) of material from the surface into the lower crust/mantle and the role of a recycled surface component seems to be one of the most consistent features of TTG chemistry (Hoffmann et al., 2019; Lewis et al., 2021). Alternately, this time may represent the accretion of an exotic Pietersburg Block against the central Kaapvaal Craton.

This phase overlaps with, and transitions into a phase dominated by long-lived (ca. 200 MYr) crustal reworking, likely in a transpressive context (Moyen et al., 2021a). There is a striking analogy with other Precambrian mobile belts, in which long-lived, syn-tectonic melting is also a feature (Chardon et al., 2009; Gapais et al., 2005; Zibra, 2020). We suggest that this evolution occurred after the closure of the rift basins (now greenstone belts), and we note the similarity with the model proposed in the Superior Province by Harris and Bédard (2015).

Although we lack a clear record for a cratonising event, such as observed with the GMS suite (and correlatives) further south, by ca. 2.7 Ga the Northern Kaapvaal crust was stable enough to accommodate large sedimentary basins [the Transvaal Supergroup; Eriksson et al., 2006] as well as brittle enough to be intruded by numerous mafic dykes (Klausen et al., 2010) and granitic plutons. One has to conclude, therefore, that the dominantly intra-crustal reworking process we describe here was sufficient to induce cratonisation. On the other hand, this area remained a "weak" portion of the Southern African lithosphere, and was for instance affected by the ca. 2.1 Ga event of the "Central Zone" of the Limpopo Belt (Schaller et al., 1999; Zeh et al., 2007).

8.1.5. Post-2.7 Ga: local granitic activity (NK.IV, B.IV)

Late and localised granitic activity occurred throughout the craton.

In the Northern Kaapvaal, this activity corresponds to the emplacement of "sanukitoid" and "hybrid" plutons, shortly (40 MYr) after the youngest of the reworking events, and as such may well represent the waning stages of the cratonisation process – that, if correct, would indeed have affected the lithospheric mantle as well.

Further south in eSwatini, a group of plutons showing variable chemistry were emplaced over a ca. 150 MYr period (Meyer et al., 1994). Combined with the isotopic evidence, perhaps the simplest explanation is that they correspond to brief, localised heating events of the by-then mostly stable lithosphere. Granulite-facies metamorphism is recorded at 2.73 Ga in eSwatini (Taylor et al., 2010), and could be a lower-crustal expression of the same, or similar event. In itself, this process is unknown from the modern Earth: granites seldom emplace away from a tectonic zone [except perhaps A-types, which these rocks are not; Meyer et al., 1994], and certainly not repeatedly over 150 MYr. The most straightforward explanation for this magmatism would be to link it to large igneous province events heating the lower crust – there are, after all, several large basaltic units emplacing as dykes or lava flows in the neoArchaean, such as the Ventersdorp Supergroup, at 2.79–2.73 Ga (Van der Westhuizen et al., 2006).

8.2. Changing regimes of crustal development

An interesting implication of this study is that the Kaapvaal crust (and, most likely, the crust of other cratons) developed under three or four distinct regimes, that are recorded in the major and trace element compositions as well as isotopic characteristics of the igneous rocks. The core value of the SWASA data set is that it provides a reference point to further investigate and validate the characteristics of each of these regimes.

8.2.1. Initial crustal accretion: near-chondritic TTG magmatism

The first style of crustal development corresponds to stages B.I and B.II of the BGGT. During this period of time, felsic crust is formed through the emplacement of a wide range of TTG rocks s.l. The fact that several types of TTGs can be identified, in addition to clasts of more potassic igneous rocks in 3.2 Ga conglomerates (Agangi et al., 2018; Sanchez-Garrido et al., 2011), suggests that a range of petrological mechanisms were operating simultaneously. The scattered remnants of stage NK.I could represent the same regime.

This mode of operation seems to be rather widespread in the early stages of the life of cratons. Dey (2013) or Laurent et al. (2014a) similarly show that in most part of the world, the early history of cratons is marked by TTGs with a slightly supra-chondritic Hf (or Nd) isotopic signature, for instance in the Eastern Dharwar craton, India or the Superior craton, North America.

The meaning of this consistently near-chondritic signature is still unclear. Three main lines of thought, not necessarily exclusive, coexist: (i) melting of an old (Hadean?), DM-like mafic crust, not further preserved, and coincidentally having an age such that it evolved to near-chondritic at the time of melting (Naeraa et al., 2012; Zeh et al., 2011); (ii) melting of younger mafic rocks (formed shortly before emplacement of the felsic rocks), with a DM signature, assimilating cryptic fragments of an older felsic crust (Bauer et al., 2017; Hoffmann and Kröner, 2018); (iii) melting of mafic rocks with a chondritic composition (Guitreau et al., 2012; Moyen and Laurent, 2018; Nägler and Kramers, 1998). Of course, the implications of the three models are wide-ranging in terms of tectonic scenarios and crustal growth curves.

8.2.2. Rifting of existing lithosphere and tapping into depleted mantle

Stage NK.II reflects a very different situation. TTGs are formed during this period, together with greenstone belts and a layered mafic complex. In contrast to the previous regime however, a depleted mantle source is clearly involved.

In the global literature, a few other examples of this situation are found. One example appears to be in the North China craton (East block), as compiled by Dey (2013). Portions of the Yilgarn craton (the Kurnalpi terrane: Champion and Cassidy, 2007; Czarnota et al., 2010; Mole et al., 2014) also show comparable features. In the Yilgarn at least, the similarities with the Northern Kaapvaal craton go further, as the region affected by this process seems to correspond to a domain of rifting and fracturing of the continent, and formation of greenstone belts.

8.2.3. Multiple ways of reworking existing lithosphere

Stages B.III, B.IV, NK.III and NK.IV reflect a third situation, one that has long been identified as occurring at the end of the life cycle of most cratons (Cawood et al., 2013, 2018; Laurent et al., 2014a). It is dominated by reworking of the existing continental crust and the formation of granites s.s., either by direct melting of the crust, or by a cycle of mantle enrichment and melting leading to the formation of sanukitoids (and related) rocks (Moyen et al., 2021c).

The balance between the two processes seems to vary in time and space: intra-crustal reworking dominates stage NK.III (and probably B.IV), stage B.III (the GMS suite) includes both, and stage NK.IV comprises mostly mantle-cycled components (Laurent et al., 2014a, 2019).

More generally, this period of recycling is well known from almost all cratons, where it can be shorter or longer. This phase typically lasts <100 MYr after the formation of the early TTG crust (Champion and Cassidy, 2007; Czarnota et al., 2010; Dey, 2013; Laurent et al., 2013), but is much longer, close to 400–500 MYr, in the Pilbara (Champion and Smithies, 2007). Likewise, the balance of intra-crustal reworking versus

mantle recycling varies depending on location.

8.2.4. Global vs. local evolutions

The three regimes we described above are known in most cratons, but it is important to note that they do not correspond to a global, linear evolution. For instance, although the Pilbara craton of Australia is broadly coeval with the BGGT, both areas were evolving under different regimes between 3.3 and 3.2 Ga (stage B.II). In the Pilbara, isotopic data reveal that the majority of granitoids formed by repeated intra-crustal reworking of the early emplaced components (Smithies et al., 2003). Concurrently, the Pilbara granitoids evolved to be more and more "evolved", rich in LILE (including K) – the "enriched TTGs" of e.g. Champion and Smithies (2007). In contrast, the BGGT at the same time was witnessing chiefly the accretion of a near-chondritic TTG crust. Likewise, rifting and depleted mantle contribution is observed in the Yilgarn (Czarnota et al., 2010) at a time where the Northern Kaapvaal witnessed mostly intra-crustal reworking. In much the same way as in the modern Earth, where different tectonic regimes (subduction, collision, rifting etc.) operate concurrently in different parts of the planet, tectonic (and crust formation) regimes of the Archaean Earth reflect a diversity of sites, whatever they were.

8.3. Geochemistry and geodynamics

One of the most discussed question of Archaean geology is the tectonic regime that was operating at the time, and ultimately, constraining it is a key goal of most Archaean studies. In this paper, we avoid, as much as we can, discussions in terms of plate tectonics. The composition of any igneous rock is the combination of the nature (and composition) of its source; the conditions of melting (pressure, temperature, fluid regime…); and any subsequent evolution (fractionation, assimilation, mixing, etc). Thus, the link between geodynamic and geochemistry is elusive, for the following reasons: (i) the link between rock composition and geodynamic sites is indirect at best. It results either from geometric considerations (e.g. melting of surface lithologies at depths >50 km implies that they have been buried, and this is reminiscent of a subduction process), or from comparison (e.g. the rocks in consideration resemble what can be found in modern volcanic arcs). (ii) plate tectonics, or any other possible alternative planetary tectonic regime, the diversity of which can be seen from the situation of terrestrial planets (Lenardic, 2018a, 2018b), affects the whole of the upper mantle (and perhaps more). In contrast, observation from igneous rocks reflect processes that happen mostly in the first 100 km of the Earth, and commonly shallower, and thus can give only a very partial image of any geodynamic regime.

This last observation, on the other hand, allows to realise that the study of igneous rocks do carry valuable information – they inform on the thermal state and, to some degree, the geometry of the crust (to uppermost mantle) system. This is of course not enough to fully qualify a geodynamic site (see for instance Fig. 13 of Moyen and Laurent, 2018), let alone the operation mode of a whole planet. But it does provide very valuable constrains, as long as they are not over-interpreted.

Of course, our (geological) experience is limited to one planet, and it is hard to totally avoid analogies. Although the following discussion tries to stay clear of modern simile as much as possible, it is hard to avoid using modern terms ("orogenic", etc.), as they are the easiest way to picture the state of a portion of the crust.

8.3.1. The initial accretion stages

From a felsic point of view, the initial accretion stages involve primarily TTG magmatism, itself the product of melting of mafic rocks at depth. Although the depth of melting is a matter of debate amongst petrologists (e.g. Hoffmann et al., 2019; Laurent et al., 2020), the need to bury material that once was at the surface becomes more and more clear (Lewis et al., 2021). Historically, the deep melting argument was taken as a major argument in favour of subduction-like processes; and conversely, demonstrating shallower melting was taken as forbidding subduction. In retrospect, both lines are not particularly strong. Many processes can result in the burial of mafic rocks even to mantle depth, not all of which are due to subduction (Chelle-Michou et al., 2022). Conversely, the generation of granitoids in modern continental arcs, above undisputable subductions zones, may well happen within the overlying crust (Collins et al., 2020), i.e. at "shallow" depths in terms of the TTG debate.

In the Kaapvaal craton, rocks from stage NK.I mostly occur as disrupted fragments and little else can be said. Stage B.I is dominated by basaltic and komatiitic rocks (in the BGB), implying significant amounts of mantle melting; but by the emplacement of the protolith of TTG gneisses in Swaziland. Assuming the two areas were not totally disconnected at that time, the coexistence of both types of magmatism, one clearly associated to the upwelling (and melting) of mantle and one with downwelling of surface lithologies, is perhaps more reminiscent of settings such as delamination, or local burial of a thick basaltic plateau (Bédard, 2013; Sizova et al., 2015). Stage B.II, in contrast, is associated with important shortening (Schmitz and Heubeck, 2021; Travers et al., 2023; van Rensburg et al., 2023), burial of coherent, relatively cold crustal fragments of tens of kilometers (Diener et al., 2005; Mühlberg et al., 2021), felsic lavas and clastic sediments with syn-depositional tectonic imbrication (Drabon and Lowe, 2021). This leads to infer some sort of "orogenic" setting, although one should immediately emphasise that this term may reflect a large range of situations, many of which are *not* akin to modern collision belts (Cagnard et al., 2006; Chardon et al., 2009). A "hot orogen" is an attractive option, permitting significant convergence and shortening but also accounting for the lack of HP/UHP metamorphism, thrust zones, etc.

8.3.2. The rifting stage

The NK.II rifting stage associates the formation of narrow greenstone belts (maybe rift basins?) splitting the pre-existing crust, clear tapping into a DM reservoir, and some TTG magmatism. Here too, the associated strain patterns have mostly been lost. A system permitting the succession, over a short period, of phases of stretching (formation of rift basins) and contraction (burial of the source of TTGs) is required. The opening and collapse of narrow basins can be a feature of a variety of tectonic environments, for example active margins (with back ac basins opening and closing), accretionary orogens, or even failed and inverted rifts (Bédard and Harris, 2014; Harris and Bédard, 2015). The common denominator of these settings is the deformation and horizontal displacement of a preexisting continental fragment.

8.3.3. Recycling stages

The long-lived, mostly intracrustal reworking of stage NK.III is associated with mostly vertical foliations and horizontal lineations (Pieterburg 2328 and Tzaneen 2330 mapsheets; Moyen et al., 2021a), with the lineation steepening close to greenstone belts (Jaguin et al., 2012a). A similar situation has been described in detail in the Yilgarn craton of Western Australia (Zibra, 2020), or in the Eastern Dharwar craton of India (Chardon and Jayananda, 2008; Chardon et al., 2008). The most likely interpretation here is, again, that of a "hot" orogen in which shortening affected a hot crust, that was unable to thicken but instead flowed laterally (Chardon et al., 2009; Gapais et al., 2005).

Little is known on the tectonic setting of stage B.III. Rare structural studies (Belcher and Kisters, 2006a) demonstrated the association of the GMS batholiths of the BGGT with vertical, transcurrent shear zones. This is in itself rather inconclusive, but not inconsistent with a similar hot orogen scenario.

Recycling involving the mantle occurred during stages B.IV and NK.IV, and was not associated with tectonic activity (beyond local readjustment around the raising plutons). Of course, in itself the presence of recycling of crustal material through the mantle requires some sort of burial, but little more can be said on its size, shape, direction and so on.

8.3.4. Archaean tectonic styles: from local to global?

From the above discussion, it seems evident that there is no unique Archaean tectonic environment. This is of course not a surprise – a chief feature of modern Earth is the range of geodynamic sites existing and operating concurrently, and it is logical to reach a similar conclusion for the Archaean Earth.

One consistent feature, perhaps, emerging from the discussion above is the deformation of a soft crust, involving some degree of horizontal motion of more or less coherent volumes of rock, and some degree of burial of surface rocks; but also large components of distributed deformation of this crust, and also some gravitational reorganisation, via the exhumation of light, partially molten (or heavily injected by granitoids) portions of the crust.

Jumping from the geometry of a given region during a geological stage, to a planet-wide conclusion, is however a daunting task. Most of what we described above could be just as easily be reconciled with processes similar to those occurring at plate boundaries (operating in a perhaps slightly warmer Earth); or, conversely, with the total lack of strain localisation and distributed deformation across the lithosphere, i.e. no plates; or a combination of both (a mostly "soft" lithosphere, with some rigid fragments indenting it). Interestingly, the community seems to slowly converge towards some form of hybrid models, featuring no real plate or plate boundaries but rather a mosaic of generally soft blocks in relative motion, colliding or indenting each other, occasionally sliding below each other and undergoing large internal strain (Bédard, 2018; Capitanio et al., 2022; Cawood et al., 2022; Chowdhury et al., 2020; Harris and Bédard, 2015; Moyen et al., 2021b; Sizova et al., 2015; Zibra, 2020).

8.4. Large databases and how they relate to geology

The interpretations in this paper are based on a large database of published analyses of granitoids (> 2300, including the new SWASA samples). This database is sorted and qualified in terms of geological history, and therefore offers the possibility to discuss the meaning of global trends and patterns.

An oft-used line of investigation is the secular evolution of igneous rock compositions. Here we have the opportunity to explore it in the light of our understanding of the rock types present (Fig. 16). In previous studies [Martin and Moyen (2002) or Condie (2005b) for instance], MgO content has been suggested to increase with time in the global Archaean record. This observation was used by these authors and by others, to infer progressive steepening (or onset) of subduction during Archaean, based on the assumption that all rocks in the database are TTGs and thus come from similar primary melts, having more or less interacted with a similar overlying peridotitic mantle wedge. In our Kaapvaal dataset (Fig. 16), MgO contents do indeed increase from ca. 3.6 to 3.2 Ga in Barberton. However, this primarily reflects the predominance of the mafic Kaap Valley pluton in the dataset during this younger period. After 3.1 Ga, on the other hand, MgO decreases. In the Northern Kaapvaal, MgO contents also increase from 3.3 to 2.7 Ga, but in this case this is mostly the result of the onset of a distinct rock type (sanukitoids and related) at ca. 2.67 Ga. Before this age, MgO contents fluctuate in a less systematic manner.

Sr contents were also used by Martin and Moyen (2002) and taken as an indicator of the depth of melting, because it is interpreted as reflecting the decreasing stability of plagioclase at higher pressure. Here, the increasing average composition that is observed in the BGGT before 3.0 Ga largely reflects the shift from stage I and II TTGs to stage III high-Sr GMS (in particular the mantle-related compositions). During stages B.I and B.II, the fluctuations are less systematic [the highest-Sr series is at ca. 3.45 Ga, as long noted; (Anhaeusser and Robb, 1980)]. Conversely, in the Northern Kaapvaal, average Sr contents actually decrease with time.

La/Yb or Sr/Y (not shown) illustrate an even more complex behavior. In the Kaapvaal Craton, both ratios show rather unclear evolutions (and certainly not a clear trend towards, for instance, more fractionated, HREE depleted compositions, as often described in global databases: Condie, 2005b; Smithies, 2000). In both sub-provinces, this reflects a change in rock types – from high Sr/Y and La/Yb TTGs (with earlier "high pressure" and younger "low pressure", in Barberton at least) to lower Sr/Y and La/Yb compositions which reflect an increase in reworked components. The coexistence of distinct regimes at the same time (reworking vs. accretion) contributes to a blurred signal.

Perhaps the most robust, and only definitive, cratonic evolution indicator observed in both domains is the progressive change towards more potassic intrusive rocks with time. This reflects that each portion of the craton increasingly switches from juvenile accretion to reworking of preexisting felsic crustal material. Somewhat dispiritingly, this observation had been made more than fifty years ago by the early workers

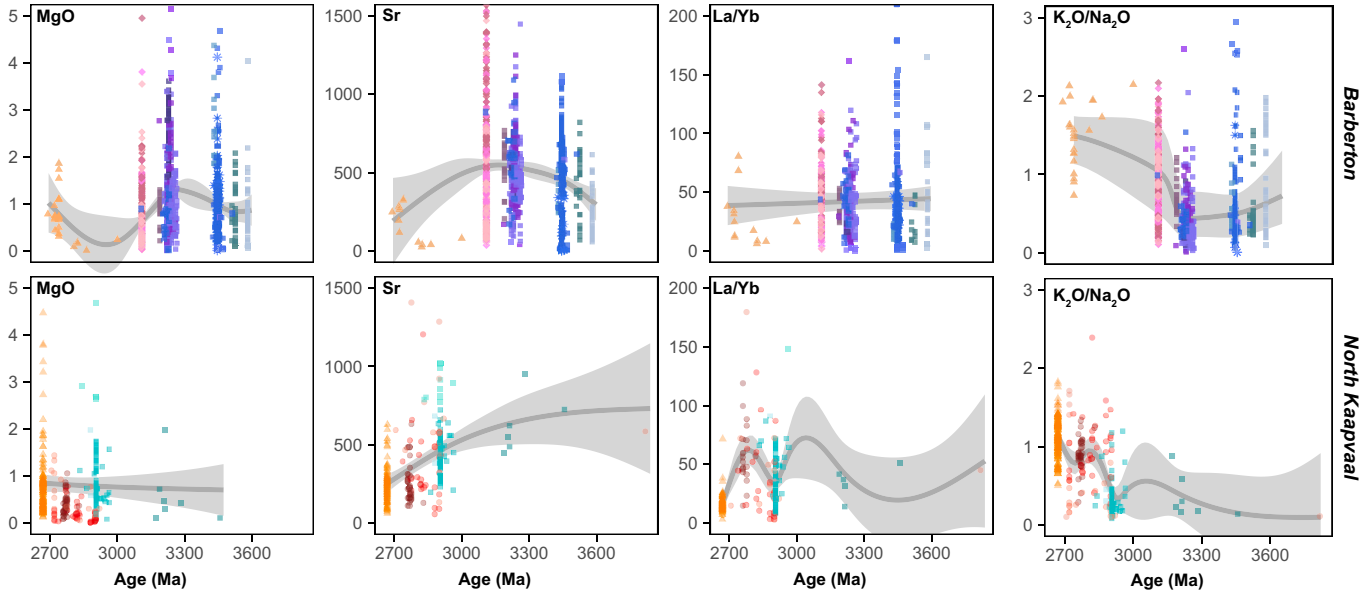

Fig. 16. Age versus composition diagrams for the BGGT (top row) and Northern Kaapvaal (lower row) granitoids, using popular indicators of "global trends". The grey bands indicate spline smoothing (Hastie and Tibshirani, 1990) to serve as a visual guide. Other symbols as in earlier figures (SWASA samples not explicitly identified).

studying Archaean terranes! (Salop and Scheinmann, 1969; Visser, 1956).

If nothing else, these examples highlight the danger of blindly relying on large databases. Such compilations are bound, by design, to include distinct rock types. The meaning of a certain geochemical signal however can be understood only in reference to its origin – interpreting high Sr/Y as depth of melting, for instance, is predicated on the assumption that (i) the rocks in consideration are chilled liquids; (ii) they all derive from a similar source, such that the only variable is the depth of melting; (iii) in a situation where the key driver is the plagioclase/garnet balance. Should any of these assumptions fail (and the second one at least is demonstrably wrong when dealing with different rock types, so it is very likely not correct for large databases), the whole reasoning collapses as has been highlighted in several studies (McCoy-West et al., 2022; Moyen, 2009).

Regional differences between cratons can also be examined in the light of our data. Periods of crustal recycling for instance (the GMS suite of Barberton stage III, and the various granites of North Kaapvaal stage III) tend to generate REE patterns with steeper slopes but more concave (higher λ1 and λ2 following O'Neill, 2016) than initial crustal accretion. One may therefore speculate that global distributions at the scale of a craton are likely to reflect the balance of different rock types, and further that the evolution of resulting sediments will show the proportion of each type cropping out at the time of erosion. It is of course an important observation on its own right, but perhaps one that tells more on the "local evolution stage" of a given craton than the global crustal evolution.

9. Conclusion: the SWASA collection – illustrating various modes of crustal development

In this contribution we do not wish to extrapolate too much regarding global tectonic patterns for the Archaean Earth. From the perspective of the felsic crust, the example of the Kaapvaal Craton reveals that 3 or 4 broad regimes can exist:

- **Accretion of an original crustal nucleus,** mostly with near-chondritic crustal material. As, in most cases, rocks from that stage are only preserved as deformed fragments in Grey Gneiss complexes, it is quite hard to discuss in more detail possible geodynamic settings. In the BGGT, this petrogenetic process appears to have occurred in a range of contexts, with the ca. 3.45 Ga plutons emplaced into a thick submerged mafic crust that did not seem to undergo much concomitant or subsequent(?) regional deformation, to the ca. 3.2 Ga plutons associated with a major deformation event involving crustal thickening (as attested by its topographic expression).
- **Rifting of pre-existing crust,** resulting in the formation of narrow rift basins (future greenstone belts) as well as more radiogenic magmatism.
- **Recycling of the crust**, petrologically with two chief modes: (i) **intra-crustal reworking**, with partial melting of the older rocks; (ii) **cycling through the mantle**, with burial of crustal components into the mantle, leading to melting of this enriched mantle. Both can occur together or separately and in varying proportions. Tectonic settings (let alone geodynamic) for these periods appear to vary, from dominated by exhumation of partially molten lower crust in granite-migmatite domes in the absence of far-field deformation (e.g. Pilbara), to long-lived melting under transcurrent to transpressive conditions (e.g. Eastern Dharwar: Chardon et al. (2011); Yilgarn: Zibra (2020); Northern Kaapvaal stage NK.III), to essentially static for the latest increments (stages B.IV and NK.IV).

The SWASA collection as presented and characterised for major and trace element compositions here serves as a basis for further detailed investigations. It has been assembled with particular attention to the coverage of the different stages and regimes outlined in this paper. Table 3 summarises the number of samples available from each magmatic stage. Although as with any record there are unavoidable biases, related to outcrop quality, accessibility and preservation biases, the collection features representative samples of each stage/regime (at least for the granitoids, Table 3). We trust that it can therefore be used as a sound basis to investigate the geochemical signatures of Archaean crust-forming processes, taking into account the diversity of regimes during the Archaean, and avoiding sketchy oversimplifications.

Declaration of competing interest

The authors declare the following financial interests/personal relationships which may be considered as potential competing interests:

JF Moyen reports financial support was provided by IRP BuCoMO. Emilie Bruand reports financial support was provided by ANR. Emilie Bruand reports financial support was provided by ClerVolc. Marc Alban Millet reports financial support was provided by NERC. Peter Cawood and Oliver Nebel report financial support was provided by ARC and by Monash University.

Data availability

Data is included as Supplementary Material

Acknowledgments

This paper draws on 20 years of experience of the first author with Kaapvaal geology. Amongst the numerous colleagues who introduced us to the region, showed us rocks, facilitated access and in general, shaped our thinking on the Craton's long and complex history, we are particularly indebted to G. Stevens and A. Kisters for 20 years of geological (and friendly!) discussions; to O. Laurent, G. Nicoli and A. Vézinet for petrological and geochronological understanding of the Northern Kaapvaal; to A. Chauvet for unraveling the complex tectonic history of the same area. In Barberton, the encyclopedic knowledge of C. Heubeck on BGB's rocks, and his willingness to share it with colleagues, is gratefully acknowledged. No paper on Kaapvaal geology would be complete without mentioning C. Anhaeusser, whose work is still a source of inspiration after 50 years, whose remarkable maps are still key references. Field work was partly funded by BuCoMO, a French-South African IRP collaboration project jointly funded by the French CNRS and the South African NRF. Massimo Raveggi is thanked for analytical assistance at Monash University. Analyses at Monash were funded by ARC grant FL160100168 to PAC. This work was supported by a NERC project NIIICE (NE/R001332/1) to MAM. We would like to thank Claire Fonquernie and Krzysztof Suchorski for support in major and trace elements analyses of part of the collection and ICP-MS lab facilities at the LMV. This work was partly supported by the French Government Laboratory of Excellence initiative n° ANR-10-LABX-0006 and by the French National Research Agency (grant ANR-21-CE49-0001-01, AMNESIA, PI EB). This is Laboratory of Excellence ClerVolc contribution number 631.

Appendix A. Sample sharing policy

The SWASA (SWAziland-South Africa) sample suite has been collected with the aim to be representative of the evolution of the Kaapvaal craton and serve as a basis for studies of crustal evolution in Archaean. Samples were collected and prepared to allow for multiple geochemical and

petrological studies of Archaean igneous processes to be performed on the same samples. This sharing policy together with request forms are available as Supplementary Material.

Sample information including description, location, age, major and trace element concentrations, of the available samples can be found in the Supplementary Material.

The SWASA sample suite is curated by the sampling team. It is intended to be an open sample suite that can be requested by any interested party, the SWASA team will consider each request on the basis of requested sample mass, study focus, novelty of the analytical work and publication plans. All requests should involve justification of each criteria.

More specifically, request that follow the following criteria will be favoured:

- Not requiring an unnecessary large and/or unjustified amount of sample mass
- Targeting of specific set of samples to test clearly outlined hypotheses
- Justify the use of combined geochemical/petrological tools
- Avoid unjustified repetition of previous measurements
- Clearly defined timeline for data generation

In cases of identical and simultaneous sample requests, teams led by or involving collaboration with researchers based in South Africa will be given preference.

Conditions of sample access are:

- The SWASA team should be included as co-author of the resulting publication as “The SWASA team” (and not as individuals).
- Data is published in open access format
- Sample powder is not to be shared further unless specific permission is sought and given by the curators
- Unused sample mass after analysis should be returned to curators

To request samples, please submit the request form along with the sample request spreadsheet available in the Supplementary Material. Requests will be considered as soon as possible by the SWASA team.

Table A1
All samples of the original SWASA collection. Three samples initially given SWASA designation, unrelated to the objectives of this work have subsequently been extracted from the collection. Some samples were taken for different purposes (e.g. sedimentary samples for detrital accessory minerals) and were not analysed for whole rock composition.

Sample	IGSN	Latitude	Longitude	Rock Type	Stage	Unit	Description	Equivalent sample from literature	Age (Ma)	Reference for age and comments	Notes
Ancient Gneiss Complex & eSwatini granitoids											
SWASA-001	CNRS0000024354	−26.471944	31.16879	Gneiss	B. I	Ngwane gneisses	Dominant banded medium grey gneiss		3600-3300	Regional age spread of AGC	
SWASA-002	CNRS0000024355	−26.471944	31.16879	Gneiss	B. I	Ngwane gneisses	Early dark phase		3600-3300	Regional age spread of AGC	
SWASA-003	CNRS0000024356	−26.588145	31.186204	Deformed granitoid	B. II	Usutu suite	Coarse grained granodiorite	AGC-317 (Kröner et al. 2019); AGC-368 (Kröner et al. 2018)	3226–3261	This locality, Kröner et al. 2018, Kröner et al., 2019	
SWASA-004	CNRS0000024357	−26.588145	31.186204	Deformed granitoid	B. II	Usutu suite	Mafic syn-plutonic dyke		3226–3261	Implied from field relations	
SWASA-005	CNRS0000024358	−26.599043	31.152043	Granitoid	B. IV	Ngwempisi pluton	Coarse grained porphyritic granite		2720	Same unit (Maphalala and Kröner 1993)	
SWASA-006	CNRS0000024359	−26.599043	31.152043	Granitoid	B. IV	Ngwempisi pluton	Fine grained cutting(?) phase		≤ 2720	Implied from field relations	
SWASA-007	CNRS0000024360	−26.76262	30.988275	Granitoid	B. I	Tsawela gneisses	Coarse grained foliated tonalite	AGC-491 (Hoffmann et al. 2016)	3450	This locality, Hoffmann et al. (2016)	
SWASA-008	CNRS0000024361	−26.76262	30.988275	Granitoid	B. I	Dyke	Dyke cutting across Tsawela Gneisses		≤ 3450	Implied from field relations	
SWASA-009	CNRS0000024362	−26.849297	30.962751	Granitoid	B. IV	Sicunusa pluton	Coarse grained porphyritic granite		2723	Same unit (Maphalala and Kröner 1993)	
SWASA-010		−26.985546	31.037572	Sediment		Pongola Supergroup, undif.	Quartzite		2940	Same unit (Gold 2006)	
SWASA-011		−27.022767	31.085344	Sediment		Pongola Supergroup, undif.	Bt-Ms arkose		2940	Same unit (Gold 2006)	
SWASA-012		−27.022767	31.085344	Sediment		Pongola Supergroup, undif.	Yellow siltstone		2940	Same unit (Gold 2006)	

(*continued on next page*)

Table A1 (*continued*)

Sample	IGSN	Latitude	Longitude	Rock Type	Stage	Unit	Description	Equivalent sample from literature	Age (Ma)	Reference for age and comments	Notes
SWASA-013	CNRS0000024366	−26.800074	30.947892	Deformed granitoid	B. I	Tsawela gneisses	Coarse grained foliated tonalite		3450	Same unit (Kröner and Tegtmeyer 1994)	
Barberton granite-greenstone terrain											
SWASA-014	CNRS0000024367	−26.617385	31.1023	Granitoid	B. III	Mpuluzi batholith	Medium grained granite		3106	Average age, same unit (Moyen et al., 2021a, b, c)	
SWASA-015	CNRS0000024368	−26.21149	30.964033	Granitoid	B. III	Mpuluzi batholith	Undeformed relatively late dark grey granite/ granodiorite		3106	Average age, same unit (Moyen et al., 2021a, b, c)	
SWASA-016	CNRS0000024369	−26.21149	30.964033	Granitoid	B. III	Mpuluzi batholith	Sheared granite		3106	Average age, same unit (Moyen et al., 2021a, b, c)	
SWASA-017	CNRS0000024370	−26.21149	30.964033	Granitoid	B. III	Mpuluzi batholith	Sheared granite (less weathered ?)		3106	Average age, same unit (Moyen et al., 2021a, b, c)	
SWASA-018	CNRS0000024371	−26.180828	30.99775	Gneiss	B. I	Steynsdorp gneisses	Foliated tonalite	SP12 (Anhaeusser and Robb 1981); BA26 (Kröner et al. 1991)	3531	This locality, Kröner at al. (1991)	
SWASA-019	CNRS0000024372	−26.098444	30.958267	Granitoid	B. III	Dalmein pluton	Dalmein granite, relatively fine grained border facies		3203	Same unit (Lana et al. 2010)	
SWASA-020	CNRS0000024373	−26.056229	30.850432	Granitoid	B. I	Theespruit pluton	Medium to coarse grained trondhjemite	TP4D (Anhaeusser and Robb, 1980); JB-17-C1 (Laurent et al. 2020); 16SA-10-1 (Wang et al. 2021); MS-30, MS31, MS-32, MS-33, MS-34, MS-35 (Mühlberg et al. 2021)	3460	This locality, Wang et al. 2021	Recent quarry near eLukwatini-Mooiplaas road
SWASA-021	CNRS0000024374	−26.056229	30.850432	Amphibolite	B. I	Theespruit pluton	Amphibolite xenolith (dark, amphibole-rich, little or no plag)	MS-28, MS-29 (Mühlberg et al. 2021)	Maybe 3530	Assumed equivalent of Sandspruit/ Theespruit Formation	
SWASA-022	CNRS0000024375	−26.056229	30.850432	Amphibolite	B. I	Theespruit pluton	Amphibolite xenolith (ordinary amp+pg+ep)				
SWASA-023	CNRS0000024376	−26.035935	30.802438	Amphibolite	B. I	Theespruit pluton	Amphibolite xenolith (ordinary amp+pg+ep)				
SWASA-024	CNRS0000024377	−26.022454	30.803912	Granitoid	B. I	Theespruit pluton	Medium to coarse grained trondhjemite	JB-17-C3 (Laurent et al. 2020); < 500 m from 17SA-9-1, 14-SA-22 (Wang et al. 2021), BB3 (Zeh et al. 2009)	3450-3453	Same unit nearby, Zeh et al. 2009; Wang et al. 2021	
SWASA-025	CNRS0000024378	−25.996874	30.677203	Granitoid	B. I	Stolzburg pluton	Foliated trondhjemite	LC17 (Anhaeusser and Robb, 1980); STZ1, STZ2 (Yearron, 2003); MS-14 (Mühlberg et al., 2021)	3435	This locality, Mühlberg et al. 2021	

(*continued on next page*)

Table A1 (*continued*)

Sample	IGSN	Latitude	Longitude	Rock Type	Stage	Unit	Description	Equivalent sample from literature	Age (Ma)	Reference for age and comments	Notes
SWASA-026	CNRS0000024379	−26.003195	30.736541	Granitoid	B. I	Stolzburg pluton	Trondhjemite	MS-15 (Mühlberg et al. 2021)	3432	This locality, Mühlberg et al. 2021	
SWASA-027		−26.002887	30.789299	Sediments/ Felsic volcanics	B. I	Theespruit Formation	Felsic schists	800 m from BKC-23 (Cutts et al. 2014); 2012-1, 2012-2 (Moyen et al., 2021a, b, c)	3523-3527	This locality, Moyen et al., 2021a, b, c	
SWASA-028	CNRS0000024381	−25.972926	30.836905	Mafic volcanics	B. I	Komati formation	Massive komatiite		ca. 3470	Same unit (Lowe and Byerly 2007; Byerly et al., 2018)	
SWASA-029	CNRS0000024382	−25.968172	30.847361	Mafic volcanics	B. I	Komati formation	Spinifex-textures komatiite (fine grained)				
SWASA-030	CNRS0000024383	−25.968172	30.847361	Mafic volcanics	B. I	Komati formation	Spinifex-textures komatiite (coarse grained)				
SWASA-031	CNRS0000024384	−25.966675	30.880636	Mafic volcanics	B. I	Hooggenoeg Formation, H2v member	Massive basalts		3440-3470	Same unit (Lowe and Byerly 2007; Byerly et al., 2018)	
SWASA-032	CNRS0000024385	−25.952648	30.880974	Mafic volcanics	B. I	Hooggenoeg Formation, H2v member	Sill(?) of doleritic material				
SWASA-033	CNRS0000024386	−25.948532	30.883053	Mafic volcanics	B. I	Hooggenoeg Formation, H3v member	Komatiite, spinifex textures		3440-3470	Same unit (Lowe and Byerly 2007; Byerly et al., 2018)	
SWASA-034	CNRS0000024387	−25.944883	30.884557	Mafic volcanics	B. I	Hooggenoeg Formation, H3v member	Silicifed basalts				
SWASA-035		−25.94442	30.884799	Sediments	B. I	Hooggenoeg formation, H3c (assumed)	Chert Float		3440-3470	Same unit (Lowe and Byerly 2007; Byerly et al., 2018)	
SWASA-036	CNRS0000024389	−25.94442	30.884799	Mafic volcanics	B. I	Hooggenoeg formation, H3c (assumed)	Strongly silicified ultramafic, fuchsite-carbonate bearing		3440-3470	Same unit (Lowe and Byerly 2007; Byerly et al., 2018)	
SWASA-037	CNRS0000024390	−26.024633	30.761932	Granitoid	B. I	Stolzburg pluton	Trondhjemite	MS-22 (Mühlberg et al. 2021); JB-17-C5-a (Laurent et al. 2020)	3442-3457	This locality, Wang et al. 2021	Disused quarry, kaNgwane crushers. Other samples from this locality (facies unspecified) include STZ21/ Q1, Q3, Q5 and Q6; STZ25 (Yearron 2003); MS-42, -43, -44, -45, -46, -47, -48, -49 (Mühlberg et al. 2021); 14SA-20-1, -20-2, 16SA-18-2, -18-3 (Wang et al. 2021)
SWASA-038	CNRS0000024391	−26.024633	30.761932	Granitoid	B. I	Stolzburg pluton	Dark sphene bearing phase	MS-23 (Mühlberg et al. 2021); JB-17-C5-b (Laurent et al., 2020)	3454	This locality, same rock (< 1 m). Laurent et al. 2020	
SWASA-039	CNRS0000024392	−26.024633	30.761932	Amphibolite	B. I	Stolzburg pluton	Amphibolite enclave		Maybe 3530	Assumed equivalent of Sandspruit/ Theespruit Formation	
SWASA-040	CNRS0000024393	−26.024633	30.761932	Granitoid	B. I	Stolzburg pluton	Garnet-bearing, undeformed trondhjemitic dyke	STZ21/Q2 (Yearron, 2003); MS24 (Mühlberg et al. 2021); probably 14-SA-10, 14SA-18-2, 14SA-20-2 (Wang et al. 2021)	3205-3225	This locality, Wang et al. 2021	
SWASA-041		−25.996973	30.663415	Amphibolite	B. I / B.II	Inyoni shear zone (amphibolite)	Grt-bearing amphibolite (float)	BAR-11-11 (François et al. 2014)	3215-3250	Age of metamorphism/ anatexis in Inyoni shear zone (Dziggel et al., 2015; François, 2014; Peng et al. 2019; Wang et al. 2019)	Emplacement age of amphibolite precursor is not known (maybe equivalent of Theespruit/ Sandspruit Formation). Samples SA124, SA126, SA127, SA128 (Peng et al.
SWASA-042	CNRS0000024395	−25.995287	30.662807	Amphibolite	B. I / B.II	Inyoni shear zone (amphibolite)	Coarse grained amphibolite (amphibole + melt "mush")				
SWASA-043	CNRS0000024396	−25.995287	30.662807	Amphibolite	B. I / B.II	Inyoni shear zone (amphibolite)	Fine grained amphibolite with incipient melting				

(*continued on next page*)

Table A1 (*continued*)

Sample	IGSN	Latitude	Longitude	Rock Type	Stage	Unit	Description	Equivalent sample from literature	Age (Ma)	Reference for age and comments	Notes
SWASA-044	CNRS0000024397	−25.995287	30.662807	Amphibolite	B. I / B.II	Inyoni shear zone (amphibolite)	Melt-rich mush (amphibole poor)				2019); 14SA-35, 15SA-30, 15SA-31 (Wang et al.
SWASA-045	CNRS0000024398	−25.995287	30.662807	Amphibolite	B. I / B.II	Inyoni shear zone (amphibolite)	Ordinary hbl+plg amphibolite (unmolten)				2019); 14SA-18-1, 16SA-20-2, 17SA-12 (Wang et al.
SWASA-046	CNRS0000024399	−25.995855	30.661629	Granitoid	B. II	Inyoni shear zone (tonalite)	Coarse-grained foliated tonalite, relatively early phase		3235-3266	Same unit, nearby, Wang et al. 2021	2021) were all taken ca. 1 km to the South.
SWASA-047		−25.998184	30.661271	Amphibolite	B. I / B.II	Inyoni shear zone (amphibolite)	Grt-bearing amphibolite		3215-3250	Age of metamorphism/ anatexis in Inyoni shear zone (Dziggel et al., 2015; François, 2014; Peng et al. 2019; Wang et al. 2019)	
SWASA-048		−25.999775	30.66165	Amphibolite	B. I / B.II	Inyoni shear zone (amphibolite)	Grt-bearing amphibolite	INY21; INY115 (Moyen et al. 2006; Nédélec et al. 2012)			
SWASA-049	CNRS0000024402	−26.043201	30.657836	Granitoid	B. III	Boesmanskop	Porph. Syenite		3096-3107	Same unit (Kamo and Davies 1994; Westraat et al. 2004)	
SWASA-050	CNRS0000024403	−26.120411	30.416927	Granitoid	B. III	Heerenveen	Core coarse grained granite, euhedral quartz	BC29 (Anhaeusser and Robb, 1980)	3118	Same unit, average age of core granite (Moyen et al., 2021a, b, c)	
SWASA-051	CNRS0000024404	−26.17208	30.443619	Granitoid	B. III	Heerenveen	Coarse grained leucogranite with pegmatite fragments		3110	Same unit, average of 3 leucogranites (Moyen et al., 2021a, b, c)	
SWASA-052	CNRS0000024405	−26.195132	30.454462	Granitoid	B. III	Heerenveen	Pink granite/qtz monzonite	HE-11-06 (Moyen et al., 2021a, b, c)	3086	This locality (Moyen et al., 2021a, b, c)	
SWASA-053	CNRS0000024406	−25.891794	30.622437	Granitoid	B. II	Nelshoogte pluton	Coarse grained foliated trondhjemite	NLG26 (Yearron 2003); KPV99-94, EKC03-9 (Schoene et al. 2008); KK89 (Zeh et al. 2009); 14SA-16 (Wang et al. 2021)	3236-3238	This locality, Schoene et al. (2008); Zeh et al. (2009); Wang et al. (2021)	Under the R38 bridge, Komati river bed. B-90-16 (de Ronde and Kamo 2000) probably also from this locality
SWASA-054	CNRS0000024407	−25.867421	30.659712	Granitoid	B. II	Nelshoogte pluton	Coarse grained foliated trondhjemite	KL7 (Anhaeusser and Robb, 1980)	3238-3238	Same unit	
SWASA-055	CNRS0000024408	−25.762466	30.81019	Granitoid	B. II	Kaap Valley pluton	Coarse grained Amph-Bt Tonalite	SKV33, SKV34 (Anhaeusser and Robb, 1980); KVY1A (Yearron 2003); 14SA-23 (Wang et al. 2021)	3222	This locality, Wang et al. 2021	
SWASA-056		−25.945831	31.108602	Sediments	B. I	Msauli chert (Mendon Formation, M1c member)	Light grey chert (with lapili)		3330-3300	Same unit (Lowe and Byerly 2007; Byerly et al., 2018)	
SWASA-057		−25.945831	31.108602	Sediments	B. I	Msauli chert (Mendon Formation, M1c member)	Black chert				
SWASA-058		−25.908362	31.09143	Sediments	B. II	Fig Tree Group (Manzimnyama Syncline)	Turbidite sandstone		ca. 3260	Same unit nearby, Drabon and Lowe 2021	
SWASA-059		−25.882409	31.089343	Sediments	B. II	Fig Tree Group (Barite Valley Syncline)	Stratiform baryte		ca. 3260	Same unit, Drabon and Lowe 2021	

(*continued on next page*)

Table A1 (*continued*)

Sample	IGSN	Latitude	Longitude	Rock Type	Stage	Unit	Description	Equivalent sample from literature	Age (Ma)	Reference for age and comments	Notes
SWASA-060		−25.791991	31.084091	Sediments	B. II	Moodies group, MdS1 (Dycedale Syncline)	Fine grained, silicified sandstone		3214-3218	Same unit nearby, Heubeck et al. 2013	250 m North of "White tidal sandstone" geotrail locality
SWASA-061		−25.791991	31.084091	Sediments	B. II	Moodies group, MdS1 (Dycedale Syncline)	Coarse grained sandstone				
SWASA-062		−25.791991	31.084091	Sediments	B. II	Moodies group, MdQ2 (Dycedale syncline)	Conglomerate				
SWASA-063		−25.791991	31.084091	Sediments	B. II	Moodies group, MdS1 (Dycedale Syncline)	Fine grained, silicified sandstone				
SWASA-064	CNRS0000024417	−25.77057	31.060641	Granitoid	B. II	Kaap Valley pluton	Coarse grained Amph Tonalite		3227-3229	This locality (Tegtmeyer and Kröner 1987; Kamo and Davis 1994)	"Barberton sand pit"
SWASA-065	CNRS0000024418	−25.941588	30.894031	Mafic volcanics	B. I	Hooggenoeg Formation, H5v member	Massive basalts		3440-3470	Same unit (Lowe and Byerly 2007; Byerly et al., 2018)	
SWASA-066	CNRS0000024419	−25.943722	30.892001	Mafic volcanics	B. I	Hooggenoeg Formation, H4v member	(ultra)mafic lava, maybe pillowed		3440-3470	Same unit (Lowe and Byerly 2007; Byerly et al., 2018)	
SWASA-067	CNRS0000024420	−25.944706	30.889175	Mafic volcanics	B. I	Hooggenoeg Formation, H4v member	Mafics immediately above H3c chert				
SWASA-068	CNRS0000024421	−25.938775	30.894178	Felsic	B. I	Hooggenoeg Formation, H6i member	Hypovolcanic felsic rock	JB-17-F3 (Laurent et al., 2020)	3455-3456	Same unit nearby (< 250 m), Laurent et al. 2020	
SWASA-069	CNRS0000024422	−25.937426	30.894098	Felsic	B. I	Hooggenoeg Formation, H6i member	Fine grained, hypovolcanic felsic rock				
SWASA-070	CNRS0000024423	−25.937161	30.894819	Felsic	B. I	Hooggenoeg Formation, H6i member	Fine grained, hypovolcanic felsic rock	JB-17-F4 (Laurent et al., 2020)			
SWASA-071		−25.8332555	30.9455949	Mafic volcanics	B. II	Welvreden formation, Pioneer Complex	Shale	See Robin-Popieul et al. 2012; Puchtel et al. 2014	3263	Same unit nearby, Puchtel et al. 2014	
SWASA-072		−25.8332555	30.9455949	Mafic volcanics	B. II	Welvreden formation, Pioneer Complex	Tuff				
SWASA-073	CNRS0000024426	−25.833849	30.943528	Mafic volcanics	B. II	Welvreden formation, Pioneer Complex	Spinifex komatiite				
SWASA-074	CNRS0000024427	−25.833849	30.943528	Mafic volcanics	B. II	Welvreden formation, Pioneer Complex	Px-bearing serpentinite				
Murchison greenstone belt, and surrounding intrusives											
SWASA-075	CNRS0000024428	−23.957799	30.371016	Felsic	NK. II	Rubbervale Formation	Felsic schists		2960-2970	Same unit, Poujol et al. 1996, Schwarz-Schampera et al., 2010	
SWASA-076		−23.957799	30.371016	Sediments	NK. II	Rubbervale Formation	Chl-qtz schists				
SWASA-077	CNRS0000024430	−23.90011	30.385077	Mafic	NK. II	Rooiwater complex	Coarse-grained Hbl gabbro		2964	Same unit, Zeh et al. 2013	
SWASA-078		−23.937789	30.412488	Mafic	NK. II	Rooiwater complex	Northernmost (lower ?) magnetite layer				
SWASA-079		−23.937789	30.412488	Mafic	NK. II	Rooiwater complex	Southernmost (upper?) magnetite layer				
SWASA-080		−23.936328	30.411668	Mafic	NK. II	Rooiwater complex	Gabbro, North (below?) magnetite layer				
SWASA-081	CNRS0000024434	−23.919676	30.54735	Felsic	NK. II	Rubbervale Formation	Rubbervale Rhyolite	TR61 (Brandl et al. 1996); Rub1, Rub2 (Zeh et al. 2013) [2 km SE]	2960-2970	Same unit nearby, Brandl et al. 1996; Zeh et al. 2013	

(*continued on next page*)

Table A1 (*continued*)

Sample	IGSN	Latitude	Longitude	Rock Type	Stage	Unit	Description	Equivalent sample from literature	Age (Ma)	Reference for age and comments	Notes
SWASA-082	CNRS0000024435	−23.923629	30.818602	Granitoid	NK. III	Lekkersmaak granite	Coarse grained, porphyritic Bt+Ms granite	Between MUR-09-63 & MUR-09-66 (Poujol et al., 2021)	2740-2795	Same unit; Zeh et al. 2009, Poujol et al. 2021	
SWASA-083	CNRS0000024436	−23.837007	30.982922	Granitoid	NK. III	Lekkersmaak granite	Fine grained Ms+Bt granite	MUR-09-67 (Poujol et al. 2021); MUR7 (Block et al., 2013)			
SWASA-084	CNRS0000024437	−23.837007	30.982922	Granitoid	NK. III	Lekkersmaak granite	Pegmatoidal Ms+Bt+Grt granitoid				
SWASA-085		−23.996568	31.115831			Phalaborwa complex	Misc rock types		2060	Same unit (Nebel et al)	
SWASA-117		−23.309442	30.723629	Mafic	NK. II ?	Giyani Greenstone belt	Metagabbro (float)		3203	Kröner et al. 2000 on a meta-andesite nearby	Surprising age - much older than the other greenstone belts or supracrustal remnants of this area
SWASA-118		−23.309442	30.723629	Mafic	NK. II ?	Giyani Greenstone belt	Metabasalt (float)	T10 (Kröner et al. 2000)			
SWASA-119		−23.3450449	30.7647294	Mafic	NK. II ?	Giyani Greenstone belt	Metabasalt (float)		< 2874	Cutting porphyry dyke in this area (TR63; Kröner et al. 2000)	
SWASA-120		−23.3442017	30.768584	Mafic	NK. II ?	Giyani Greenstone belt	Ultramafic (float)				
SWASA-121		−23.3442017	30.768584	Mafic	NK. II ?	Giyani Greenstone belt	coarse grained gabbro/ pyroxenite				
SWASA-122		−23.338955	30.774517	Mafic	NK. II ?	Giyani Greenstone belt	Fresh fine grained gabbro (float)				
SWASA-123		−23.338955	30.774517	Mafic	NK. II ?	Giyani Greenstone belt	coarse grained gabbro/ pyroxenite				
Pietersburg Greenstone belt and granitoids to the South											
SWASA-086	CNRS0000024446	−23.940629	29.94803	Granitoid	NK. III	Duiwelskloof batholith	Fine grained granodiorite	DWK-01 (Laurent & Zeh 2015)	2840	Same locality, Laurent & Zeh 2015	
SWASA-087	CNRS0000024447	−23.941785	29.949844	Amphibolite	NK. II ?	Duiwelskloof batholith	Amphibolite		Maybe 2940	By analogy with GLG-2	
SWASA-088	CNRS0000024448	−23.941785	29.949844	Amphibolite	NK. II / NK. III	Duiwelskloof batholith	Amphibolite with leucocratic veins				
SWASA-089	CNRS0000024449	−23.92851	29.894978	Gneiss	NK. II	Groot Letaba Gneisses	Dark grey gneiss	LP-17-10 (Maulny 2019)	2962	Same rock (< 1 m), Maulny 2019	R71 Roadcut, ca. 20 km E. of Mankweng
SWASA-090	CNRS0000024450	−23.92851	29.894978	Vein in gneiss	NK. III	Groot Letaba Gneisses	Late, horizontal pegmatite vein		Maybe 2860	By analogy with similar features regionally (Vézinet et al. 2018)	
SWASA-091	CNRS0000024451	−23.92851	29.894978	Gneiss	NK. III	Groot Letaba Gneisses	Coarse-grained gneiss	LP-17-14 (Maulny 2019)	2862	Same rock (< 1 m), Maulny 2019	
SWASA-092	CNRS0000024452	−23.92851	29.894978	Gneiss	NK. III	Groot Letaba Gneisses	Coarse grained gneiss, with white veins		Maybe 2860	By analogy with similar features regionally (Vézinet et al. 2018)	
SWASA-093	CNRS0000024453	−23.92851	29.894978	Amphibolite	NK. II ?	Groot Letaba Gneisses	Amphibolite dyke		Maybe 2940	By analogy with GLG-2	
SWASA-094	CNRS0000024454	−23.92851	29.894978	Vein in gneiss	NK. III	Groot Letaba Gneisses	Garnet-bearing leucocratic melt	LP-17-11 (Moyen et al. in prep.)	ca. 2860	By analogy with similar features regionally (Vézinet et al. 2018)	
SWASA-095	CNRS0000024455	−23.92851	29.894978	Amphibolite	NK. II	Groot Letaba Gneisses	Amphibolite enclave	GLG-2 (Laurent & Zeh 2015)	2942	Same rock (< 1m), Laurent & Zeh 2015	
SWASA-096	CNRS0000024456	−23.932402	29.864066	Gneiss	NK. II	Groot Letaba Gneisses	Gneiss with some injections	MAK-G2 (Laurent & Zeh 2015)	2945	This locality, Laurent & Zeh 2015	

(*continued on next page*)

Table A1 (*continued*)

Sample	IGSN	Latitude	Longitude	Rock Type	Stage	Unit	Description	Equivalent sample from literature	Age (Ma)	Reference for age and comments	Notes
SWASA-097	CNRS0000024457	−23.932402	29.864066	Vein in gneiss	NK. III	Groot Letaba Gneisses	Synfolial leucocratic material	LP-17-13a (Moyen et al. in prep.)	ca. 2860	Same rock (< 1 m), Moyen & Paquette unpub.	
SWASA-098	CNRS0000024458	−23.932402	29.864066	Gneiss	NK. II	Groot Letaba Gneisses	Gneiss (stage II), perhaps less injected than 96	MAK-G2 (Laurent & Zeh 2015); LP-17-13c (Moyen et al. in prep.)	2945	This locality, Laurent & Zeh 2015	
SWASA-099	CNRS0000024459	−23.913273	29.782784	Granitoid	NK. III	Turfloop	Medium grained grey granite	TUR-11 (Laurent & Zeh 2015)	2773	Same unit, Laurent & Zeh 2015	
SWASA-100	CNRS0000024460	−23.913273	29.782784	Granitoid	NK. III	Turfloop	White/pink coarse grained, accidental magnetite				
SWASA-101	CNRS0000024461	−23.871968	29.747585	Granitoid	NK. III	Turfloop	Granite, sightly porph, some layering				
SWASA-102	CNRS0000024462	−23.765948	29.787273	Amphibolite	NK. II	Pietersburg greenstone belt	Greenschist to amphibolite facies metamafic		Maybe 2950	Typical age for Pietersburg Greenstone Belt; de Wit et al. 1993; Kröner et al. 2000	
SWASA-103		−23.765948	29.787273	Sediments	NK. II	Pietersburg greenstone belt	Ferrugineous chert				
SWASA-153		−24.017776	29.370201	Sediments	NK. II	Pietersburg greenstone belt	Chert clast breccia	PB102 (Zeh & Gerdes 2013)	2880	Same unit nearby, Zeh & Gerdes 2013	
SWASA-154		−24.017776	29.370201	Sediments	NK. II	Pietersburg greenstone belt	Dark spotted qz+bt schist				
SWASA-155		−24.017776	29.370201	Sediments	NK. II	Pietersburg greenstone belt	quartzite / quartz rich Qz+Ms schist				
Northern Kaapvaal / Limpopo Southern marginal zone											
SWASA-104	CNRS0000024467	−23.513335	30.001584	Gneiss	NK. II	Goudplaas Gneisses	Grey gneiss	R36-D3 (Vézinet et al. 2018); GHR-G1 (Laurent and Zeh 2015)	2880	This locality, Laurent & Zeh 2015	
SWASA-105	CNRS0000024468	−23.513335	30.001584	Vein in gneiss	NK. III	Goudplaas Gneisses	Late leucosome, with granitic to pegmatitic texture	R36-D1; R36-D2 (Vézinet et al. 2018)	Maybe 2850 to 2760	By analogy with similar features regionally (Vézinet et al. 2018)	
SWASA-106	CNRS0000024469	−23.513335	30.001584	Vein in gneiss	NK. III	Goudplaas Gneisses	Amphibole bearing vein	R36-D4 (Vézinet et al. 2018)			
SWASA-107	CNRS0000024470	−23.515988	30.047167	Gneiss	NK. I	Goudplaas Gneisses	Dark hbl-tonalite (stage I)	GBHR1 (Laurent and zeh 2015); R36-B5 (Vézinet et al. 2018)	3340-3280	This locality, Laurent and Zeh 2015 (core and rims, respectively)	Goudplaas locality
SWASA-108	CNRS0000024471	−23.515988	30.047167	Gneiss	NK. III	Goudplaas Gneisses	Light foliated gneisses (stage II??)	GBHR4 (Laurent and Zeh 2015); R36-B4; R36-B6 (Vézinet et al. 2018)	2847	This locality, Laurent and Zeh (2015)	
SWASA-109	CNRS0000024472	−23.515988	30.047167	Vein in gneiss	NK. III	Goudplaas Gneisses	Pink pegmatoid (stage III - early)	GH-2 (Laurent and Zeh 2015)	2790	This locality, Laurent and Zeh (2015)	
SWASA-110	CNRS0000024473	−23.515988	30.047167	Vein in gneiss	NK. III	Goudplaas Gneisses	White plag pegmatoid (stage III - late)	GBHR2 (Laurent and Zeh 2015)	2767	This locality, Laurent and Zeh (2015)	
SWASA-111	CNRS0000024474	−23.515988	30.047167	Granitoid	NK. IV	Goudplaas Gneisses	Cutting pink granite dyke (stage IV)	GBHR3 (Laurent and Zeh 2015); R36-B3 (Vézinet et al. 2018)	2674	This locality, Laurent and Zeh (2015)	
SWASA-112	CNRS0000024475	−23.515988	30.047167	Vein in gneiss	NK. IV	Goudplaas Gneisses	Pegmatite post stage IV dyke		< 2674	Implied from field relations	
SWASA-113	CNRS0000024476	−23.515988	30.047167	Vein in gneiss	NK. III	Goudplaas Gneisses	Euhedral amphibole accumulation in dark tonalite	R36-B1 (Vézinet et al. 2018)	Maybe 2850 to 2760	By analogy with similar features regionally	

(*continued on next page*)

Table A1 (*continued*)

Sample	IGSN	Latitude	Longitude	Rock Type	Stage	Unit	Description	Equivalent sample from literature	Age (Ma)	Reference for age and comments	Notes
										(Vézinet et al. 2018)	
SWASA-114	CNRS0000024477	−23.363717	30.223853	Gneiss	NK. I	Goudplaas Gneisses	Dark gneiss with melt injections and leucosomes	R578-G1 (Vézinet et al. 2018)	3213	This locality, Vézinet et al. (2018)	
SWASA-115	CNRS0000024478	−23.363717	30.223853	Vein in gneiss	NK. III	Goudplaas Gneisses	Amphibole + melt pocket	R578-G2 (Vézinet et al. 2018)	Maybe 2850 to 2760	By analogy with similar features regionally (Vézinet et al. 2018)	
SWASA-116	CNRS0000024479	−23.331147	30.263944	Gneiss	NK. I	Goudplaas Gneisses	Light-colored strongly foliated gneiss, altered	R578-F1 (Vézinet et al. 2018)	3457	This locality, Vézinet et al. (2018)	
SWASA-124	CNRS0000024480	−23.310888	29.821189	Sediments	NK. III ?	Bandelierkop metapelites	Semipelite, garnet-poor		Max. deposition age estimated at 2733 for Bandelierkop pelites (in other locations) [Nicoli et al., 2015]		Bandelierkop quarry
SWASA-125	CNRS0000024481	−23.310888	29.821189	Sediments	NK. III ?	Bandelierkop metapelites	semipelite, garnet-rich, dark				
SWASA-126	CNRS0000024482	−23.310888	29.821189	Sediments	NK. III ?	Bandelierkop metapelites	semipelite, melt+garnet rich		Melting at 2716 for grt-bearing leucosomes and 2712 for Opx-bearing leucosomes (Taylor et al. 2014, both from this locality)		
SWASA-127	CNRS0000024483	−23.310888	29.821189	Sediments	NK. III ?	Bandelierkop metapelites	small garnet leucosome				
SWASA-128	CNRS0000024484	−23.310888	29.821189	Sediments	NK. III ?	Bandelierkop metapelites	garnet-poor leucosome				
SWASA-129	CNRS0000024485	−23.310888	29.821189	Sediments	NK. III ?	Bandelierkop metapelites	opx-leucosome				
SWASA-130	CNRS0000024486	−23.310888	29.821189	Sediments	NK. III ?	Bandelierkop metapelites	pelite				
SWASA-131	CNRS0000024487	−23.310888	29.821189	Sediments	NK. III ?	Bandelierkop metapelites	grt-leucosome in pelite				
SWASA-132	CNRS0000024488	−23.437595	29.745044	Granitoid	NK. IV	Matok pluton	Capricorn phase (medium grained)	MAT1 (Laurent et al., 2014a, b, c)	2680	Same unit (Laurent et al. 2013)	
SWASA-133	CNRS0000024489	−23.441549	29.746393	Gneiss	NK. II	Baviaanskloof Gneisses	Grey gneiss, Capricorn South quarry	CQ-E3 (Vézinet et al. 2018)	2922	This locality, Vézinet et al. (2018)	Capricorn quarry (South). Actual outcrop covered by rubble since 2018.
SWASA-134	CNRS0000024490	−23.441549	29.746393	Vein in gneiss	NK. III	Baviaanskloof Gneisses	Pink pegmatoid, Capricorn Capricorn South quarry	LP-17-01 (Moyen et al. In prep); CQ-E1 (Vézinet et al. 2018)	2812	This locality, Moyen and Paquette (unpub.)	
SWASA-135	CNRS0000024491	−23.441549	29.746393	Vein in gneiss	NK. III	Baviaanskloof Gneisses	Melt + crd patch on grey gneiss, Capricorn South quarry	CQ-E2; CQ-E4 (Vézinet et al. 2018)	< 2812; perhaps 2715 ?	Implied from field relations; 2715 is the age of pelite melting in the area.	
SWASA-136	CNRS0000024492	−23.432091	29.764682	Vein in gneiss	NK. II	Baviaanskloof Gneisses	Ordinary melt, rare grt/crd, Capricorn North quarry	CQ-C3; CQ-C4 (Vézinet et al. 2018)	2920	Vézinet (2019); maybe inherited	Capricorn quarry (North)
SWASA-137	CNRS0000024493	−23.432091	29.764682	Gneiss	NK. II / NK. III	Baviaanskloof Gneisses	Heterogeneous gneiss + liquid + grt, Capricorn North quarry	CQ-C1; CQ-C2 (Vézinet et al. 2018)	Maybe 2920 to 2850	By analogy with nearby samples - emplacement age 2920, melting 2850, reheating 2715 ?	
SWASA-138	CNRS0000024494	−23.432202	29.765467	Vein in gneiss	NK. III	Baviaanskloof Gneisses	Grt+crd vein in gneiss, Capricon North quarry	LP-17-02 (Moyen et al. In prep)	2850/2713	Monazite ages (Moyen and Paquette, unpub)	
SWASA-139	CNRS0000024495	−23.525552	29.703535	Granitoid	NK. IV	Matok pluton	Diorite	MAT9, MAT10 (Laurent et al., 2014a, b, c)	2680	Same unit (Laurent et al. 2013)	Magma mixing visible on the outcrop, possibly heterogeneous samples
SWASA-140	CNRS0000024496	−23.525552	29.703535	Granitoid	NK. IV	Matok pluton	Mxed granodiorite	MAT11 to 14 (Laurent et al., 2014a, b, c)	2679	MAT13, Laurent et al. 2013	
SWASA-141	CNRS0000024497	−23.525552	29.703535	Granitoid	NK. IV	Matok pluton	Late pink aplite/ pegmatite		< 2680	Implied from field relations	
SWASA-142	CNRS0000024498	−23.748342	29.312272	Granitoid	NK. IV	Moletsi pluton	Dark porphyritic fine grained grd	MOL-2c (Laurent et al. 2013)	2688	This locality, Laurent et al. 2013	
SWASA-143	CNRS0000024499	−23.748342	29.312272	Granitoid	NK. IV	Moletsi pluton	(heterogeneous) porph pink granite	MOL-2a (Laurent et al. 2013)	2688	Implied from field relations (comagmatic)	

(*continued on next page*)

Table A1 (*continued*)

Sample	IGSN	Latitude	Longitude	Rock Type	Stage	Unit	Description	Equivalent sample from literature	Age (Ma)	Reference for age and comments	Notes
SWASA-144	CNRS0000024500	−23.700327	29.305093	Granitoid	NK. IV	Moletsi pluton	Coarse grained pink granite	MOL5c (Laurent et al. 2013)	2685	This locality, Laurent et al. 2013	
SWASA-145	CNRS0000024501	−23.700327	29.305093	Granitoid	NK. IV	Moletsi pluton	Dark porphyritic fine grained grd, late dyke	MOL5a (Laurent et al. 2013)	< 2685	Implied from field relations	
SWASA-146	CNRS0000024502	−23.724145	28.984544	Granitoid	NK. IV	Matlala pluton	Coarse grained pink granite		2693	Implied from field relations (comagmatic)	
SWASA-147	CNRS0000024503	−23.724145	28.984544	Granitoid	NK. IV	Matlala pluton	Dark porphyritic fine grained granodiorite	ca. 1 km from MTL43 (Laurent et al. 2013)	2693	Same unit nearby (Laurent et al. 2013)	
SWASA-148	CNRS0000024504	−23.759212	29.045686	Granitoid	NK. IV	Matlala pluton	Coarse grained pink granite	ca. 1 km from MTL31 (Laurent et al. 2013)	2690	Same unit nearby (Laurent et al. 2013)	
SWASA-149	CNRS0000024505	−23.792538	29.127546	Vein in gneiss	NK. II	Hout River Gneisses	Trondhjemitic gneiss	HRG1 (Laurent et al. 2013)	2953	Laurent & Zeh 2015	
SWASA-150	CNRS0000024506	−23.792538	29.127546	Amphibolite	NK. II	Hout River Gneisses	Amphibolite		Maybe 2940-2950	Typical age of amphibolites regionally	
SWASA-151	CNRS0000024507	−23.792538	29.127546	Vein in gneiss	NK. III	Hout River Gneisses	Pink fine grained granite	HRG2 (Laurent et al. 2013)	2833	Laurent & Zeh 2015	
SWASA-152	CNRS0000024508	−23.945224	29.129752	Granitoid	NK. IV	Mashashane pluton	Dark porphyritic fine grained grd	MAS23 (Laurent et al. 2013)	2680	Same unit, Laurent et al. 2013	

Comments on the terms used in the table: **(i) Rock type.** *Granitoid*: undeformed or weakkly deformed igneous rock, preserving original igneous textures; or more deformed portion of a pluton dominantly preserved. *Deformed granitoid*: granitoid having undergone solid-state deformation; no portion of the pluton preserves igneous textures. *Gneiss*: Composite gneiss (or portion of a composite gneiss), solid state deformation, generally evidence for multiple igneous, anatectic or metamorphic events, commonly multiple phases transposed. *Vein in gneiss*: leucosomes, small dykes and masses of aplite, pegmatite, granite; generally cutting the gneissic fabric. May represent in-situ melting or injection. **(ii) Equivalent sample** means same rock type, same unit, same locality (or close). Sometimes same block/dyke/ledge. **(iii) Ages** prefixed by "*Maybe*" are best estimate based on regional geology, no actual data. **(iv). Reference for ages** use the following conventions: *Same rock*: sample taken from the same facies and the same block/ledge. Normally < 1 m. *This locality*: on the same outcrop, facies can be correlated to SWASA sample. Often within < 10 m. *Same unit, nearby*: same stratigraphic/lithological unit, within < 1 km. *Same unit*: same stratigraphic/lithological unit.

Appendix B. Supplementary data

Supplementary data to this article can be found online at https://doi.org/10.1016/j.earscirev.2024.104680.

References

Agangi, A., Hofmann, A., Elburg, M.A., 2018. A review of Palaeoarchaean felsic volcanism in the eastern Kaapvaal craton: linking plutonic and volcanic records. Geosci. Front. 9, 667–688.

Anhaeusser, C.R., 1983. The geology of the Schapenburg greenstone remnant and surrounding Archaean granitic terrane south of Badplaas, Eastern Trasvaal, Contributions to the geology of the Barberton Mountain land. Geological Society of South Africa, pp. 31–44.

Anhaeusser, C.R., 2006. A reevaluation of Archean intracratonic terrane boundaries on the Kaapvaal Craton, South Africa: Collisional suture zones? Special Papers of the Geological Society of America, 405, p. 193.

Anhaeusser, C., 2019. The geology and tectonic evolution of the northwest part of the Barberton Greenstone Belt, South Africa: A review. S. Afr. J. Geol. 122, 421–454.

Anhaeusser, C.R., Robb, L.J., 1980. Regional and detailed field and geochemical studies of archean trondhjemitic gneisses, migmatites and greenstone xenoliths in the southern part of the Barberton mountain land, South Africa. Precambrian Res. 11, 373–397.

Anhaeusser, C.R., Robb, L.J., 1983a. Chemical analyses of granitoid rocks from the Barberton Mountain Land, 9. Geological Society of South Africa Special Publication, pp. 189–219.

Anhaeusser, C.R., Robb, L.J., 1983b. Geological and geochemical characteristics of the Heeenveen and Mpuluzi batholiths south of the Barberton greenstone belt, and premliminary thoughts on their petrogenesis, Contributions to the geology of the Barberton Mountain land. Geological Society of South Africa, pp. 131–151.

Anhaeusser, C.R., Robb, L.J., Viljoen, M.J., 1981. Provisonnal Geological Map of the Barberton Greenstone Belt and Surrounding Granitic Terrane, Eastern Transvaal and Swaziland (1:250 000). Geological Society of South Africa Special Publication. Geological Society of South Africa.

Anhaeusser, C.R., Robb, L.J., Viljoen, M.J., 1983. Notes on the provisionnal geological map of the Barberton greenstone belt and surrounding granitic terrane, eastern Transvaal and Swaziland (1:250 000 color map). Trans. Geol. Soc. S. Afr. 9, 221–223.

Armstrong, R.L., 1981. Radiogenic isotopes: the case for crustal recycling on a near-steady-state no-continental-growth Earth. Philos. Trans. R. Soc. Lond. 301, 443–472.

Bauer, A.M., Fisher, C.M., Vervoort, J.D., Bowring, S.A., 2017. Coupled zircon Lu–Hf and U–Pb isotopic analyses of the oldest terrestrial crust, the> 4.03 Ga Acasta Gneiss Complex. Earth Planet. Sci. Lett. 458, 37–48.

Bédard, J.H., 2013. How many arcs can dance on the head of a plume?: A 'Comment'on: A critical assessment of Neoarchean 'plume only'geodynamics: evidence from the Superior province, by Derek Wyman, Precambrian Research, 2012. Precambrian Res. 229, 189–197.

Bédard, J.H., 2018. Stagnant lids and mantle overturns: Implications for Archaean tectonics, magmagenesis, crustal growth, mantle evolution, and the start of plate tectonics. Geosci. Front. 9, 19–49.

Bédard, J.H., Harris, L.B., 2014. Neoarchean disaggregation and reassembly of the Superior craton. Geology G35770, 35771.

Belcher, R.W., Kisters, A.F.M., 2006a. Progressive adjustments of ascent and emplacement controls during incremental construction of the 3.1 Ga Heerenveen batholith, South Africa. J. Struct. Geol. 28, 1406–1421.

Belcher, R.W., Kisters, A.F.M., 2006b. Syntectonic emplacement and deformation of the Heerenveen batholith: conjectures on the structural setting of the 3.1 Ga granite magmatism in the Barberton granite-greenstone terrain, South Africa. Geol. Soc. Am. Spec. Publ. 405, 211–231.

Block, S., Moyen, J.F., Zeh, A., Poujol, M., Jaguin, J., Paquette, J.L., 2013. The Murchison Greenstone Belt, South Africa: Accreted slivers with contrasting metamorphic conditions. Precambrian Res. 227, 77–98.

Bonin, B., Janousek, V., Moyen, J.F., 2020. Chemical variation, modal composition and classification of granitoids. In: Janousek, V., Bonin, B., Collins, W.J., Farina, F., Bowden, P. (Eds.), Post-Archean Granitic Rocks: Petrogenetic Processes and Tectonic Environments. Geological Society of London, pp. 9–51.

Brey, G.P., Shu, Q., 2018. The birth, growth and ageing of the Kaapvaal subcratonic mantle. Mineral. Petrol. 112, 23–41.

Byerly, G., Lowe, D., Heubeck, C., 2018. Geologic Evolution of the Barberton Greenstone Belt–A Unique Record of Crustal Development, Surface Processes, and Early Life 3.55 to 3.20 Ga. Earth's Oldest Rocks, 2nd edn. Elsevier, Berlin.

Cagnard, F., Durrieu, N., Gapais, D., Brun, J.P., Ehlers, C., 2006. Crustal thickening and lateral flow during compression of hot lithospheres, with particular reference to Precambrian times. Terra Nova 18, 72–78.
Capitanio, F.A., Nebel, O., Moyen, J.F., Cawood, P.A., 2022. Craton Formation in early Earth Mantle Convection Regimes. J. Geophys. Res. Solid Earth 127.
Cawood, P.A., Hawkesworth, C., Dhuime, B., 2013. The continental record and the generation of continental crust. Geol. Soc. Am. Bull. 125, 14–32.
Cawood, P.A., Chowdhury, P., Mulder, J.A., Hawkesworth, C.J., Capitanio, F.A., Gunawardana, P.M., Nebel, O., 2022. Secular Evolution of Continents and the Earth System.
Champion, D.C., Cassidy, K.F., 2007. An overview of the Yilgarn Craton and its crustal evolution. In: Bierlein, F.P., Knox-Robinson, C.M. (Eds.), Kalgoorlie 07' Conference. Proceedings of Geoconferences (WA) Inc. Geoscience Australia Record, pp. 13–35.
Champion, D.C., Sheraton, J.W., 1997. Geochemistry and Nd isotope systematics of Archaean of the Eastern Goldfields, Yilgarn Craton, Australia: implications for crustal growth processes. Precambrian Res. 83.
Champion, D.C., Smithies, R.H., 2007. Geochemistry of Paleoarchean granites of the East Pilbara Terrane, Pilbara Craton, Western Australia: Implications for early Archean crustal growth. In: Van Kranendonk, M.J., Smithies, R.H., Bennett, V. (Eds.), Earth's Oldest Rocks. Elsevier, pp. 369–410.
Chardon, D., Jayananda, M., 2008. Three-dimensional field perspective on deformation, flow, and growth of the lower continental crust (Dharwar craton, India). Tectonics 27, TC1014.
Chardon, D., Jayananda, M., Chetty, T.R.K., Peucat, J.J., 2008. Precambrian continental strain and shear zone patterns: south Indian case. J. Geophys. Res. Solid Earth 113.
Chardon, D., Gapais, D., Cagnard, F., 2009. Flow of ultra-hot orogens: A view from the Precambrian, clues for the Phanerozoic. Tectonophysics 477, 105–118.
Chardon, D., Jayananda, M., Peucat, J.J., 2011. Lateral constrictional flow of hot orogenic crust: Insights from the Neoarchean of South India, geological and geophysical implications for orogenic Plateaux. Geochem. Geophys. Geosyst. 12, Q02005.
Chavagnac, V., 2004. A geochemical and Nd isotopic study of Barberton komatiites (South Africa): implication for the Archean mantle. Lithos 75, 253–281.
Chelle-Michou, C., McCarthy, A., Moyen, J.-F., Cawood, P., Capitanio, F., 2022. Make subduction diverse again. Earth Sci. Rev. 226, 103966.
Chowdhury, P., Chakraborty, S., Gerya, T.V., Cawood, P.A., Capitanio, F.A., 2020. Peel-back controlled lithospheric convergence explains the secular transitions in Archean metamorphism and magmatism. Earth Planet. Sci. Lett. 538, 116224.
Clemens, J.D., Belcher, R.W., Kisters, A.F.M., 2010. The Heerenveen Batholith, Barberton Mountain Land, South Africa: Mesoarchaean, Potassic, Felsic Magmas formed by Melting of an Ancient Subduction complex. J. Petrol. 51, 1099.
Collins, W.J., Murphy, J.B., Johnson, T.E., Huang, H., 2020. Critical role for water in the formation of continental crust. Nat 13 (5), 331–338.
Compston, W., Kröner, A., 1988. Multiple zircon growth within early Archean tonalitic gneiss from the Ancient Gneiss complex, Swaziland. Earth Planet. Sci. Lett. 87, 13–28.
Condie, K.C., 2005a. High field strength element ratios in Archean basalts: a window to evolving sources of mantle plumes? Lithos 79, 491–504.
Condie, K.C., 2005b. TTGs and adakites: are they both slab melts? Lithos 80, 33–44.
Couzinié, S., Laurent, O., Moyen, J.F., Zeh, A., Bouilhol, P., Villaros, A., 2017. Post-collisional magmas: Isotopically camouflaged contributors to crustal growth. In: Goldschmidt Conference, Paris.
Czarnota, K., Champion, D., Goscombe, B., Blewett, R., Cassidy, K., Henson, P., Groenewald, P., 2010. Geodynamics of the eastern Yilgarn Craton. Precambrian Res. 183, 175–202.
Dey, S., 2013. Evolution of Archaean crust in the Dharwar craton: the Nd isotope record. Precambrian Res. 227, 227–246.
Dhuime, B., Wuestefeld, A., Hawkesworth, C.J., 2015. Emergence of modern continental crust about 3 billion years ago. Nat. Geosci. 8, 552–555.
Diener, J., Stevens, G., Kisters, A.F.M., Poujol, M., 2005. Metamorphism and exhumation of the basal parts of the Barberton greenstone belt, South Africa: Constraining the rates of mid-Archaean tectonism. Precambrian Res. 143, 87–112.
Drabon, N., Lowe, D.R., 2021. Progressive accretion recorded in sedimentary rocks of the 3.28– 3.23 Ga Fig tree Group, Barberton Greenstone Belt. GSA Bull. 134, 5–6.
Drabon, N., Byerly, B.L., Byerly, G.R., Wooden, J.L., Keller, C.B., Lowe, D.R., 2021. Heterogeneous Hadean crust with ambient mantle affinity recorded in detrital zircons of the Green Sandstone Bed, South Africa. Proc. Natl. Acad. Sci. 118, e2004370118.
Dziggel, A., Stevens, G., Poujol, M., Anhaeusser, C.R., Armstrong, R.A., 2002. Metamorphism of the granite-greenstone terrane South of the Barberton greenstone belt, South Africa: an insight into the tectono-thermal evolution of the 'lower' portions of the Onverwacht group. Precambrian Res. 114, 221–247.
Eglington, B., Armstrong, R., 2004. The Kaapvaal Craton and adjacent orogens, southern Africa: a geochronological database and overview of the geological development of the craton. S. Afr. J. Geol. 107, 13–32.
Elburg, M.A., Poujol, M., 2020. Lu-Hf analyses of zircon from the Makoppa Dome and Amalia-Kraaipan area: implications for evolution of the Kimberley and Pietersburg blocks of the Kaapvaal Craton. S. Afr. J. Geol. 2020 (123), 369–380.
Eriksson, P., Altermann, W., Hartzer, F., Johnson, M., Anhaeusser, C., Thomas, R., 2006. The Transvaal Supergroup and its precursors. Geol. S. Afr. 237–260.
Fedo, C.M., Wayne Nesbitt, H., Young, G.M., 1995. Unraveling the effects of potassium metasomatism in sedimentary rocks and paleosols, with implications for paleoweathering conditions and provenance. Geology 23, 921–924.
Fouch, M.J., James, D.E., VanDecar, J.C., Van der Lee, S., Group, K.S., 2004. Mantle seismic structure beneath the Kaapvaal and Zimbabwe Cratons. S. Afr. J. Geol. 107, 33–44.
Fowler, M., Rollinson, H., 2012. Phanerozoic sanukitoids from Caledonian Scotland: implications for Archean subduction. Geology 40, 1079–1082.
Furnes, H., Robins, B., de Wit, M.J., 2012. Geochemistry and petrology of lavas in the upper Onverwacht Suite, Barberton Mountain land, South Africa. S. Afr. J. Geol. 115, 171–210.
Gapais, D., Potrel, A., Machado, N., Hallot, E., 2005. Kinematics of long-lasting Paleoproterozoic transpression within the Thompson Nickel Belt, Manitoba, Canada. Tectonics 24.
Greber, N.D., Dauphas, N., 2019. The chemistry of fine-grained terrigenous sediments reveals a chemically evolved Paleoarchean emerged crust. Geochim. Cosmochim. Acta 255, 247–264.
Greber, N.D., Dauphas, N., Bekker, A., Ptáček, M.P., Bindeman, I.N., Hofmann, A., 2017. Titanium isotopic evidence for felsic crust and plate tectonics 3.5 billion years ago. Science 357, 1271–1274.
Griffin, W., Pearson, N., Belousova, E., Jackson, S., Van Achterbergh, E., O'Reilly, S.Y., Shee, S., 2000. The Hf isotope composition of cratonic mantle: LAM-MC-ICPMS analysis of zircon megacrysts in kimberlites. Geochim. Cosmochim. Acta 64, 133–147.
Guitreau, M., Blichert-Toft, J., Martin, H., Mojzsis, S.J., Albarède, F., 2012. Hafnium isotope evidence from Archean granitic rocks for deep-mantle origin of continental crust. Earth Planet. Sci. Lett. 337-338, 211–223.
Harris, L.B., Bédard, J.H., 2015. Interactions between continent-like 'drift', rifting and mantle flow on Venus: gravity interpretations and Earth analogues. Geol. Soc. Lond. Spec. Publ. 401, 327–356.
Hastie, T., Tibshirani, R., 1990. Generalized Additive Models. In: Monographs on Statistics & Applied Probability. Chapman and Hall/CRC, p. 1.
Hawkesworth, C.J., Cawood, P.A., Dhuime, B., 2020. The Evolution of the Continental Crust and the Onset of Plate Tectonics. Front. Earth Sci. 8.
Heilimo, E., Halla, J., Andersen, T., Huhma, H., 2013. Neoarchean crustal recycling and mantle metasomatism: Hf–Nd–Pb–O isotope evidence from sanukitoids of the Fennoscandian shield. Precambrian Res. 228, 250–266.
Henderson, D.R., Long, L.E., Barton Jr., J.M., 2000. Isotopic ages and chemical and isotopic composition of the Archaean Turfloop batholith, Pietersburg granite-greenstone terrane, Kaapvaal craton, South Africa. S. Afr. J. Geol. 103, 38–46.
Heubeck, C., Lowe, D.R., 1999. Sedimentary petrography and provenance of Archean Moodies group, Barberton Greenstone belt. Geol. Soc. Am. Spec. Pap. 329, 259–286.
Heubeck, C., Engelhardt, J., Byerly, G.R., Zeh, A., Sell, B., Luber, T., Lowe, D.R., 2013. Timing of deposition and deformation of the Moodies Group (Barberton Greenstone Belt, South Africa): Very-high-resolution of Archaean surface processes. Precambrian Res. 231, 236–262.
Hoffmann, J., Kröner, A., 2018. Early Archaean crustal evolution in southern Africa—an updated record of the Ancient Gneiss complex of Swaziland. In: Earth's Oldest Rocks, 2nd edn. Elsevier, Amsterdam, pp. 553–567.
Hoffmann, J.E., Zhang, C., Moyen, J.-F., Nagel, T.J., 2019. The formation of tonalites-trondjhemites-granodiorites and of the early continental crust. In: Van Kranendonk, M., Bennett, V., Hoffmann, J.E. (Eds.), Earth Oldest Rocks, 2nd ed. Elsevier, pp. 133–168.
Hofmann, A., Harris, C., 2008. Silica alteration zones in the Barberton greenstone belt: a window into subseafloor processes 3.5–3.3 Ga ago. Chem. Geol. 257, 221–239.
Jaguin, J., Gapais, D., Poujol, M., Boulvais, P., Moyen, J.-F., 2012a. The Murchison greenstone belt (South Africa): a general tectonic framework. S. Afr. J. Geol. 115, 65–76.
Jaguin, J., Poujol, M., Boulvais, P., Robb, L., Paquette, J.-L., 2012b. Metallogeny of precious and base metal mineralization in the Murchison Greenstone Belt, South Africa: indications from U–Pb and Pb–Pb geochronology. Mineral. Deposita 47, 739–747.
Jochum, K.P., Weis, U., Schwager, B., Stoll, B., Wilson, S.A., Haug, G.H., Andreae, M.O., Enzweiler, J., 2016. Reference Values following ISO guidelines for frequently Requested Rock Reference Materials. Geostand. Geoanal. Res. 40, 333–350.
Johnson, M., Anhaeusser, C., Thomas, R., 2006. The Geological Society of South Africa. Johannesburg Council for Geoscience.
Klausen, M., Söderlund, U., Olsson, J., Ernst, R., Armoogam, M., Mkhize, S., Petzer, G., 2010. Petrological discrimination among Precambrian dyke swarms: eastern Kaapvaal craton (South Africa). Precambrian Res. 183, 501–522.
Korenaga, J., 2018. Estimating the formation age distribution of continental crust by unmixing zircon ages. Earth Planet. Sci. Lett. 482, 388–395.
Kramers, J.D., McCourt, S., van Reenen, D., 2006. The Limpopo belt. In: Johnson, M.R. W., Anhaeusser, C.R., Thomas, R.J. (Eds.), The Geology of South Africa. Council for Geosciences, Pretoria, pp. 209–236.
Kramers, J.D., Henzen, M., Steidle, L., 2014. Greenstone belts at the northernmost edge of the Kaapvaal Craton: timing of tectonic events and a possible crustal fluid source. Precambrian Res. 253, 96–113.
Kreissig, K., Nägler, T.F., Kramers, J.D., Van Reenen, D., Smit, C.A., 2000. An isotopic and geochemical study of the northern Kaapvaal Craton and the Southern marginal Zone of the Limpopo Belt: are they juxtaposed terranes? Lithos 50, 1–25.
Kröner, A., Brandl, G., Jaeckel, P., 1996a. Single zircon age for the felsic Rubbervale Formation, Murchison greenstone belt, South Africa. S. Afr. J. Geol. 99, 229–234.
Kröner, A., Hegner, E., Wendt, J.I., Byerly, G.R., 1996b. The oldest part of the Barberton granitoid-greenstone terrain, South Africa: evidence for crust formation between 3.5 and 3.7 Ga. Precambrian Res. 78, 105–124.
Kröner, A., Jaeckel, P., Brandl, G., 2000. Single zircon ages for felsic to intermediate rocks from the Pietersburg and Giyani greenstone belts and bordering granitoid orthogneisses, northern Kaapvaal Craton, South Africa. S. Afr. J. Geol. 30, 773–793.
Kröner, A., Hoffmann, J.E., Xie, H., Münker, C., Hegner, E., Wan, Y., Hofmann, A., Liu, D., Yang, J., 2014. Generation of early Archaean grey gneisses through melting

of older crust in the eastern Kaapvaal craton, southern Africa. Precambrian Res. 255, 823–846.
Kröner, A., Hoffmann, J.E., Wong, J.M., Geng, H.-Y., Schneider, K.P., Xie, H., Yang, J.-H., Nhleko, N., 2019. Archaean crystalline rocks of the Eastern Kaapvaal Craton, the Archaean Geology of the Kaapvaal Craton, Southern Africa. Springer, pp. 1–32.
Lahaye, Y., Arndt, N., Byerly, G., Chauvel, C., Fourcade, S., Gruau, G., 1995. The influence of alteration on the trace-element and Nd isotopic compositions of komatiites. Chem. Geol. 126, 43–64.
Lana, C., Tohver, E., Cawood, P., 2010. Quantifying rates of dome-and-keel formation in the Barberton granitoid-greenstone belt, South Africa. Precambrian Res. 177, 199–211.
Laurent, O., 2012. Les changements géodynamiques à la transition Archéen-Protérozoïque : étude des granitoïdes de la marge Nord du craton du Kaapvaal (Afrique du Sud), Laboratoire Magmas et Volcans. Université Blaise Pascal, Clermont-Ferrand, p. 531.
Laurent, O., Zeh, A., 2015. A linear Hf isotope-age array despite different granitoid sources and complex Archean geodynamics: example from the Pietersburg block (South Africa). Earth Planet. Sci. Lett. 430, 326–338.
Laurent, O., Paquette, J.-L., Martin, H., Doucelance, R., Moyen, J.-F., 2013. LA-ICP-MS dating of zircons from Meso- and Neoarchean granitoids of the Pietersburg block (South Africa): Crustal evolution at the northern margin of the Kaapvaal craton. Precambrian Res. 230, 209–226.
Laurent, O., Martin, H., Moyen, J.-F., Doucelance, R., 2014a. The diversity and evolution of late-Archaean granitoids: evidence for the onset of "modern-style" plate tectonics between 3.0 and 2.5 Ga. Lithos 205, 208–235.
Laurent, O., Rapopo, M., Stevens, G., Moyen, J.-F., Martin, H., Doucelance, R., Bosq, C., 2014b. Contrasting petrogenesis of Mg-K and Fe-K granitoids and implications for postcollisional magmatism: case study from the late-Archaean Matok pluton (Pietersburg block, South Africa). Lithos 196-197, 131–149.
Laurent, O., Rapopo, M., Stevens, G., Moyen, J.F., Martin, H., Doucelance, R., 2014c. Contrasting petrogenesis of Mg-K and Fe-K granitoids and implications for post-collisional magmatism: case study from the late-Archaean Matok pluton (South Africa). EGU, Vienna pp. EGU2014-5341.
Laurent, O., Zeh, A., Brandl, G., Vézinet, A., Wilson, A., 2019. Granitoids and Greenstone Belts of the Pietersburg Block—Witnesses of an Archaean Accretionary Orogen along the Northern Edge of the Kaapvaal Craton. In: A, K., A, H. (Eds.), The Archaean Geology of the Kaapvaal Craton, Southern Africa. Springer.
Laurent, O., Björnsen, J., Wotzlaw, J.-F., Bretscher, S., Pimenta Silva, M., Moyen, J.F., Ulmer, P., Bachmann, O., 2020. Earth's earliest granitoids are crystal-rich magma reservoirs tapped by silicic eruptions. Nat. Geosci. 13, 163–169.
Lenardic, A., 2018a. The diversity of tectonic modes and thoughts about transitions between them. Philos. Trans. R. Soc. A Math. Phys. Eng. Sci. 376, 20170416.
Lenardic, A., 2018b. Volcanic-Tectonic modes and planetary life potential. In: Handbook of Exoplanets, pp. 2897–2916.
Lewis, J.A., Hoffmann, J.E., Schwarzenbach, E.M., Strauss, H., Liesegang, M., Rosing, M. T., 2021. Sulfur isotope evidence for surface-derived sulfur in Eoarchean TTGs. Earth Planet. Sci. Lett. 576, 117218.
Lowe, D., Byerly, G., Heubeck, C., 2012. Geologic Map of the West-Central Barberton Greenstone Belt, South Africa, Scale 1: 25,000. In: Geological Society of America Map and Chart Series.
Madlakana, N., Stevens, G., 2018. Plagioclase disequilibrium induced during fluid-absent biotite-breakdown melting in metapelites. J. Metamorph. Geol. 36, 1097–1116.
Madlakana, N., Stevens, G., Bracciali, L., 2020. Paleoproterozoic amphibolite facies retrogression and exhumation of Archean metapelitic granulites in the Southern marginal Zone of the Limpopo Belt, South Africa. Precambr. Res. 337, 105532.
Marsh, J.S., 2006. The Dominion Group. The Geology of South Africa. Council for Geoscience, Pretoria, pp. 149–154.
Martin, H., Moyen, J.-F., 2002. Secular changes in TTG composition as markers of the progressive cooling of the Earth. Geology 30, 319–322.
Martin, H., Smithies, R., Rapp, R., Moyen, J., Champion, D., 2005. An overview of adakite, tonalite-trondhjemite-granodiorite (TTG), and sanukitoid: relationships and some implications for crustal evolution. Lithos 79, 1–24.
McCarthy, T.S., 2006. The Witwatersrand Supergroup. The Geology of South Africa. Council for Geoscience, Pretoria, pp. 155–186.
McCoy-West, A.J., Chowdhury, P., Burton, K.W., Sossi, P., Nowell, G.M., Fitton, J.G., Kerr, A.C., Cawood, P.A., Williams, H.M., 2019. Extensive crustal extraction in Earth's early history inferred from molybdenum isotopes. Nat. Geosci. 12, 946–951.
McCoy-West, A.J., Millet, M.-A., Nowell, G.M., Nebel, O., Burton, K.W., 2020. Simultaneous measurement of neodymium stable and radiogenic isotopes from a single aliquot using a double spike. J. Anal. At. Spectrom. 35, 388–402.
McCoy-West, A.J., Mortimer, N., Burton, K.W., Ireland, T.R., Cawood, P.A., 2022. Re-initiation of plutonism at the Gondwana margin after a magmatic hiatus: the bimodal Permian-Triassic Longwood Suite, New Zealand. Gondwana Res. 105, 432–449.
Meyer, F.M., Robb, L.J., Reimold, W.U., de Bruiyn, H., 1994. Contrasting low and high-ca plutons in the Barberton Mountain Land, southern Africa. Lithos 32, 63–76.
Mole, D.R., Fiorentini, M.L., Thebaud, N., Cassidy, K.F., McCuaig, T.C., Kirkland, C.L., Romano, S.S., Doublier, M.P., Belousova, E.A., Barnes, S.J., 2014. Archean komatiite volcanism controlled by the evolution of early continents. Proc. Natl. Acad. Sci. 111, 10083–10088.
Moyen, J.-F., 2009. High Sr/Y and La/Yb ratios: the meaning of the "adakitic signature". Lithos 112, 556–574.
Moyen, J.-F., 2011. The composite Archaean grey gneisses: Petrological significance, and evidence for a non-unique tectonic setting for Archaean crustal growth. Lithos 123, 21–36.
Moyen, J.F., 2020. Archaean granitoids: Classification, petrology, geochemistry and origin. In: Dey, S., Moyen, J.F. (Eds.), Archean Granitoids of India: Windows into Early Earth Tectonics. Geological Society of London.
Moyen, J.-F., Laurent, O., 2018. Archaean tectonic systems: a view from igneous rocks. Lithos 302-303, 99–125.
Moyen, J.-F., Martin, H., 2012. Forty years of TTG research. Lithos 148, 312–336.
Moyen, J.-F., Stevens, G., Kisters, A.F.M., Belcher, R.W., Lemirre, B., 2018. TTG plutons of the Barberton granitoid-greenstone terrain, South Africa. In: Van Kranendonk, M., Bennett, V., Hoffmann, J.E. (Eds.), Earth Oldest Rocks, 2nd ed. Elsevier, pp. 615–654.
Moyen, J.-F., Chauvet, A., Vézinet, A., Paquette, J.-L., Cochelin, B., Bruand, E., Diener, J., Stevens, G., 2021a. 200 Ma de deformation et de fusion partielle dans la croute Archéenne: la marge Nord du Craton du Kaapvaal, Afrique du Sud, 27e édition de la Réunion des Sciences de la Terre.
Moyen, J.-F., Laurent, O., Cawood, P.A., Nebel, O., Capitanio, F., Chelle-Michou, C., Mac Carthy, A., 2021b. Weighing the evidence: do Archaean igneous compositions forbid, allow, suggest or require plate tectonics?. In: Goldschmidt 2021 Virtual 4–9 July.
Moyen, J.-F., Zeh, A., Cuney, M., Dziggel, A., Carrouée, S., 2021c. The multiple ways of recycling Archaean crust : a case study from the ca. 3.1 Ga granitoids from the Barberton Greenstone Belt, South Africa. Precambrian Res. 353 article 105998.
Mühlberg, M., Stevens, G., Moyen, J.-F., Kisters, A.F.M., Lana, C., 2021. Thermal evolution of the Stolzburg Block, Barberton granitoid-greenstone terrain, South Africa: Implications for Paleoarchean tectonic processes. Precambrian Res. 359, 106082.
Naeraa, T., Scherstén, A., Rosing, M., Kemp, A., Hoffmann, J., Kokfelt, T., Whitehouse, M., 2012. Hafnium isotope evidence for a transition in the dynamics of continental growth 3.2 Gyr ago. Nature 485, 627–630.
Nägler, T.F., Kramers, J., 1998. Nd isotopic evolution of the upper mantle during the Precambrian: models, data and the uncertainty of both. Precambrian Res. 91, 233–252.
Nesbitt, H.W., Young, G.M., 1982. Early Proterozoic climates and plate motions inferred from major element chemistry of lutites. Nature 299, 715–717.
Nguuri, T., Gore, J., James, D., Webb, S., Wright, C., Zengeni, T., Gwavava, O., Snoke, J., Group, K.S., 2001. Crustal structure beneath southern Africa and its implications for the formation and evolution of the Kaapvaal and Zimbabwe cratons. Geophys. Res. Lett. 28, 2501–2504.
Nicoli, G., Stevens, G., Moyen, J.-F., Frei, D., 2015. Rapid evolution from sediment to anatectic granulite in an Archean continental collision zone: the example of the Bandelierkop Formation metapelites, South marginal Zone, Limpopo Belt, South Africa. J. Metamorph. Geol. 33, 177–202.
Nicoli, G., Stevens, G., Moyen, J.F., Vézinet, A., Mayne, M., 2017. Insights into the complexity of crustal differentiation from K2O-poor leucosomes within metapelitic migmatites: Southern marginal Zone of the Limpopo Belt, South Africa. J. Metamorph. Geol. 35, 999–1022.
O'Connor, J.T., 1965. A classification for quartz-rich igneous rocks based on feldspar ratios. U.S. Geological Survey Professionnal Paper, 525, pp. 79–84.
Ohta, T., Arai, H., 2007. Statistical empirical index of chemical weathering in igneous rocks: A new tool for evaluating the degree of weathering. Chem. Geol. 240, 280–297.
O'Neill, H.S.C., 2016. The smoothness and shapes of chondrite-normalized rare earth element patterns in basalts. J. Petrol. 57, 1463–1508.
Parman, S.W., Grove, T.L., Dann, J.C., 2001. The production of Barberton komatiites in an Archean subduction zone. Geophys. Res. Lett. 28, 2513–2516.
Passeraub, M., Wuest, T., Kreissig, K., Smit, C., Kramers, J.D., 1999. Structure, metamorphism, and geochronology of the Rhenosterkoppies greenstone belt, South Africa. S. Afr. J. Geol. 102, 323–334.
Pearce, J.A., 2008. Geochemical fingerprinting of oceanic basalts with applications to ophiolite classification and the search for Archean oceanic crust. Lithos 100, 14–48.
Poujol, M., 2001. U-Pb isotopic evidence for episodic granitoid emplacement in the Murchison greenstone belt, South Africa. J. Afr. Earth Sci. 33, 155–163.
Poujol, M., Anhaeusser, C.R., 2001. The Johannesburg dome, South Africa: new single zircon U-Pb isotopic evidence for early Archaean granite-greenstone development within the central Kaapvaal craton. Precambrian Res. 108, 139–157.
Poujol, M., Robb, L.J., 1999. New U-Pb ages on gneisses and pegmatite from South of the Murchison greenstone belt, South Africa. S. Afr. J. Geol. 102, 93–97.
Poujol, M., Robb, L.J., Anhaeusser, C.R., Gericke, B., 2003. A review of the geochronological constraints on the evolution of the Kaapvaal craton, South Africa. Precambrian Res. 127, 181–213.
Poujol, M., Jaguin, J., Moyen, J.-F., Boulvais, P., Paquette, J.L., 2021. Archean S-Type granites: petrology, geochemistry and geochronology of the Lekkersmaak and Willie plutons, Kaapvaal Craton, South Africa. S. Afr. J. Geol. 124, 87–110.
Puchtel, I.S., Walker, R.J., Touboul, M., Nisbet, E.G., Byerly, G.R., 2014. Insights into early Earth from the Pt–Re–Os isotope and highly siderophile element abundance systematics of Barberton komatiites. Geochim. Cosmochim. Acta 125, 394–413.
Reimold, W.U., Gibson, R.L., 1996. Geology and evolution of the Vredefort impact structure, South Africa. J. Afr. Earth Sci. 23, 125–162.
van Rensburg, D.J., Heubeck, C., Reimann, S., 2021. Volcanoes in the estuaries: Insights into Earth's oldest (3.22 Ga) terrestrial microbial habitats, Moodies Group, Barberton Greenstone Belt. Precambrian Res. 365, 106325.
van Rensburg, D.J., Heubeck, C., Reimann, S., 2023. Constraints from the Ntaba Mhlope Syncline and the Mkomozane Homocline, Moodies Group (3.22 Ga), Eswatini, on the deformation of the southern margin of the Barberton greenstone belt. J. Afr. Earth Sci. 205, 104989.
Robb, L.J., 1978. A general geological description of the Archaean granitic terrane between Nelspruit and Bushbuckridge, Eastern Transvaal. Trans. Geol. Soc. S. Afr. 81, 331–338.

Robb, L.J., Anhaeusser, C.R., 1983. Chemical and petrogenetic characteristics of Archaean tonalite-trondhjemite gneiss plutons in the Barberton mountain land. Geol. Soc. S. Afr. Spec. Publ. 9, 103–116.
Robb, L.J., Anhaeusser, C.R., Van Nierop, D.A., 1983. The recognition of the Nelspruit batholith north of the Barberton greenstone belt and its significance in terms of Archaean crustal evolution, pp. 117–130.
Robb, L.J., Barton Jr., J.M., Kable, E.J.D., Wallace, R.C., 1986. Geology, geochemistry and isotopic characteristics of the Archaean Kaap Valley pluton, Barberton mountain land, South Africa. Precambrian Res. 31, 1–36.
Robb, L., Brandl, G., Anhaeusser, C., Poujol, M., 2006. Archaean granitoid intrusions. Geol. S. Afr. 57–94.
Robinson, P., 2003. XRF analysis of flux-fused discs. In: Geoanalysis 2003, The 5th International Conference on the Analysis of Geological and Environmental Materials, 2003. Wiley-Blackwell.
Rudnick, R.L., Gao, S., 2014. 4.1 - Composition of the Continental Crust. In: Holland, H. D., Turekian, K.K. (Eds.), Treatise on Geochemistry, Second edition. Elsevier, Oxford, pp. 1–51.
Salop, L.I., Scheinmann, Y.M., 1969. Tectonic history and structure of plateforms and shields. Tectonophysics 7, 565–597.
Sanchez-Garrido, C., Stevens, G., Armstrong, R., Moyen, J.-F., Martin, H., Doucelance, R., 2011. Diversity in Earth's early felsic crust: Paleo-Archean peraluminous granites of the Barberton greenstone belt. Geology 39, 963–966.
Schaller, M., Steiner, O., Studer, I., Holzer, L., Herwegh, M., Kramers, J.D., 1999. Exhumation of Limpopo Central Zone granulites and dextral continent-scale transcurrent movement at 2000 Ma along the Palala shear zone, Northern Provinve, South Africa. Precambrian Res. 96, 263–288.
Schmitz, M., Heubeck, C., 2021. Constraints on deformation mechanisms of the Barberton Greenstone Belt from regional stratigraphic and structural data of the synorogenic Moodies Group. Precambrian Res. 362, 106177.
Schneider, K., Hoffmann, J., Münker, C., Patyniak, M., Sprung, P., Roerdink, D., Garbe-Schönberg, D., Kröner, A., 2019. Petrogenetic evolution of metabasalts and metakomatiites of the lower Onverwacht Group, Barberton Greenstone Belt (South Africa). Chem. Geol. 511, 152–177.
Scholl, D.W., von Huene, R., 2007. Crustal recycling at modern subduction zones applied to the past—issues of growth and preservation of continental basement crust, mantle geochemistry, and supercontinent reconstruction. Geol. Soc. Am. Mem. 200, 9–32.
Scholl, D.W., von Huene, R., 2009. Implications of estimated magmatic additions and recycling losses at the subduction zones of accretionary (non-collisional) and collisional (suturing) orogens. Geol. Soc. Lond. Spec. Publ. 318, 105–125.
Schwarz-Schampera, U., Terblanche, H., Oberthür, T., 2010. Volcanic-hosted massive sulfide deposits in the Murchison greenstone belt, South Africa. Mineral. Deposita 45, 113–145.
Shirey, S.B., Hanson, G.N., 1984. Mantle-derived Archaean monzodiorites and trachyandesites. Nature 310, 222–224.
Sizova, E., Gerya, T., Stüwe, K., Brown, M., 2015. Generation of felsic crust in the Archean: A geodynamic modelingperspective. Precambrian Res. 271, 198–224.
Smithies, R.H., 2000. The Archaean tonalite-trondhjemite-granodiorite (TTG) series is not an analogue of Cenozoic adakite. Earth Planet. Sci. Lett. 182, 115–125.
Smithies, R., Champion, D., Cassidy, K., 2003. Formation of Earth's early Archaean continental crust. Precambrian Res. 127, 89–101.
Stern, C.R., 2011. Subduction erosion: rates, mechanisms, and its role in arc magmatism and the evolution of the continental crust and mantle. Gondwana Res. 20, 284–308.
Stern, R.J., Scholl, D.W., 2010. Yin and yang of continental crust creation and destruction by plate tectonic processes. Int. Geol. Rev. 52, 1–31.
Stevens, G., Moyen, J.-F., 2007. Metamorphism in the Barberton Granite Greenstone Terrain: A record of Paleoarchean accretion. In: Van Kranendonk, M.J., Smithies, R. H., Bennett, V. (Eds.), Earth's Oldest Rocks. Elsevier, pp. 669–698.
Stevens, G., van Reenen, D., 1992. Partial melting and the origin of metapelitic granulites in the Southern marginal Zone of the Limpopo Belt, South Africa. Precambrian Res. 55, 303–319.
Tang, M., Chen, K., Rudnick, R.L., 2016. Archean upper crust transition from mafic to felsic marks the onset of plate tectonics. Science 351, 372–375.
Taylor, S.R., McLennan, S.M., 1985. The Continental Crust: Its Composition and Evolution. Blackwell Scientific Publications, Oxford, UK (312 pp.).
Taylor, J., Stevens, G., Armstrong, R., Kisters, A.F.M., 2010. Granulite facies anatexis in the Ancient Gneiss complex, Swaziland, at 2.73 Ga: Mid-crustal metamorphic evidence for mantle heating of the Kaapvaal craton during Ventersdorp magmatism. Precambrian Res. 177, 88–102.
Taylor, J., Nicoli, G., Stevens, G., Frei, D., Moyen, J.F., 2014. The processes that control leucosome compositions in metasedimentary granulites: perspectives from the Southern marginal Zone migmatites, Limpopo Belt, South Africa. J. Metamorph. Geol. 32, 713–742.
Toulkeridis, T., Clauer, N., Kroner, A., Reimer, T., Todt, W., 1999. Characterization, provenance, and tectonic setting of Fig tree greywackes from the archaean Barberton Greenstone Belt, South Africa. Sediment. Geol. 124, 113–129.
Travers, L., Chauvet, A., Lehmann, J., 2023. Structure and distribution of the Gold-Related Quartz Vein Systems in the Southwestern Part of the Barberton Greenstone Belt (South Africa, Eswatini). Minerals 13, 1034.
Trépanier, S., Mathieu, L., Daigneault, R., Faure, S., 2016. Precursors predicted by artificial neural networks for mass balance calculations: Quantifying hydrothermal alteration in volcanic rocks. Comput. Geosci. 89, 32–43.
Van der Westhuizen, W.A., De Bruiyn, H., Meintjies, P.G., 2006. The Ventersdorp Supergroup. The Geology of South Africa. Council for Geoscience, Pretoria, pp. 187–208.
Van Reenen, D.D., Smit, C.A., Perchuk, A.L., Huizenga, J.M., Safonov, O.G., Gerya, T.V., 2019. The Neoarchaean Limpopo orogeny: Exhumation and regional-scale gravitational crustal overturn driven by a granulite diapir. In: The Archaean Geology of the Kaapvaal Craton, Southern Africa. Springer, pp. 185–224.
Vearncombe, J.R., Barton Jr., J.M., Cheshire, P.E., De Beer, J.H., Stettler, E.H., Brandl, G., 1992. Geology, geophysics and mineralization of the Murchison schist belt, Rooiwater complex and surrounding granitoids, Memoirs. Geological survey of South Africa (now Council for Geosciences), p. 139.
Vézinet, A., Moyen, J.F., Stevens, G., Nicoli, G., Couzinié, S., 2018. A record of 0.5 Ga of evolution of the continental crust along the northern edge of the Kaapvaal craton, South Africa: consequences for the understanding of Archaean geodynamic processes. Precambrian Res. 305, 310–326.
Visser, D.J.L., 1956. The Geology of the Barberton Area. Geological Survey of South Africa.
Watson, J.S., 1996. Fast, simple method of powder pellet preparation for X-ray fluorescence analysis. X-Ray Spectrom. 25, 173–174.
Wilson, A., 1982. 1: 250 000 Geological Map of Swaziland, with Explanatory Notes. Swaziland Geological Survey and Mines Department, Mbabane, Swaziland.
de Wit, M.J., Jones, M.G., Buchanan, D.L., 1992a. The geology and tectonic evolution of the Pietersburg greenstone belt, South Africa. Precambrian Res. 55, 123–153.
de Wit, M.J., Roering, C., Hart, R.J., Armstrong, R.A., de Ronde, C.E.J., Green, R.W.E., Tredoux, M., Peberdy, E., Hart, R.A., 1992b. Formation of an Archaean continent. Nature 357, 553–562.
de Wit, M.J., van Reenen, D., Roering, C., 1992c. Geologic observations across a tectono-metamorphic boundary in the Babangu area, Giyani (Sutherland) greenstone belt, South Africa. Precambrian Res. 55, 111–122.
de Wit, M., Furnes, H., MacLennan, S., Doucouré, M., Schoene, B., Weckmann, U., Martinez, U., Bowring, S., 2018. Paleoarchean bedrock lithologies across the Makhonjwa Mountains of South Africa and Swaziland linked to geochemical, magnetic and tectonic data reveal early plate tectonic genes flanking subduction margins. Geosci. Front. 9, 603–665.
Zeh, A., Gerdes, A., Klemd, R., Barton, J.M., 2007. Archaean to Proterozoic crustal evolution in the central zone of the Limpopo Belt (South Africa–Botswana): constraints from combined U–Pb and Lu–Hf isotope analyses of zircon. J. Petrol. 48, 1605–1639.
Zeh, A., Gerdes, A., Barton, J.M., 2009. Archean accretion and crustal evolution of the Kalahari Craton—the zircon age and Hf isotope record of granitic rocks from Barberton/Swaziland to the Francistown Arc. J. Petrol. 50, 933.
Zeh, A., Gerdes, A., Millonig, L., 2011. Hafnium isotope record of the Ancient Gneiss complex, Swaziland, southern Africa: evidence for Archaean crust–mantle formation and crust reworking between 3.66 and 2.73 Ga. J. Geol. Soc. Lond. 168, 953–964.
Zeh, A., Jaguin, J., Poujol, M., Boulvais, P., Block, S., Paquette, J.L., 2013. Juvenile crust formation in the northeastern Kaapvaal Craton at 2.97 Ga—Implications for Archean terrane accretion, and the source of the Pietersburg gold. Precambrian Res. 233, 20–43.
Zeh, A., Ovtcharova, M., Wilson, A.H., Schaltegger, U., 2015. The Bushveld complex was emplaced and cooled in less than one million years–results of zirconology, and geotectonic implications. Earth Planet. Sci. Lett. 418, 103–114.
Zibra, I., 2020. Neoarchean structural evolution of the Murchison Domain (Yilgarn Craton). Precambrian Res. 105719.